SISSA - SCUOLA
INTERNAZIONALE
SUPERIORE
DI STUDI AVANZATI
TRIESTE
Strada Costiera 11

# ISAS - INTERNATIONAL SCHOOL FOR ADVANCED STUDIES

THESIS FOR THE TITLE OF

"MAGISTER PHILOSOPHIAE"

# ONE DIMENSIONAL COLLISIONLESS COSMOLOGICAL MODEL WITH SHELL CROSSING

Section: Astrophysics

Supervisor: Prof. D.W. Sciama

Candidate: Roberto Scaramella

Academic Year: 1985/86

TRIESTE

# ABSTRACT

The present work has been on nonlinear collapses of density perturbations in Cosmology, which are related to the problem of galaxy formation. In this theory, still unsettled today, much stress has recently been put on the gravitational role of possible massive collisionless particles. From both linear and nonlinear studies we see that if these particles had significant velocities during the cosmic expansion highly flattened structures would be the most like to be developed from the collapses. This leads naturally to the study of one-dimensional models.

The simple case with only the collisionless component has an analytic solution if the matter is represented by a finite number of planes. This solution, though, can't be exploited without a complex bookkeeping of the planes themselves, fact that requires the use of a computer. The simplicity of the model is compensated for by the unique feature of working directly with solutions: apart from roundoff errors the only possible concern on results is due to the discretness of the treatment.

The main purpose in this approach is to become able to explore a much broader sample of initial conditions than those usually considered in the literature, in order

to get a more extended knowledge on the collapse process. Initially the work consisted in building a code, which was then tested thoroughly. Finally, results have been obtained with this code both with the usual initial conditions and with initial random fields of different magnitudes for the planes velocities. These latter cases, never considered fully before, partially confirm the naive expectation of an inverse relationship between initial velocity magnitudes and final density contrast at the center of planar symmetry. However even over 5 orders of magnitude in the initial velocity dispersion, in fact, the velocities of the planes appear to be of the same order of magnitude for all cases. It is also found that sometimes for high initial velocities a ridge forms not at the center but at the outer boundary.

# TABLE OF CONTENTS

# CHAPTER I

## Introduction and survey

——*Missing light, Dark matter problem*

There is a well known and long standing discrepancy between the value of the luminous mass that is observed in the Universe and the mass inferred by dynamical arguments when one assumes stable configurations; this "dark matter" or "missing light" problem is one of the most outstanding problems in astrophysics.

In the present work we study some dynamical properties of the gravitational collapse of collisionless matter, which is thought to be responsible for the problem.

—— *Main observational results*

The mass discrepancy arises observationally on a wide range of length scales, enhancing the importance of the problem. On a local scale there is the so called Oort limit on the unseen matter in the galactic disk (Oort 1932, 1960). This limit, determined from the dispersion of stellar velocities perpendicular to the galactic plane, suggests a value of $M/M_{luminous} \geq 2$ (Bahcall 1984)

On somewhat larger galactic scales the observed rotation velocities of many spiral galaxies appear to approach constant values at large distances well beyond the confines of their luminous disks. These observations (Rubin 1982) may imply the existance of massive invisible halos surrounding spiral galaxies with $M(r) \propto r$ (Peebles 1980).

On still larger distance scales the Virial theorem applied to clusters of galaxies (Zwicky 1930) implies $M/M_{luminous} > 100$ ! (Hoffmann et al. 1980; Salpeter 1984).

This discrepancy clearly suggests the presence of an unseen massive component which dominates the gravitational dynamics of massive systems on a wide range of length scales unless one is willing to modify the law of gravitation itself (Milgrom 1983).

——*Dark matter and the Inflationary Universe*

There are also theoretical reasons suggesting the presence of gravitational components up to now unaccounted for.

Besides the increased stability that is acquired by a spiral galaxy when it is embedded in a larger massive halo, two more arguments are drawn from Cosmology: one is from the new inflationary theory and the other from theories of the early stages of galaxy formation.

The Inflation theory among other things predicts a universe with zero or very nearly zero global curvature (Guth 1981; Linde 1982). This avoids the incredible fine tuning ($\sim 10^{-54}$) required to insure that the ratio of the actual mass density to the critical one, $\Omega_0 \sim 1$ , is observed. In this inflationary model $\Omega_0 = 1$ to high

accuracy while by contrast $\Omega_{0\,luminous} \sim 3 \cdot 10^{-2}$ (Peebles 1980) is the mass density in luminous matter. Thus the inflationary theory requires copious non luminous matter.

——*Dark matter and early stages of galaxy formation*

In the gravitational instability theory small primordial departures from the uniform background density of Friedmann models give rise to the present day non-linear structure of the Universe. Their inefficient law of growth (at most as a power law with exponent of order unity; Lifshitz 1940; Zel'dovich and Novikov 1983; Peebles 1980) leads to a great inconsistency: in the standard hot Big Bang model matter and radiation are strongly coupled up to the epoch of "recombination" (redshift $\sim$ 1000) when the matter (mostly Hydrogen) becomes neutral and transparent to radiation. Prior to recombination baryonic matter and radiation were closely coupled, and any density fluctuations are found to be accompanied by a comparable temperature fluctuation in the radiation background. Observations of the cosmic microwave background imply $\delta T/T < 5 \cdot 10^{-5}$ on scales $\sim$ 5′ (Uson and Wilkinson 1984). This imposes very stringent limits on baryon density inhomogeneities present at $1+z \sim$ 1000, at least on scales larger to the one related to the Silk mass (Silk 1968).

This and the flatness problem seem to have a solution if most of the mass of the universe is in a collisionless, non baryonic, initially diffuse component. (If the matter needed to get $\Omega_0 = 1$ were in baryons unseen because they are in the form

of Jupiters or very faint cold stars serious problems with the present cosmological abundance of deuterium would arise).

Many different candidates for the collisionless matter have been proposed in various models of particle physics. All these hypothetical massive particles have the characteristic of being basically non interacting, apart from gravitational forces, after a few seconds from the Big Bang (Pagels 1984). Hence their density perturbation can usually grow much more than the baryonic ones (locked in acoustic waves by radiation pressure) between the end of the radiation-dominated era and recombination (a factor $\sim 30\ \Omega h^2$ in redshift). After decoupling the baryons can fall in the potential wells already built by these Wimps (weakly interacting particles, also darkinos). Because perturbations in the Wimps begin to grow before decoupling, smaller primordial fluctuations can lead to the formation of bound structure while still meeting the constraints from the as yet undetected fluctuation in the microwave background.

From the point of view of perturbations once the masses and number of wimps are adjusted to give $\Omega_0 = 1$, the only important feature of these particles is their velocity distribution. As they are collisionless, Wimps interpenetrate and mix on the so called "free-streaming" distance. This is the distance travelled during the fraction of cosmological time in which their velocities differ noticeably from zero (peculiar velocities of free particles dacay due to the expansion; see next chapter). The result is to completely erase their density perturbations on such scales — collisionless damping — giving a lower limit on the mass spectrum which can

collapse (this depends also on the initial perturbation spectrum; Peebles 1980; Carr and Silk 1983).

It is convenient to group the possible unseen particles into three categories: high (hot), medium (warm), or small (cold) velocities. The linear calculations show that density perturbations survive only on large scales (supercluster) for the hot case, large and medium (cluster) scales for the warm case, and all scales (down to $\sim$ globular cluster) for the cold case (Bond and Szalay 1983; Szalay and Zel'dovich 1982; Peebles 1980b; Blumenthal et al. 1982). These features have led to the two different current pictures of galaxy formation: from large scales down to small ones (fragmentation, pancakes, top-down scenario) or the opposite trend from small scales to large ones (hierarchical clustering, bottom-up scenario). The former scenario, favored by Zel'dovich and the Russian school (Zel'dovich 1970; Shandarin 1981b; Doroshkevich et al. 1975) arises when hot particles are dominant; the latter, proposed by Peebles (Peebles 1982b), when cold particles are the most important ones.

Unfortunately while both scenarios explain some observed features of the structure of the universe, each runs into difficulties. No single model seems to be able to fulfill all the constraints (Melott 1982; Shapiro et al. 1983; Centrella 1980; Peebles 1982a; White et al. 1983) without extreme initial conditions (Melott 1985). Recently researchers have begun to question some of the fundamental assumptions of the theory. For example, galaxies may not be good tracers of the overall matter distribution (biased galaxy formation; Shaeffer and Silk 1985; Davis et al. 1985).

Clearly a major role in the whole complicated process is played by the non linear regime when density perturbations are so enhanced that the linear standard treatment in separate Fourier components is no longer valid.

In the last few years some authors have tackled this difficult problem through complex many-particle numerical codes (Melott 1983; Wilson et al. 1985; Centrella and Melott 1985; Shapiro and Struck-Marcell 1985; Shandarin 1981a). Because of their sophistication and consequent long running times, these codes have generally covered only a very small range of initial conditions. However, the codes have provided numerical confirmation that highly flattened structures — the Zel'dovich pancakes — always emerge naturally from 3–D calculations of hot particles. Since this important result has been verified for only a limited range of initial conditions we are motivated to carry out the detailed study of planar structures undertaken in this thesis.

The goal of having great accuracy, flexibility and reliability favors a very simple model not including too many competing simultaneous effects. Accordingly the model chosen here is one-dimensional and plane symmetric with collisionless matter as the only component. The matter is represented by a number of equal planes which interact gravitationally but are free to interpenetrate each other.

This simple model bears less direct correspondence with a possible physical reality than the more sophisticated ones, but its great interest results from its very simplicity: it is almost an analytically solvable model ! The Zel'dovich approximate solution becomes **exact** in one dimension in the absence of shell crossing. Between

each crossing of planes a unique solution exists as will be shown in the next chapter. Of course it is possible to include shell crossing using a computer not to numerically integrate the equation of motion but just to handle the immense bookkeeping required to keep track of all the crossings.

The appeal of this approach is now evident: apart from roundoff errors and discreteness problems *the results are absolutely exact.*

Moreover this powerful approach, besides giving information on the behavior of the most important component of many more precise physical models, allows us also to study some aspects of the process of "violent relaxation" — the virialization of collisionless gravitating systems — in expanding coordinates (Lynden-Bell 1967; Shu 1978; Lecar and Cohen 1971; Tremaine 1985; Severne and Luwel 1980).

# CHAPTER II

## The theory

——*Cosmological models*

Very briefly we will recall the basic features of the Friedmann models considered here (Weinberg 1975; Peebles 1980a).

From the hypothesis of isotropy and homogeneity of the universe one can derive the Robertson-Walker metric

$$ds^2 = dt^2 - \frac{a(t)^2\, dr^2}{1 - kr^2} - a(t)^2\, r^2\, (d\theta^2 + sin\theta^2\, d\phi^2) \qquad (1)$$

where $c \equiv 1$ , $k$ is the curvature constant and $a(t)$ is the dimensionless expansion parameter. Assuming the energy-momentum tensor to be that of a a perfect fluid, the $_{0,0}$ component (time-time) of the Einstein equations is

$$\left(\frac{\dot{a}}{a}\right)^2 = \frac{8\pi}{3} G\rho - \frac{k}{a^2} \qquad (2)$$

where $\rho$ is the energy density.

A note on the conventions used here: the present time at which both the time variable and the expansion factor are normalized is always denoted by the subscript $_0$ while background values are denoted by the subscript $_b$ . Hence $\rho_0$ indicates

the actual value of the energy density and $t_0 \equiv 1$, $a_0 \equiv 1$ . The Hubble parameter is defined as $H(t) \equiv \dot{a}/a$ and the redshift as $1 + z \equiv a_0/a = a^{-1}$ .

As it is evident from eq.(2) the global curvature is reklated to the energy content: define the critical density to be $\rho_c \equiv 3H^2/(8\pi G)$ and $\Omega \equiv \rho/\rho_c$. Then according to wheter $\Omega$ is greater, smaller or equal to unity it follows that $k = 1$, $-1$, $0$ , and the universe is called closed, open, or marginally open.

The simplest case, $k = 0$ , is the classical Einstein-de Sitter model (hereafter E. d. S. ) which, if only non relativistic matter is present, has $\rho = (6\pi G t^2)^{-1}$ and $a \sim t^{\frac{2}{3}}$.

The closed case has a solution for $a(t)$ which is a cycloid while the open case has formally the same solution as the closed one, provided that the trigonometric functions are replaced by their hyperbolic analogues. Still, as long as $(1+z) \gg \Omega_0^{-1}$ , the closed and open case don't differ appreciably from the E. d. S. case which therefore plays a major role.

Finally, although today radiation no longer is dynamically important, because of the faster decrease with expansion of the radiation density ($\rho_{rad} \propto a^{-4}$ as opposed to $\rho_{matter} \propto a^3$), radiation was in fact dominant at

$$1 + z > 1 + z_{eq} \equiv \rho_{0_{matter}}/\rho_{0_{photons}} \cong 40000\,\Omega h^2 \qquad (3)$$

(when $H_0 = 100\,h\,kmsec^{-1}Mpc^{-1}$).

For $z \gg z_{eq}$ $\quad \rho \simeq \rho_{rel} \sim a^{-4}$ and $t \sim a^2$ ;

for $z \ll z_{eq}$ $\quad \rho \simeq \rho_{matter} \sim a^{-3}$ and $t \sim a^{\frac{2}{3}}$ .

——*Evolution of density perturbations*

If one is concerned with phenomena which are confined within the causal horizon, as in our case, it is legitimate to use the Newtonian approximation because the physical quantities are well defined (Peebles 1980a) and one needs not to be concerned with the gauge problems which arise in the full treatment (Bardeen 1980; Press and Vishniac 1980).

It is then useful to define *comoving coordinates*

$$\mathbf{q} \equiv \frac{\mathbf{x}}{a} \tag{4}$$

for points separated by a (proper) vector $\mathbf{x}$ at time $t$.

This implies that $\mathbf{q}$ is a a constant for a background observer, at rest with respect to the Hubble flow. Following Peebles (Peebles 1980a) one can show that for a perfect pressureless fluid (dust) the $_{0,0}$ field equation reduces to $\nabla_x^2 \Phi = 4\pi G\rho$ where $\Phi$ is the scalar gravitational potential; therefore in the background model an observer at $\mathbf{x} = 0$ measures the potential $\Phi_b = \frac{2}{3}\pi G\rho_b x^2$ . It is also useful to have an equation for $\ddot{a}$ ; differentiating eq.(2) with respect to time one gets

$$\ddot{a} = -\frac{4}{3}\pi G\rho_b\, a^2 \tag{5}$$

Doing the same with eq.(4) one has

$$\dot{\mathbf{x}} \equiv \mathbf{u} = a\dot{\mathbf{q}} + \mathbf{q}\dot{a} \equiv \dot{a}\mathbf{q} + \mathbf{v} \tag{6}$$

where $\mathbf{v} \equiv a\dot{\mathbf{q}}$ is the *peculiar velocity*, that is the velocity which a particle has with respect to an observer comoving with the background (these obviously have $\mathbf{v} \equiv 0$ by definition).

Through a slick manipulation of the Lagrangian (Peebles 1980a) one can factorize out the general expansion and consider the dynamics in the $q$ space (comoving grid), which is a more convenient coordinate system.

If we define the new gravitational potential as $\phi \equiv \Phi + \frac{1}{2} a \ddot{a} q^2$ , the field equation for this potential is

$$\nabla_q^2 \phi = 4\pi G \rho a^2 + 3a^2 \ddot{a} = 4\pi G a^2 [\rho(\mathbf{q}, t) - \rho_b(t)] \tag{7}$$

and the source for the new potential is the departure of the density from the background value.

The equation of motion for a particle of mass $m$ is $\dot{\mathbf{p}} = -m \nabla_q \phi$ where $\mathbf{p} \equiv m a^2 \dot{\mathbf{q}}$ . Rewriting in terms of the peculiar velocity one gets

$$\dot{\mathbf{v}} + \frac{\dot{a}}{a} \mathbf{v} + \frac{1}{a} \nabla \phi = 0 \tag{8}$$

and this equation shows clearly a very important effect: when *particles* are *free* ($\nabla \phi \equiv 0$) $|\mathbf{v}| \sim a^{-1}$ , and the *peculiar velocities decay* !

This is a purely kinematic effect (cosmic drag), which has profound consequences on the efficiency of gravitational instability process.

It is worthwhile noting that, since $\dot{\mathbf{q}} \sim \mathbf{v}/a$, it follows that $\dot{\mathbf{q}} \sim a^{-2}$ for free particles.

Applying the change of coordinates to the standard equations of continuity and momentum for a pressureless fluid, after some manipulations one can get the basic

equation for the evolution of the density contrast $\Delta$ , defined as $\Delta \equiv (\rho - \rho_b)/\rho_b$ which is

$$\ddot{\Delta} + 2\frac{\dot{a}}{a}\dot{\Delta} - 4\pi G\rho_b\Delta = 0 \tag{9}$$

This equation has the following solutions (Peebles 1980a):

— E. d. S.

$$\Delta(a) = A(q)\,a + B(q)\,a^{-\frac{3}{2}} \tag{10}$$

where $A$ and $B$ are specified by initial conditions.

— $k \neq 0$

Defining $s \equiv |\Omega^{-1} - 1| = (a/a_0)|\Omega_0^{-1} - 1|$ , changing variable from $a$ to $s$ and taking advantage of eq.(2) rewritten as

$$\left(\frac{\dot{a}}{a}\right) = \frac{8}{3}\pi G\rho_b\left[1 + \left(\frac{1}{\Omega_0} - 1\right)\frac{a(t)}{a_0}\right] \tag{11}$$

one can express eq.(2) as

$$\frac{d^2}{ds^2}\Delta + \frac{(3 \pm 4s)}{2s(1 \pm s)}\frac{d}{ds}\Delta - \frac{3\Delta}{2s^2(1 \pm s)} = 0 \tag{12}$$

where the + and − correspond to $\Omega > 1$ and $\Omega < 1$ respectively.

The solution of eq.(12) can be expressed as sum of a growing and a decaying solution (Groth and Peebles 1975). The main feature, growth rate at most as a modest power of time, holds also for $\Omega > 1$ if we consider the expansion phase.

——*Zel'dovich theory*

Zel'ldovich (1970) proposed an approximate solution for the non linear phase based on the assumption that the motion of a particle can be described by (q constant)

$$\mathbf{x} = a(t)\,\mathbf{q} + b(t)\,\mathbf{s}(\mathbf{q}) \tag{13}$$

This equation implies that the deviations from the Hubble flow (when $b(t)$ or $\mathrm{s(q)} \equiv 0 \rightarrow \mathrm{x} = a\mathrm{q}$ ) evolve in a self similar manner because they factor into one function depending only on time and another depending only on a given profile of coordinates.

This assumption of course is equivalent to a similar behaviour of $\delta\rho/\rho$ for small deviations.

How is eq.(13) related with $\Delta$ and eq.(9) ? One can take advantage of mass conservation and set

$$dm = \rho\, d^3x = <\rho> a(t)^3\, d^3q \tag{14}$$

(remember that for matter $\rho \sim a^{-3}$). Therefore

$$\rho = \frac{<\rho>}{a^{-3}\left[\frac{D(\mathrm{x})}{D(\mathrm{q})}\right]} \tag{15}$$

where $D(\mathrm{x})/D(\mathrm{q})$ is the Jacobian of the transformation of coordinates $\mathrm{x} = \mathrm{x(q)}$ and can be thought as a deformation tensor.

An appropriate coordinate system can be chosen locally in such a way that the tensor becomes diagonal and the density relation becomes simpler:

$$\rho = \frac{<\rho>}{[(1-\frac{b}{a}\alpha)(1-\frac{b}{a}\beta)(1-\frac{b}{a}\gamma)]} \tag{16}$$

where $b/a$ depends only on time and $\alpha$,$\beta$,$\gamma$, the eigenvalues of the deformation tensor, depend only on $\mathrm{s(q)}$ and its derivatives.

The quantities $\alpha$,$\beta$,$\gamma$, characterize the deformation along the three orthogonal principal axes of the deformation tensor:

$$\alpha = -\frac{\partial s_1}{\partial q_1} \qquad \beta = -\frac{\partial s_2}{\partial q_2} \qquad \gamma = -\frac{\partial s_3}{\partial q_3} \tag{17}$$

For small deformations eq.(16) becomes

$$\rho \cong < \rho > \left[1 + (\alpha + \beta + \gamma)\,\frac{b}{a}\right] \tag{18}$$

and we can see that $\delta\rho/\rho = f(q)\,(b/a)$ where $f(q) = \alpha + \beta + \gamma$ ; the density perturbation grows preserving its slope.

It can also be seen from eq.(16) that the density goes to infinity when one of the three factors in the denominator becomes zero. This happens because all the particles have the same value for the coordinate along the principal axis corresponding to the largest value among $\alpha$, $\beta$, $\gamma$. Therefore all the particles are in a plane – "pancake" configuration – and a caustic is formed in the density profile (we always consider $p = 0$ ).

After this stage the approximation breaks down because s is no longer a single-valued function of q (multistreams).

How good is the approximate solution ? Following Doroshkevich et al.(1975) one requires that $\hat{\rho}$ satisfies $\hat{\rho} = -\frac{1}{4\pi G}\,\nabla_x \mathbf{w}$ where $\mathbf{w} = \ddot{\mathbf{x}} = \ddot{a}\,\mathbf{q} - \ddot{b}\,\mathbf{s}(\mathbf{q})$ , that is the density $\hat{\rho}$ produces the acceleration field $\mathbf{w}(\mathbf{q}, t)$ .

If $\rho = \hat{\rho}$ we have an exact (selfconsistent) solution, therefore it is useful to define the fractional error $\epsilon = (\hat{\rho} - \rho)/\rho$. At the beginning

$$\Delta \equiv \frac{\rho - < \rho >}{< \rho >} \sim t^{\frac{2}{3}} \ll 1 \tag{19}$$

and $\epsilon = 0$.

Now, expressing $\hat{\rho}$ and $\rho$ in the coordinate system in which the deformation tensor is diagonal, we can show after some manipulations that

$$\epsilon = \frac{-a^2(\ddot{b} + 2\frac{\ddot{a}}{a}b)\, J_1 \; + \; ab\,(2\ddot{b} + \frac{\ddot{a}}{a}\, b)\, J_2 \; - \; 3b^2\ddot{b}\, J_3}{3\, a^2\ddot{a}} \tag{20}$$

where the J's are invariants of the "reduced" deformation tensor $\frac{\partial s_i}{\partial q_k}$ :

$$J_1 = \alpha + \beta + \gamma \qquad J_2 = \alpha\beta + \alpha\gamma + \beta\gamma \qquad J_3 = \alpha\beta\gamma \tag{21}$$

This is an important result because it shows that $\epsilon$ doesn't depend on the coordinate system as it is a function of the invariants only .

Now if one requires the coefficient of $J_1$ to be identically zero we have that $\epsilon$ is of second order in $\partial s_i/\partial q_k$ if we are in more than one dimension. In this case $\epsilon \neq 0$ and the theory is an approximation. But if we limit ourselves to the *one-dimensional* case we have that only one of $\partial s_i/\partial q_k \neq 0$ , say $\alpha$, and with $\beta \equiv 0$, $\gamma \equiv 0$ it follows that *also* $\epsilon \equiv 0$ . Therefore if

$$\frac{\ddot{b}}{b} + 2\,\frac{\ddot{a}}{a} = 0 \tag{22}$$

is satisfied we have an *exact solution* to our nonlinear problem. It is this important fact that motivates our studying a one dimensional model.

We have now the task of determining $b(t)$ from eq.(22). For this purpose it is convenient to change variables from the time to $a(t)$ itself. Let a prime $'$ denote $d/da$ : so, considering $b = b(a)$ we have $\dot{b} = b'\,\dot{a}$ and $\ddot{b} = b''\dot{a}^2 + b'\ddot{a}$ ; substituting in eq.(22) we get

$$\frac{b''\dot{a}^2}{b} + \ddot{a}\left(\frac{b'}{b} + \frac{2}{a}\right) = 0 \tag{23}$$

Combining the cosmological equations (2) and (5) we have $\dot{a}^2 = -2a\ddot{a} + k$ so eq.(23) can be rewritten as

$$-k\frac{b''}{b} = \ddot{a}\left(-2a\frac{b''}{b} + \frac{b'}{b} + \frac{2}{a}\right) \tag{24}$$

The simplest case is the E. d. S. model: in this case $k = 0$ and we get

$$-2\,a\,\frac{b''}{b} + \frac{b'}{b} + \frac{2}{a} = 0 \tag{25}$$

which is an Euler type equation, with solution $b(a) = A_1 a^2 + A_2 a^{-\frac{1}{2}}$. And if we consider the ratio $b(a)/a$ we again find the law of growth $\delta\rho/\rho \sim a$ (cf. eq. 10).

If instead $k \neq 0$, after some manipulations eq.(24) can be rewritten with $x \equiv \alpha a$, $\alpha = k/2$ as

$$x(x-1)\frac{d^2}{dx^2}b - \frac{\alpha}{2}\frac{d}{dx}b - \alpha^2 b = 0 \tag{26}$$

which has the hypergeometric function as solution.

——*The 1–D planar model*

As discussed at the end of chapter I the goal is to study the dynamics of a pressureless fluid in expanding coordinates.

From the theory developed in the previous section we have seen that choosing to work in one dimension allows us to have exact solutions of the equation of motion. Therefore in the calculation presented here the fluid is split into $2N$ planes of equal mass in a symmetrical configuration with respect to the origin. Because of this assumed symmetry one can limit the study just to one side of the zone of interest (the $N$ planes to the "right", for instance).

This implies also that whenever a plane collapses through the origin its mirror image does the same and enters the zone under study at the same instant but with opposite velocity. In this regard the plane appears to "bounce" elastically on the inner boundary and there is no net flux of planes through the midplane.

Let's now examine in some detail the equations involved.

In the unperturbed picture all planes are separated by a distance $\xi_b\, a(t)$ and the common surface density is $\sigma(t) = \rho_b(t)\, \xi_b\, a(t)$.

The equation of motion in Newtonian approximation for the given $m^{th}$ plane is (Peebles 1980a)

$$\frac{d^2}{dt^2}\, x_m = -\frac{4\pi}{3} G\, \rho_b(t)\, x_m - 4\pi G\, \delta M\,(x_m, t) \tag{27}$$

where $\delta M(x_m, t)$ is the excess of mass/area betwen $x_m$ and $x = 0$ with respect to the background:

$$\delta M\,(x_m, t) \equiv M\,(x_m, t) - M_b\,(x_m, t) = \sigma(t)\, K(t) - \rho_b(t)\, x_m \tag{28}$$

Here the function $K(x_m)$ counts the actual number of planes between the one labelled $m$ (included) and the origin.

Defining now the *fractional deviation of position* from the background value, $\delta$, as

$$\delta_m(t) \equiv \frac{x_m(t) - x_{m_b}}{x_{m_b}} = \frac{q_m(t) - q_{m_b}}{q_{m_b}} \tag{29}$$

we have

$$x_m(t) = x_{m_b}\,[1 + \delta_m(t)] = m\, \xi_b\, a(t)\,[1 + \delta_m(t)] \tag{30}$$

Taking the second time derivative of this equation one gets

$$\ddot{x}_m \;=\; m\,\xi_b\,\{\ddot{a}(t)\,[1+\delta_m(t)]\;+\;2\dot{a}(t)\dot{\delta}_m(t)\;+\;a(t)\,\ddot{\delta}_m(t)\} \tag{31}$$

But eq.(27) can be written as

$$\ddot{x}_m \;=\; -\frac{4\pi}{3}\,\rho_b\,x_m\;-4\pi G\,\rho_b(t)\,[\,\xi_b\,a(t)\,K(x_m)\;-\;x_m] \tag{32}$$

Equating these two equations, using the cosmological equation (2) we have

$$\ddot{\delta}_m(t)\;+\;2\,\frac{\dot{a}}{a}\,\dot{\delta}_m(t)\;-\;4\pi G\,\rho_b\left\{\delta_m(t)\;-\;\left[\frac{K(x_m)}{m}\;-\;1\right]\right\}\;=\;0 \tag{33}$$

Let's define $[K(x_m)/m]\;-\;1\equiv S(t,m)$ as a "source function", which is *zero if no shell crossing has occurred* (in this case $K(x_m)\;=\;m$), and assumes rational values otherwise.

Finally we can write

$$\ddot{\delta}_m(t)\;+\;2\,\frac{\dot{a}}{a}\,\dot{\delta}_m(t)\;-\;4\pi G\,\rho_b\,[\,\delta_m(t)\;-\;S(m,t)]\;=\;0 \tag{34}$$

which is our basic equation. Immediatly one sees the formal identity between eq.(9) for $\Delta\;=\;\delta\rho/\rho$ and the above equation for $\delta\;=\;\delta x/x$ when $S\;=\;0$, or between $\delta-S$ and $\Delta$ if $S\neq 0$ but $\dot{S}\equiv 0$. (Although strictly speaking $\dot{S}$ is a sum of $\delta$ functions, this has no practical relevance for the above argument.)

We already have the solutions for $\Delta$ according to the model of the universe. Denoting by $_+$ the growing solution and $_-$ the decaying one we have

$$\delta_m(t)\;=\;A_+\,D_+(t)\;+\;A_-\,D_-(t)\;+\;S(t,m) \tag{35}$$

with $A_\pm$ constants as long as $S(t,m)$ is a constant, i. e. between the shell crossings of m with its closest neighbours.

Thus we have an exact solution for the motion of a plane as long as its source term is constant. Whenever $S$ changes we obtain a *new* solution of the same form but with different coefficients $A_+$ and $A_-$ until $S$ changes again.

Therefore the logical scheme for our calculation is simple: (1) $x_m(t)$ is varied according to eq.(30) and eq.(35) until a shell crossing happens at $t = \tilde{t}$, say; (2) for $t \geq \tilde{t}$ up to a new crossing $x_m(t)$ is varied as before but now with the new law for $\delta$ given by $(t \geq \tilde{t})$

$$\delta_m(t) = A'_+ D_+(t) A'_- D_-(t) + S(t,m) \tag{36}$$

with the new coefficients $A'_+$ and $A'_-$ given by

$$\begin{aligned} A'_+ &= \mathcal{D}^{-1} \{ [\delta_m(\tilde{t}) - S(\tilde{t}_+, m)] \dot{D}_-(\tilde{t}) - \dot{\delta}_m(\tilde{t}) D_-(\tilde{t}) \} \\ A'_- &= \mathcal{D}^{-1} \{ D_+(\tilde{t}) \dot{\delta}_m(\tilde{t}) - \dot{D}_+(\tilde{t}) [\delta_m(\tilde{t}) - S(\tilde{t}, m)] \} \end{aligned} \tag{37}$$

where $\mathcal{D} \equiv [D_+(\tilde{t}) \dot{D}_-(\tilde{t}) - \dot{D}_+(\tilde{t}) D_-(\tilde{t})]$ and $S(\tilde{t}_+, m)$ is the new source function, calculated *after* the crossing has taken place.

——*Initial conditions*

Once a given profile of density contrast is specified we can determine $\delta^{in}(q)$ as follows. Rewrite eq.(13)) with $x(t) = a(t) q(t)$ as

$$q(t) = q_b - \frac{b(t)}{a(t)} s(q_b) \tag{38}$$

Eq.(16) now in one dimension reads

$$\rho(q,t) = \frac{\rho_b}{\left[1 - \frac{b(t)}{a(t)}\frac{\partial s}{\partial q}\right]} \tag{39}$$

so

$$\frac{\partial s}{\partial q} = \frac{a(t)}{b(t)}\left[1 - \left(\frac{\rho_b}{\rho(q,t)}\right)\right] \tag{40}$$

Integrating this equation with $S(0) = 0$ we have

$$\begin{aligned} \frac{b(t)}{a(t)}\, s(q) &= \int_0^q \left[1 - \frac{\rho_b}{\rho(q')}\right] dq' = q - \int_0^q \frac{\rho_b}{\rho(q')}\, dq' \\ &= q - \int_0^q \frac{dq'}{[1+\Delta(q')]} \end{aligned} \tag{41}$$

Therefore the initial value of eq.(38) is

$$q^{in} = q_b - q_b + \int_0^{q_b} \frac{dq'}{[1+\Delta(q')]} \tag{42}$$

but from eq. (29) we have

$$\delta^{in}(q_b) = \frac{q^{in} - q_b}{q_b} \tag{43}$$

so

$$\delta^{in}(q_b) = \frac{1}{q_b}\left\{\int_0^{q_b} \frac{dq'}{[1+\Delta(q')]} - q_b\right\} \tag{44}$$

or

$$\delta^{in}(q_b) = \frac{1}{q_b}\int_0^{q_b} dq' \left[\frac{-\Delta(q')}{1+\Delta(q')}\right] \tag{45}$$

which is the relation sought between the initial density profile and the fractional displacement. Note that this is correctly negative when there is an overdensity near the center (the planes are to "the left" of their background positions).

# CHAPTER III

*The code*

——*Main features*

As seen at the end of chapter II the position of a plane, say $m$, is given by

$$x_m(t) \;=\; a(t)\, q_m(t) \;=\; a(t)\, q_{b_m}\,[1 + \delta_m(t)\,] \tag{1}$$

and all the dynamics is contained in the evolution of $\delta$ ( $a(t)$ is known from the background). It is more convenient to adopt $a$ as the independent variable so $\delta = \delta(a)$ and to consider the *comoving equation of motion.*

Therefore one has

$$q_m(a) \;=\; q_{m_b}\,[1 + \delta_m(a)] \tag{2}$$

and

$$\delta_m(a) \;=\; B_+\, G_+(a) \;+\; B_-\, G_-(a) \;+\; S(a, m) \tag{3}$$

as basic equations. For E. d. S. $\quad G_+(a) = a, \;\; G_-(a) = a^{-\frac{3}{2}}$

The model assumes bilateral symmetry across the origin so one can treat just half of the number of planes involved, say $N$, provided that as soon as one plane

hits the origin its "velocity" $q' \equiv \frac{d}{da}\, q(a)$ is reversed in sign and a new solution is calculated from eq.(2–37). This mechanism – "reflection" or "bouncing" – simulates the fact that when a plane, passing through the origin, leaves the zone under study – the "right" – its symmetrical partner, following a mirror path, pops into the zone with the same speed but opposite velocity.

The region studied thus far has been in comoving space ($q$ space) with a range normalized to unity:

$$q_m \in [\ 0,\ 1\ ]; \quad \text{accordingly we have for } \delta\ : \quad \delta \in \left[\ -1,\ 1 - \frac{1}{q_{b_m}}\right] \qquad (4)$$

Let's examine now the crossing mechanism. At a *given instant* in principle one can have: two adjacent planes crossing at one point (defined as simple crossing); more than two planes crossing at the same point; or two simple crossings that happen contemporaneously in two different positions; or any combination of the above cases (define the situation as a degenerate crossing whenever is not a simple one).

Appropriate methods to handle all these phenomena have been devised but their detailed description is too long and complicated to be given here (use has been done of some of the subroutines described in "Numerical Recipes", Press et al. 1985).

——*Method*

The fate of a given plane in between crossings is completely determined by the background position $q_{b_m}$; the coefficients $B_+$ and $B_-$ for the law of growth of $\delta_m$, and the plane's ordinal place, that is the number of planes which are between

it and the origin; the latter is needed to calculate the value of the source function $S(a,m)$.

To these 4 quantities, different for each plane, the two values of $G_+(a)$ and $G_-(a)$ must be added. Moreover to handle the crossing we also need the first derivative of these functions, $G'_+(a)$ and $G'_-(a)$, and the "velocity" $q'_m$ of each plane:

$$\frac{d}{da}\,q \;\equiv\; q'_m \;=\; q_{m_b}\,[B_+\,G'_+(a) \;+\; B_-\,G'_-(a)] \tag{5}$$

The total is 5 variables for each plane plus 4 global ones. Their number is almost doubled, though, because of the following: when does a crossing happen? Because we have the exact law of motion for each plane we could solve exactly for $\hat{a}$ and $\tilde{a}$ the conditions

$$q_{m+1}(\tilde{a}) \;=\; q_m(\tilde{a}) \qquad \text{and} \qquad q_m(\hat{a}) \;=\; q_{m-1}(\hat{a}) \tag{6}$$

for all planes, then find the smallest among the $a$ 's calculated, say $\tilde{a}$, advance all $\delta$ 's up to $\tilde{a}$, cross the two planes involved and finally repeat the procedure.

This is not very efficient. To solve for $a$ with a reasonable accuracy (we don't want to spoil the advantage of working with the exact solution !) requires a considerable amount of time, and to do so for all planes when most of the values refer to fictitious solutions (fictitious because before that hypothetical crossing, others will have happened, thus changing the solution), seems not to be the best idea.

Still with a slight modification the method described above is perfectly workable. The difference consists in having a trial step, in updating the new positions

– now "tentative" – accordingly, then to search to see how many crossings have happened and which planes are involved. Once this is done, one can solve eq.(6) for the appropriate planes among these few planes only, then choose the smallest $da$, update the true, old quantities and so on.

Clearly in this way the time spent calculating eq.(6) decreases by a huge factor (2N over a few) and this compensates for the additional labor of "fishing for crossings" and of having to store old and tentative values for all the relevant quantities.

The last remark concerns the boundary conditions at $q = 1$. For the present work *periodic boundary conditions* have been assumed: this implies that planes "bounce" *at both boundaries* and their total number is conserved. We will see in the next chapter how this choice affects some of the results.

——*Tests*

Obviously whenever a numerical code is devised to solve a problem the first concern is about its trustworthiness and the reliability of its results.

In the present case at the lowest level there is a enhanced capability for the user to "see" what is happening at almost every operation through a degree of "verbosity" (degree of information written on the screen for a single cycle). This, combined with the possibility of choosing the initial conditions down to a single plane, permits one to follow in a detailed manner almost any sort of scenario (what happens when a single plane plows with high velocity through several which are still, just to mention one among many) and test and debug in this way the numerous subroutines needed in the simulation.

Of course this is not enough. Two more highly significant tests have been performed, in which we use the code to obtain a general solution with a special choice of initial conditions and then compare with results found by other authors.

——*Analytic test*

As can be seen by eq.(2–35) and eq.(2–30) if one starts with the very peculiar initial conditions of having $\delta_m^{in} < 0$ constant for all planes and zero velocities, that is a step function for the overdensity $\Delta > 0$ (see eq. 2–45), all the $\delta$'s will have the *same numerical evolution* up to the extreme range of allowed values , $\delta_m = -1$ (eq. 4).

This implies that all planes will collapse at the center at some time *without any shell crossing having occurred.*

Because of this last condition an analytic solution can be derived.

First one should note the situation at the instant of the degeneracy. When all the planes reach the origin they do so with different velocities with magnitudes ordered like the original label of the planes themselves.

Because of the symmetry the same process happened on the imaginary "left" zone ($\tilde{N}$ planes), so one should see emerge from the origin first the $\tilde{N}^{th}$ plane which has the greatest speed, then the $(\tilde{N}-1)^{th}$ and so on. With our bouncing scheme one should see the $N$ planes act like a fan (better: a spring), falling onto the origin, coming back, falling again ... and preserving their initial order throughout all the cycles.

The routine which treats the degenerate cases did indeed do a fine job in runs of this kind, because the initial order was always preserved.

Besides the qualitative feature a *quantitative* check has been performed; to see how this worked out we need to derive some formulas.

In Newtonian approximation we have (Peebles 1980a)

$$\ddot{x} \;=\; -\frac{4\pi}{3} G\,\rho_b(t)\,x \;-\; 4\pi G\,\delta M(x,t) \tag{7}$$

where $M(x,t)$ is the mass between 0 and $x$:

$$\delta M(x,t) \;=\; M(x,t) - M_b \;=\; M(x,t) - \rho_b(t)\,x \tag{8}$$

In the E. d. S. model eq.(7) becomes

$$\begin{aligned} \ddot{x} \;&=\; -\frac{4\pi}{3} G\,\rho_b(t)\,[-2x] \;-\; 4\pi G\,M(x,t) \\ &=\; \frac{4}{9}\,\frac{x}{t^2} \;-\; 4\pi G\,M(x,t) \end{aligned} \tag{9}$$

If we now have *no shell crossings* the mass between 0 and $x$ no longer depends on $x$, only on time:

$$M(x,t) \;=\; M(t) \;=\; \left(\frac{t}{t_{in}}\right)^{-\frac{4}{3}} M_{in} \tag{10}$$

because $M \sim \sigma \sim a^2 \sim t^{-\frac{4}{3}}$ where the surface density $\sigma$ decreases with the expansion.

Let's examine now the initial mass:

$$M_{in} \;=\; \rho_{in}\,x_{in} \;=\; \rho_{b_{in}}\,(1+\Delta)\,x_{in} \tag{11}$$

where $\Delta$ can usually be a function of the initial position but will be taken here to be constant.

The last term in eq.(9) in this way becomes

$$4\pi G\, M(t) \;=\; 4\pi G \left(\frac{t_{in}}{t}\right)^{\frac{4}{3}} \rho_{b_{in}}\,(1+\Delta)\,x_{in} \;=\; \frac{2\,x_{in}}{3t_{in}^2}\left(\frac{t_{in}}{t}\right)^{\frac{4}{3}} \tag{12}$$

and substituting it back in eq.(9) we get

$$\ddot{x} \;=\; \frac{4}{9}\frac{x}{t^2} - \frac{2}{3}\frac{x_{in}}{t_{in}^2}\,(1+\Delta)\left(\frac{t_{in}}{t}\right)^{\frac{4}{3}} \tag{13}$$

It is useful to change variables to $w \equiv x/x_{in}$, $\tau \equiv t/t_{in}$ so as to get

$$\frac{d^2\,w}{d\tau^2} - \frac{4}{9}\frac{w}{\tau^2} \;=\; -\frac{2}{3}\,(1+\Delta)\,\tau^{-\frac{4}{3}} \tag{14}$$

The solution of this equation is

$$w \;=\; A_1\,\tau^{\frac{4}{3}} + A_2\,\tau^{\frac{1}{3}} + (1+\Delta)\,\tau^{\frac{2}{3}} \tag{15}$$

For our purposes it is more convenient to express it in terms of the parameter $a$.

With $\alpha \equiv a/a_{in}$ and $\tau = \alpha^{\frac{2}{3}}$ we have

$$w(a) \;=\; A_1\,\alpha^2 + A_2\,\alpha^{-\frac{1}{2}} + (1+\Delta)\,\alpha \tag{16}$$

The coefficients $A_1$ and $A_2$ can be determined from the initial conditions by solving the system

$$\begin{array}{l} a \;=\; a_{in} \\ \\ \alpha \;=\; 1 \\ \\ x \;=\; x_{in} \end{array} \qquad \begin{cases} 1 \;=\; A_1 + A_2 + (1+\Delta) \\ \\ \dfrac{a_{in}}{x_{in}}\left(\dfrac{d}{da}\,x\right)_{in} \;=\; 2\,A_1 - \dfrac{1}{2}\,A_2 + (1+\Delta) \end{cases} \tag{17}$$

A run was made with the following initial conditions:

$$a_{in} = 10^{-3} \qquad \left(\frac{d}{da}\delta\right)_{in} = 0 \qquad \Delta = 1 \qquad q_b = 0.9 \tag{18}$$

This implies (cf. eq. 2–45)

$$\delta_{in} = -0.5 \qquad q_{in} = q_b\,(1+\delta_{in}) = 0.45 \tag{19}$$

The initial part of the evolution of $q(a)$ and $x(a) = a\,q(a)$ is shown in fig.(1). The zeros correspond to degenerate collapses onto the origin: at these instants the "velocity" $q'$ is reversed and a new law of motion is calculated. The "velocity" behavior is shown in fig.(2).

Now use eq.(17) to determine $A_1$ and $A_2$: from

$$x(a) = a\,q_b\,[1+\delta(a)] \qquad x' = \frac{x(a)}{a} + a\,q_b\,\delta'(a) \tag{20}$$

we have

$$\left(\frac{a\,x'}{x}\right)_{in} = 1 \qquad \text{because} \qquad \delta'(a_{in}) = 0 \tag{21}$$

Therefore we find

$$A_1 = -\frac{3}{5} \qquad A_2 = -\frac{2}{5} \tag{22}$$

and $x(a)$ should follow the theoretical law of motion

$$x(a) = x_{in}\left[-\frac{3}{5}\left(\frac{a}{a_{in}}\right) - \frac{2}{5}\left(\frac{a}{a_{in}}\right)^{-\frac{1}{2}} + 2\left(\frac{a}{a_{in}}\right)\right] \tag{23}$$

In fig.(3) we show the excellent agreement between eq.(23) (solid line) and the values computed (crosses).

Of course the solution (23) is valid until the degeneracy forms: then the planes bounce and a new solution must be calculated. The latter has the same functional form due to the self similarity of the initial conditions (Fillmore and Goldreich 1984).

——*Canonical case and comparison with other authors' work*

As already mentioned in chapter I several authors performed calculations on nonlinear collapses in cosmological models (Melott 1982, 1983; White et al. 1983; Shapiro and Struck-Marcell 1985; Shandarin 1981a) with codes which usually describe several processes at once and often operate in more than one dimension. This of course makes it difficult to look for comparisons. Most of the cases treated in the literature, though, assume as initial conditions for the overdensity the shape given when only one Fourier component of small amplitude is present and assume velocities which are small compared to those dimensionally appropriate to the time and length scale of interest.

The motivation of these assumptions lies in the output from the linear phase of the evolution of density perturbations driven by hot dark matter.

Let's now apply these assumptions to our model. Rewrite here eq.(2–42):

$$q_{in} = \int_0^{q_b} \frac{dq'}{[1+\Delta(q')]}$$

When $|\Delta(q)| \ll 1$ this becomes

$$q_{in} \cong \int_0^{q_b} dq' \,[1-\Delta(q')] \tag{24}$$

Thus if $\Delta(q) = \sum \Delta_k \cos kq = \Delta \cos mq$, then with the crude assumption that only one term, $k = m$, is dominant, we get

$$q_{in} = q_b - \int_0^{q_b} \Delta \cos mq \, dq = q_b - \Delta \frac{\sin mq_b}{m} \tag{25}$$

and

$$\delta_{in} = -\Delta \frac{\sin mq_b}{mq_b} \tag{26}$$

It is convenient to normalize such that $m = \pi$ (remember that $0 \leq q \leq 1$).

Examine now the velocity that a particle would get in going from $q_b$ to $q_{in}$ : the peculiar velocity is (cf. eq. 2–6) $v = \dot{x} - a\dot{q}$. Substituting $x = a\,q_b - b(t)\,s$ we have

$$v_{in} = [\dot{a}\,q_b - \dot{b}\,s_{in}] - \dot{a}\,q_{in} = -b\,s_{in}\left(\frac{\dot{b}}{b} - \frac{\dot{a}}{a}\right) \tag{27}$$

For E. d. S. $a \sim t^{\frac{2}{3}}$ and $b \sim a^2 \sim t^{\frac{4}{3}}$ so

$$v_{in} = -b\,s_{in}\left(\frac{4}{3t} - \frac{2}{3t}\right) = -\frac{2}{3}\frac{b}{t}\,s_{in} \quad \text{or} \quad v_{in} = -\frac{2}{3}\,a_{in}^{\frac{1}{2}}\,s_{in} \tag{28}$$

Therefore several runs were made with eq.(26) and eq.(28) as initial conditions, and their complete description is reported with other results in the next chapter.

Here, being interested only in making comparisons, we show only the final result of the more suitable case, whose parameters are:

$$a_{in} = 10^{-3} \qquad a_{fin} = 1 \qquad \Delta = 10^{-2} \qquad N_{planes} = 100 \tag{29}$$

In fig.(4) is shown the phase space in comoving coordinates, which is very similar to fig.(2f) of Shapiro and Struck-Marcell (1985) and fig.(8a) of Melott (1983).

# CHAPTER IV

*Numerical results*

——*Canonical case*

As mentioned at the end of the previous chapter runs were made with initial conditions chosen to match as closely as possible models that have already appeared in the literature (Melott 1982; Centrella and Melott 1985; Shapiro and Struck-Marcell 1985). This was done both to gain some insight on certain controversial issues (Melott 1985; Tremaine 1985) and to test the code.

All of our runs assume an Einstein-De Sitter universe and all but one employ 100 planes.

As initial conditions we chose to consider cosinusoidal density perturbations with amplitude $\Delta = 1$ % and half wavelength equal to the size of the zone studied (in our dimensionless units this means $\lambda = 2$ ).

This initial perturbation has been assumed to have already gone through a long linear evolution by the time the calculation begins.

Thus we assume that only the growing mode ($\sim\ a$) is present initially (so $B_- \equiv 0$ in eq. 3–3). This implies in turn that all planes have a net inward bulk peculiar velocity.

The initial velocity and mass profiles are shown in fig.(5) and the same is done for $z = 10,\ 3,\ 0$ in fig.(6-8). The mass fraction profile, *normalized to the box*, is shown together with the phase space diagram in order to have a better visual correlation between mass profile and the distribution of the planes.

The evolutionary sequence is evident. First planes fall in an orderly fashion toward the origin. Then the first planes to hit the origin bounce and form a first counterstream.

These planes decelerate and collapse again later, giving birth to a second counterstream, and so on.

It is perhaps easier to visualize what is happening by considering a plot of the phase space which is linear in the comoving coordinate. Looking at fig.(9) one can see the characteristic pattern of a well ordered collapse: a spiral wound around the origin (remember the existance of a symmetric part !).

Other important conclusions can be drawn: the "snapshot" shows a system which is very far from ergodic (sometimes with appropriate initial conditions the motion is even self similar; see end of chapter III).

There are strong density enhancements when a counterstream inverts its velocity – "turnaround" – and at these locations the mass profile has a steep rise. This correspondence can be better seen in fig.(10) where both phase space and mass

profile (normalized to the box) are shown for $z = 6$ . This effect is due to the fact that planes spend more time close to the turnarounds because there they slow down (quite similar to the behaviour of a comet at aphelion, for instance).

All these qualitative results agree quite well with those shown by Shapiro and Struck-Marcell (1985) and Melott (1983).

At this stage one crucial question that must be addressed is: "How does the number of planes affect the results?"

Evidently 100 planes are not enough to get good statistics. Unfortunately there are time constraints on the computations. To see how things vary, a run was made with the same initial conditions, but with 300 planes.

It was found that the required CPU time for the calculation was larger by a factor of almost 20 : 8.5 hrs. for 300 planes vs. 0.5 hrs. for 100 planes on a VAX 11-750. The increase in CPU vs. number of planes $N$ appears to be even greater than $\sim N^2$ . Of course more cases are needed to confirm this trend.

This nonlinear scaling is due to the different number of tentative crossings (for definitions see the third section of chapter III), number of real crossings and number of bounces at the origin; the former are $2.5 \cdot 10^4$ , $1.4 \cdot 10^4$ , 209 , for 100 planes and $2.4 \cdot 10^5$ , $1.3 \cdot 10^5$ , 637 , for 300 planes.

If we plot the final results of the N=300 case we see that there is just a more continuous description of the streams in phase space, not any substantial difference is seen in fig.(11) from fig.(4).

If we plot the mass fraction for both cases at $z = 2,\ 1,\ 0$, we can see that there is a small difference at the very beginning of the curve.(Fig. 12-14) .

Except for this the agreement is excellent. The difference is of course due to the grainier mapping of the N=100 case.

Because of the much greater cost in terms of CPU it seems therefore convenient to use a number of planes greater than 100 only when a really precise result is needed.

To explore extensively the parameter space N=100 seems to give fine results with a reasonable expense of computer time. On the other hand when we consider the effects of random "thermal" motions it seems reasonable to improve the statistics of the final output by combining the results of a few independent runs with a moderate number of planes.

——*Initial random velocities*

One of the main purposes of this work is to examine the effect of random velocities on the evolution of density perturbations is (for a non self consistent approach see Sukhurov 1982).

To gain general information on the effects of initial velocity fields for a wide range of characteristic thermal speeds we consider gaussian velocity distributions for the shells at $z = 1000$ and study a range of five orders of magnitude in the initial velocity dispersion.

Because we choose a non dimensional description the appropriate velocity scale is the ratio of the length scale of our zone to $t_{in}$, the age of the universe at the beginning of our calculation.

This peculiar velocity scale, $\tilde{v}$ , in our units, is

$$\tilde{v} = \frac{x_{tot}}{t_{in}} = \frac{a_{in}\, q_{tot}}{t_{in}} = \frac{q_{tot}}{\sqrt{a_{in}}} = a_{in}^{-\frac{1}{2}} \tag{1}$$

where we have made use of (1) $t \sim a^{\frac{3}{2}}$ for E. d. S. , (2) $q_{tot} = 1$ , and (3) $t = a = 1$ at the present time ($z = 0$).

We choose the velocity dispersion of our assumed gaussian distribution (with zero mean velocity) to be a fraction, $\mathcal{F}$ , of $\tilde{v}$ at $t_{in}$ :

$$v_{r.m.s.} = \mathcal{F}\,\tilde{v} \tag{2}$$

Five values for $\mathcal{F}$ have been studied, $\mathcal{F} = 1,\ 10^{-1},\ 10^{-2},\ 10^{-3},\ 10^{-4}$ . Each of these was run four different times with different randomly selected velocities, (cases a, b, c, d) to accumulate statistics.

In all cases the initial density perturbation was the same as in the canonical case, $\Delta(q) = 10^{-2}\, cos\pi q$ , so each plane had the same initial position as in our run with no random motion.

In order to see consistently the effect of the *magnitude* of the velocities alone on the subsequent evolution, we assigned all the shells the same value of the peculiar velocity in units of $\mathcal{F}\tilde{v}$ in a run for the different values of $\mathcal{F}$ considered.

The first step is to show what happens without velocities ($\mathcal{F} = 0$) to have a benchmark to compare with.

This case, referred to as the "cold" case, is very similar in outcome to the canonical case shown previously. This can be seen in the following figures.

In fig.(15) the initial mass profile is shown, while in fig.(16-19) the phase space and mass profile are plotted at four different time slices ($z = 10,\ 3,\ 1,\ 0$).

The effect of the gravitational field induced by the small initial overdensity can be appreciated by considering how much the velocities found here differ from adiabatic, in which the velocities would simply decrease like $v \sim 1/a$ .

Therefore, going back in time, if one increased the vertical scale of the graphs like $1/a$ , as has been done here, nearly adiabatic evolution with $a\,v$ = constant would have very similar limiting velocities in the different slices as a fraction of the entire length of the vertical axis.

This is not the case however, as can easily be seen. Moreover a numerical inspection reveals that almost all planes have $\mid v_p \mid \leq 0.5$ from $z = 0$ instead of having a variation of a factor 4.

The evolution of the mass fraction is shown for the same time slices. The most interesting feature is the cusp seen in the graph for $z = 3$ which corresponds to the high concentration of planes at the turnaround of the first counterstream. Later more counterstreams have developed and accordingly more cusps are seen although not in such a pronounced way.

To gain more insight into the temporal evolution of this cold case, a run was made into the "future" ($a > 1$), to see if the regularity of the counterstreams' formation and shape continued also after the expansion factor has increased by many times over the value at the first collapse ($z \sim 7$).

The fig.(20), which shows the phase space for $a = 70$ (this would correspond to an age of $\sim 10^{13}$ years !), confirms that it is indeed so. Although there are only

a few points for each counterstream, the very regular pattern of their arcs can still be noted.

The system seems to be still far from a virialized state.

Let's examine now the runs with random peculiar velocities, concentrating on case a to start with. In fig.(21) are shown the initial conditions which are the same for all the a-subcases once the magnitude of the velocities is appropriately scaled.

In fig.(22-25) are shown both phase space distribution and mass fraction (the latter always normalized to the box) for $z = 500$ for $\mathcal{F} = 1,\ 10^{-1},\ 10^{-2},\ 10^{-3}$ .

After just a factor 2 in the expansion the first differences due to different velocity amplitudes already appear: for high velocities ($\mathcal{F} = 1,\ 10^{-1}$) the initial mass profile begins to look less smooth because the planes have already moved appreciably, while for low velocities ($\mathcal{F} = 10^{-3}$) the gravitational effect starts taking place and accelerates the planes inward, shifting the average velocity toward negative values.

In fig.(26-29) is shown the $z = 100$ time slice. Because the axes for the velocities have been scaled down by the adiabatic factor 10 we can see that, as expected, for high velocities the extra kinetic energy input has overcome the gravitational field and the motion has indeed been almost adiabatic.

In contrast, for low initial velocities (hence less initial kinetic energy) the behavior is exactly the opposite: only 4 out of 100 planes happen to be in the adiabatiacally rescaled initial phase space !

In fig.(30-34) are shown the final mass profile and phase space for all the $\mathcal{F}$ values.

Because it would be too long and tedious to show here detailed graphs of all the other three cases, it is convenient now to examine the *combined results* of cases a, b, c, and d relative to the *same* $\mathcal{F}$ value.

In fig.(35) are shown for comparison the final mass profile for the cold case (solid line), for $\mathcal{F} = 10^{-4}$ (short dash) and for $\mathcal{F} = 1$ (point-dash).

The naive intuition that with low velocities the collapse is dominated by gravitation, is nicely confirmed. Indeed the $\mathcal{F} = 10^{-4}$ case closely matches the cold case, while the $\mathcal{F} = 1$ case appears to be much more diffuse with almost half of the total mass close to the outer boundary.

The same position encloses $\sim$ 90 % of the mass in the cold case. In fig.(36) are shown the remaining results: cold, solid line; $\mathcal{F} = 10^{-3}$ , short dash; $\mathcal{F} = 10^{-2}$ , point-dash; $\mathcal{F} = 10^{-1}$ , long dash-short dash.

The $\mathcal{F} = 10^{-3}$ case is a bit less condensed in the inner region ($\log q < 0.5$) than the cold case but its curve has almost the same shape. Two turnarounds appear to be at the same place in the cold and $\mathcal{F} = 10^{-3}$ runs, while the third and innermost, present in the cold case, is absent in the $\mathcal{F} = 10^{-3}$ case.

The $\mathcal{F} = 10^{-2}$ run begins to show the feature, already noted for the $\mathcal{F} = 1$ case, of mass accumulation ($\sim$ 30 %) at the outer boundary, but the remaining part of the curve, although displaced to the right (more rarefaction) seems to be still similar to the $\mathcal{F} = 10^{-3}$ case.

The $\mathcal{F} = 10^{-1}$ case is completely different on the other hand. There is a pronounced mass localization into two well separated and definite regions, with

$\sim$ 30% of the mass in the inner region ($\log q < -1.5$) and almost 60 % confined to a thin shell near the outer boundary. This is surprising at first glance because one would have naively expected a smooth transition, ordered according to increasing values of $\mathcal{F}$, from the cold case up to the "hot" ($\mathcal{F} = 1$) one.

An examination of fig.(37-40) where all the final values of the four cases with $\mathcal{F} = 10^{-1}$ are shown yields the confirmation of this general trend: all cases have a significant fraction of the planes close to the outer boundary. Because of the heavy weight of the single case b (which has $\sim$ 90 % of the mass at the outer region !) more ample statistics would probably give a lower value for the fraction of the mass concentrated at the outer bondary. Nevertheless the trend remains.

A possible explanation could be the already-mentioned effect that the initial peculiar velocities have on both the energy and the distance that a plane can travel.

In expanding coordinates the energy is not conserved. Through the cosmic virial theorem (Peebles 1980a) one can only set limits on the total energy variation, or otherwise verify its differential decrease when working with the equations of motion (Melott 1982).

Therefore the following considerations are not rigorous at all but can still give some insight into the results.

The argument is that beacuse of the peculiarity of our model (e.g. role of the background values, adimensionality) one can think of the initial gravitational binding "energy" to be of the order of the initial density contrast, that is $\sim 10^{-2}$ .

Now one can compare this value with the typical initial kinetic "energy" which, going as the square of the characteristic average velocity, is proportional to $\mathcal{F}^2$ .

Therefore we can roughly expect that a fraction of planes will be unbound when $\mathcal{F} \sim 10^{-1}$ or greater, and they will tend to accumulate at the outer boundary.

The other effect which is of utmost importance when velocity fields are present is "collisionless damping". This effect is due to the free-streaming properties of collisionless particles and it is responsible for the low-mass cutoff that hot or warm Wimp's density perturbations have after the linear growth phase.

For a *free particle* we can easily calculate the *diffusion length*, which is the distance travelled by the particle before its peculiar velocity is completely annihilated by the cosmic drag.

Because $dx = v_p\, dt$, if we rewrite it in terms of comoving cordinates we have

$$dq = \frac{v_p}{a}\, dt \tag{3}$$

Integrating this equation we find the *comoving diffusion length* $q_D$, comoving distance travelled by a free particle between $t_i$ and $t$, as

$$q_D = \int_{t_1}^{t} d\tau\, \frac{v_p(\tau)}{a} \tag{4}$$

But $v_p(t) = (a_i/a)\, v_p(t_i)$ for a free particle and we assumed $v_p(t_i) = (\mathcal{F}\, q_{tot}\, a_i)/t_i$ so, making use of the E. d. S. relation $(a/a_i) = (t/t_i)^{\frac{2}{3}}$ we get

$$\begin{aligned} q_D &= \int_{t_i}^{t} d\tau \left(\frac{a_i}{a}\right)^2 \frac{\mathcal{F}\, q_{tot}}{t_i} \\ &= \int_{t_i}^{t} \frac{d\tau}{t_i}\, \mathcal{F}\, q_{tot} \left(\frac{t_i}{\tau}\right)^{\frac{4}{3}} \\ &= 3\, \mathcal{F}\, q_{tot} \left[1 - \left(\frac{t_i}{t}\right)^{\frac{1}{3}}\right] \end{aligned} \tag{5}$$

This can be rewritten as

$$\frac{q_D}{q_{tot}} = 3\mathcal{F}\left[1 - \left(\frac{a_i}{a}\right)^{\frac{1}{2}}\right] \tag{6}$$

and we see that the average plane, if it were free, would at most travel a distance

$$q_{D_\infty} = 3\mathcal{F}\, q_{tot} \tag{7}$$

But one third of this maximum distance is almost covered in the very first doubling of the expansion factor!

For $(a/a_i) = 9/4$ in fact $q_D/q_{tot} = \mathcal{F}$ . It is evident then that already for $z = 500$ the small initial density perturbation will have been washed out for $\mathcal{F} \sim 1$ . It is convenient now to examine the final phase space for the average of cases a, b, c, and d for a given value of $\mathcal{F}$ because the former carries more infrmation than the density profile.

Because the outer boundary region is also of interest the same data are displayed twice, once in a graph which is linear in the comoving position and once in one which is logarithmic in the latter variable.

First examine the cold case: the linear and the logarithmic plot of its final $(z = 0)$ phase space for 100 planes are shown in fig.(41) and fig.(42). We note its regular spirals, completely similar to the canonical case; the only difference is in the current position of turnarounds because the latter case started to bounce earlier than the former because it had a net inward ordered initial velocity.

In fig.(43) and fig.(44) we have the same for $\mathcal{F} = 10^{-4}$ and we can immediatly see that the difference from the cold case is really minimal: the greater density

which appear to be now at the center is mainly due to the difference in the number of planes plotted (here and afterwards 400).

In fig.(45) and fig.(46) is shown the case $\mathcal{F} = 10^{-3}$ . This case begins to differ from the previous one in the inner region. As already noted from the mass profile, here the innermost stream has disappeared, while the others are still fairly recognizable. A certain local clumpiness in the streams also begins to appear on a fine scale.

Fig.(47) and fig.(48) are relative for the case $\mathcal{F} = 10^{-2}$ . Here we already have a fraction of planes swept out at the outer boundary and these are well separated from the others. The latter seem not to have a definite structure anymore nor to have collapsed at the center (yet?). They show an evident local clumpiness, though.

In fig.(49) and fig.(50) is presented the result for the case $\mathcal{F} = 10^{-1}$ . The planes seem to be evenly divided between the two regions at the boundaries. These two regions are then well distinct and apart one from each other. The planes there, although spatially dense still have a fair spread in velocities and lack the local small scale clumpiness seen in the previous case.

Let's see now the last case, $\mathcal{F} = 1$ , shown in fig.(51) and fig.(52). We find the same global feature observed for $\mathcal{F} = 10^{-1}$ : most of the planes are evenly split in two defined regions close to the boundaries. There are two differences from the previous case, though. First the single zones now have a greater spatial extent; second there isn't a complete void region between the two of them. In fact,a bridge-like feature is present, which is made up of two opposite streams of planes with opposite velocities.

With a more detailed examination of the single runs for $\mathcal{F} = 1$ we see that this double feature is a superposition effect: out of four runs two give clustering at the center and two at the outer boundary. This can be seen, for instance, in fig.(53) and in fig.(54) where the case d is shown for $z = 3$ and $z = 0$. Another interesting problem which arises is given by the relative degree of local clumpiness that is different for different values of $\mathcal{F}$.

Our opinion is that this is mainly due to the large graininess of such a small number of planes used. If we waited enough time probably this local clumpiness would also show in the cases with high $\mathcal{F}$. The relaxation process is in fact due here to the two body encounters (crossings) and we can expect a non monotonic behaviour with different number of planes: if the planes are really few their encounters have big effects on their orbits, but they are rare and so the process is slow. If we instead are representing an ideal continuum situation (this would not be the case if, for instance we were simulating a small stellar cluster), this would of course require a great number of planes to get in this way a large amount of crossing per characteristic time. These crossing on the other hand would have very little effect and so if we had to represent a fluid with only random velocity fields any small clumpiness would look suspicious. If we averaged different infact this clumpiness would probably not persist anymore.

It is also interesting to consider the role of the chosen boundary conditions: would the ridge on the external boundary for high $\mathcal{F}$ value have formed at all or would the planes have just ended spread out much further apart, "frozen" by the cosmic drag?

It is difficult to evaluate the competing effects of local relaxation and gravitational pull versus the thermal drift. Nevertheless if a ridge were still formed with a non reflecting external boundary, the ridge itself would not probably occur at the same place for a different initial velocity distribution (same $\mathcal{F}$ but different random draw). The periodic outer boundary condition has the effect of a seed on a possible ridge formation because all the planes that do not have enough energy to make the complete journey to the other part of the zone are compelled to stay in its vicinity and quickly relax there.

——*Conclusions*

The code that has been devised and tested seems to give the opportunity of getting information on a broad variety of different cases and its results can have multiple purposes. More specifically one can acquire at an abstract level broader knowledge of: gravitational physics in expanding cooordinates, of the statistical properties inherent in the phenomenon of violent relaxation (Lynden-Bell 1967, Shu 1978, Lecar and Cohen 1971; Cuperman et al. 1971; Hohl 1968) which, because of its intrinsic difficulty has never been treated as a main specific goal in expanding coordinates (for the analogous model in non expanding coordinates see Severne et al. 1984), and finally of the dominant component in current popular models, helping in understanding their features and tsting previous results. For instance at a first glance for the canonical case the run made with 300 planes doesn't rule out at all the claim of Melott (1982) that more than 10% of the mass is concentrated in a core which is 1% of the wavelength, a result on which some doubts have been

cast. From the graph in fig.(14) it seems that the mass fraction within $10^{-2}$ is $\geq 15\%$ , but a more careful study is needed because of the high sensitivity to the inital conditions.

Working on the main issue addressed in the present work, the effect of random velocity fields on a small density perturbation, has confirmed the coarse trend that was naively expected (high velocities give more diffusion) but with some interesting features: among them the formation of ridges at the outer boundary and the fact that the accelerations due to collapses and cosmic drag give rise after a factor 1000 in expansion to peculiar velocities which seem to be of the same order of magnitude. This occurs despite huge differences in their initial values (5 orders of magnitudes). The final velocity fields are still highly ordered when the initial phase space has no or very little mixing. This confirms one of the main aspects of the collisionless gravitating systems: the relaxation time for highly ordered system is *much* greater than the dynamical time.

Some limitations evidenced during the work suggest perhaps the need for a better algorithm to allow the routine use of a larger number of planes. This would minimize the spurious effects of the excessive discreteness of working with a few hundreds of planes. Some of these effects can in fact not be overcome by combining statistically the final results of many different runs. We mainly refer to the degree of local clumpiness which in some cases could have a crucial role.

We have seen in fact that also for high initial velocities a strong tendency to clustering seems to be present. In this case, though, we could expect that for the

same range in expansion the final degree of clumpiness would be inversely proportional to the total number of planes used in runs with the same initial value for $\mathcal{F}$.

As for possible future development of this problem besides the study of the aforementioned statistical connections and improvements of the code itself, the next stage could be the study of different initial density contrast profiles: from the linear studies usually there emerges a whole Fourier spectrum and there is the strong possibility that the final results could change quite a bit when the whole spectrum is initially taken into account instead of a single component, albeit dominant. This can be particularly true in the case of warm Wimps that have a spectrum less sharply peaked than that of hot Wimps but still with a cutoff such that the one-dimensional model can be applicable. Besides the initial conditions we have seen that also the boundary conditions sometimes play quite a role and it is then also of interest to see what happens when they are modified.

It will also be of interest to compare the resultsof this treatment with those of a completely different approach, namely working with distribution functions in phase space. In this way we can evaluate the discrete approach versus the continuum one.

# FIGURES

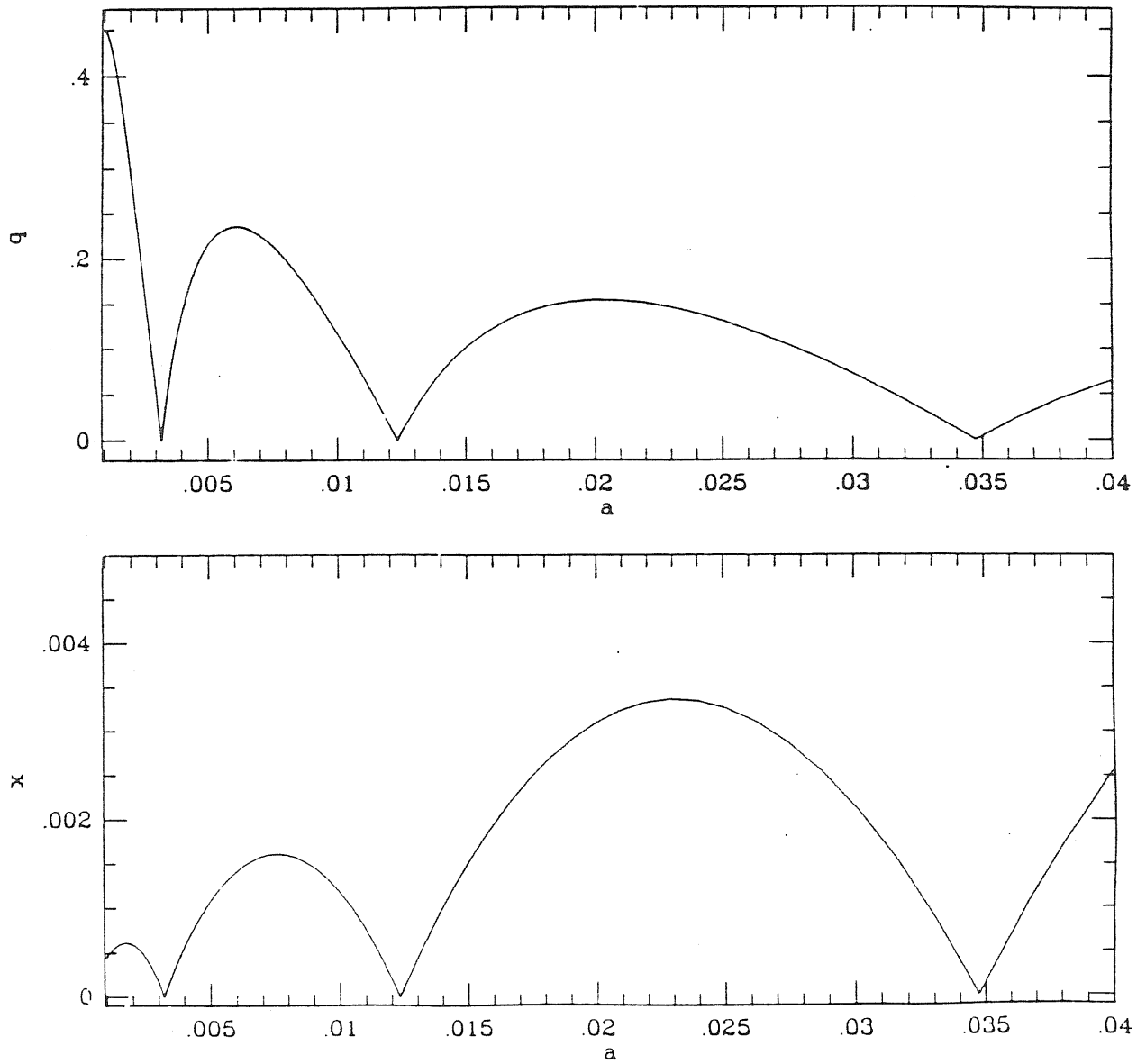


**Figure 1.** Analytic case: proper (x) and comoving (q) position of last plane.

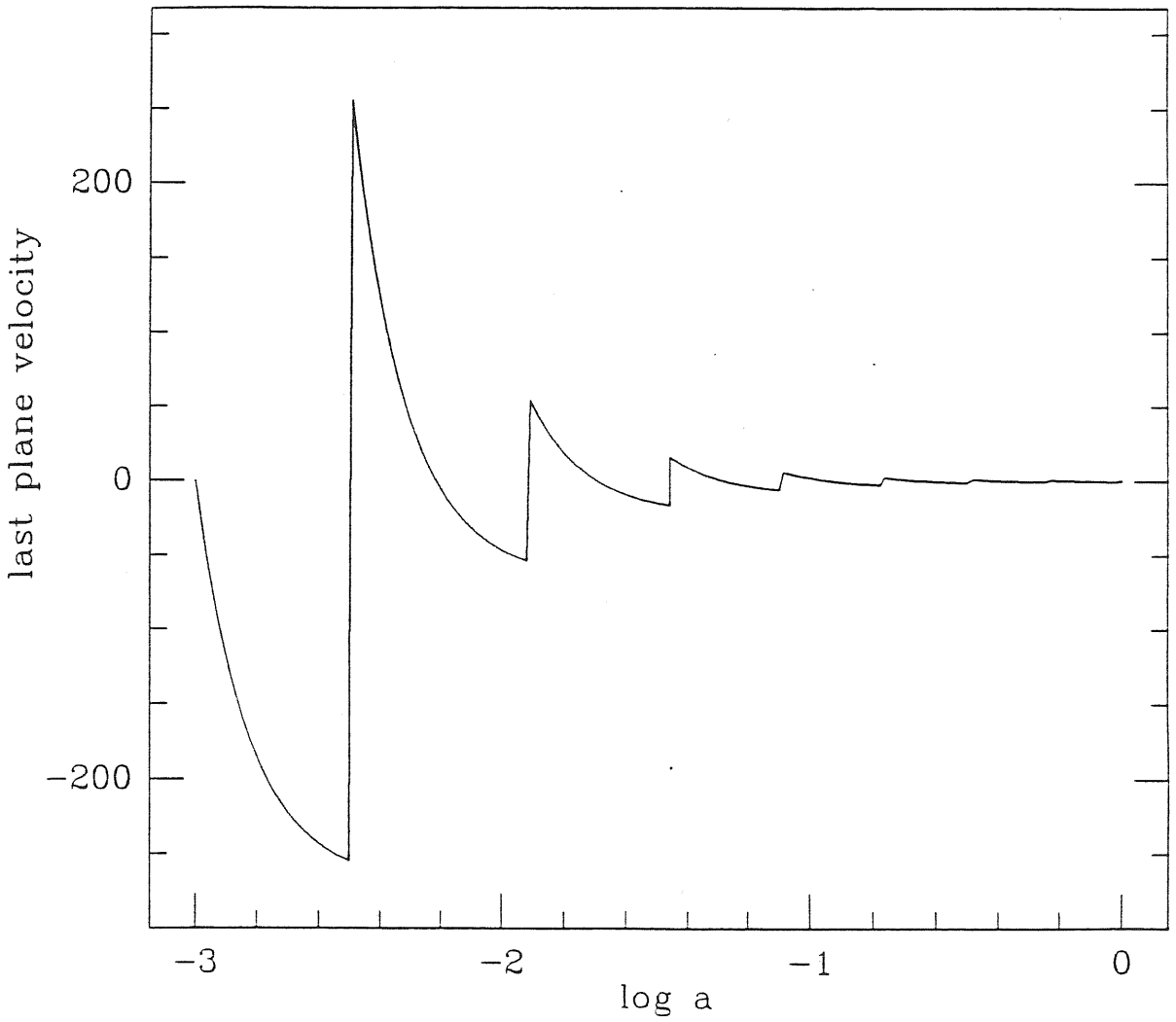


**Figure 2.** Analytic case: last plane velocity.

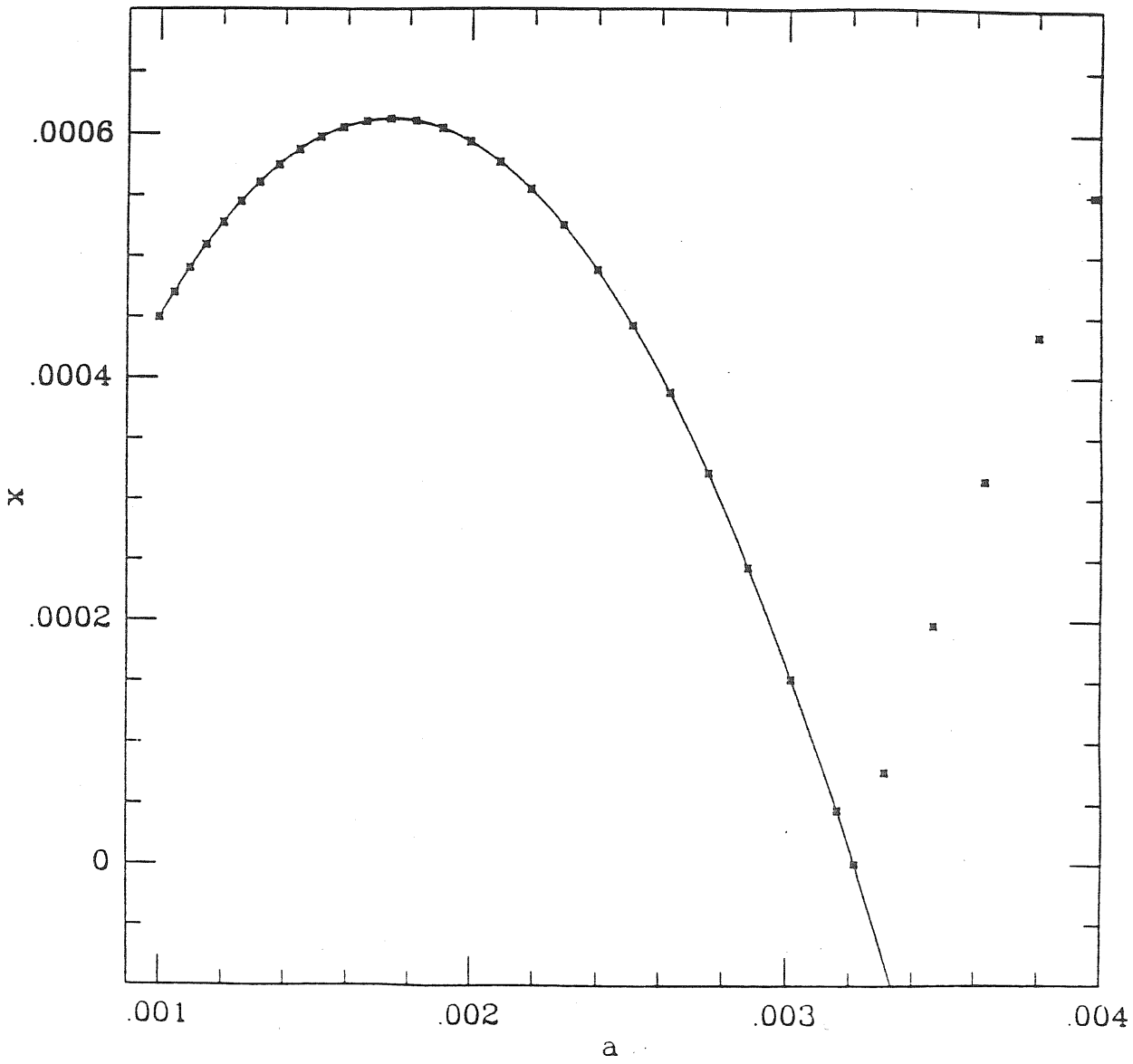


**Figure 3.** Analytic case: fit curve (solid line), last plane position (crosses).

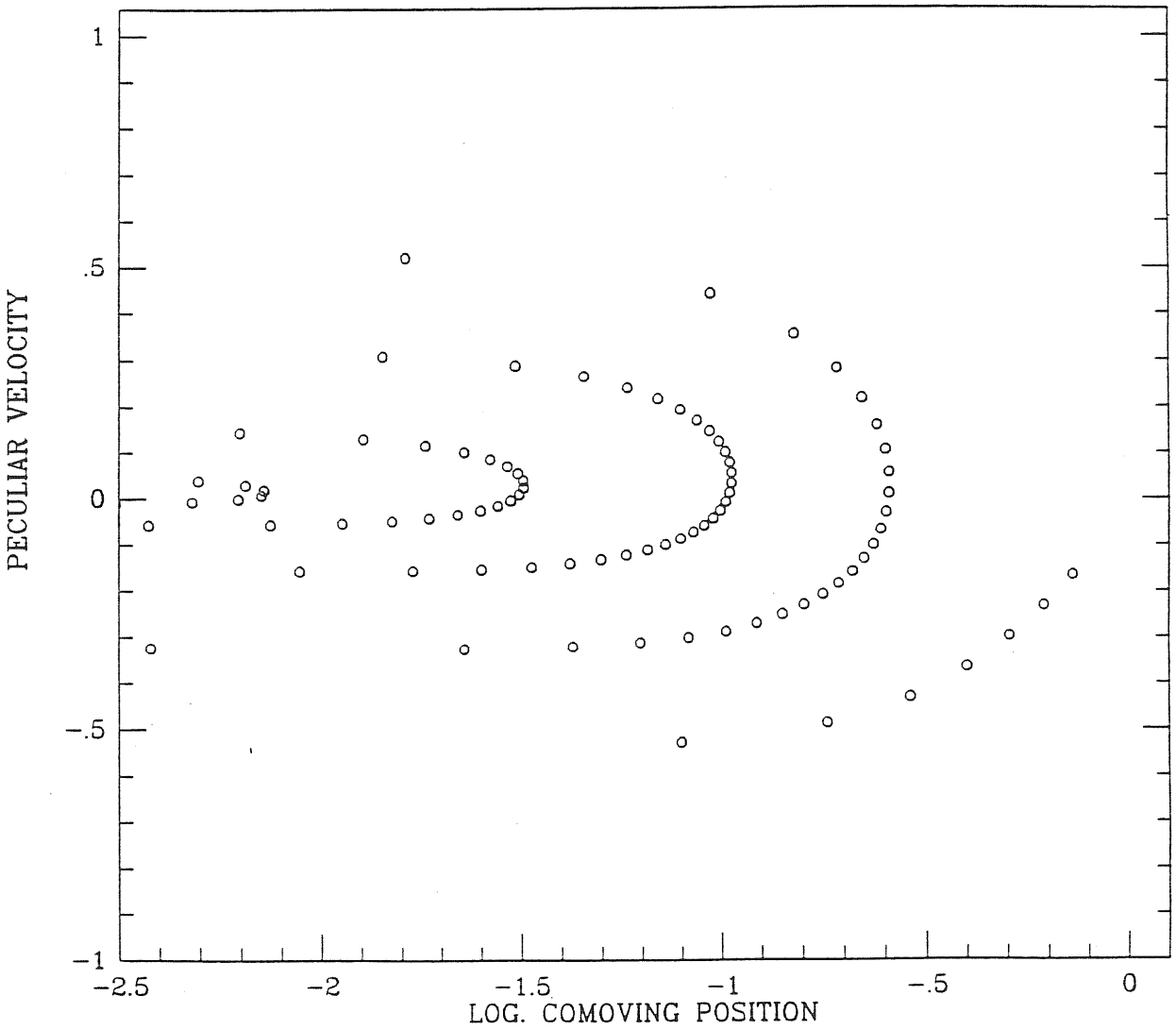


**Figure 4.** Canonical case: z=0 (final values); 100 planes.

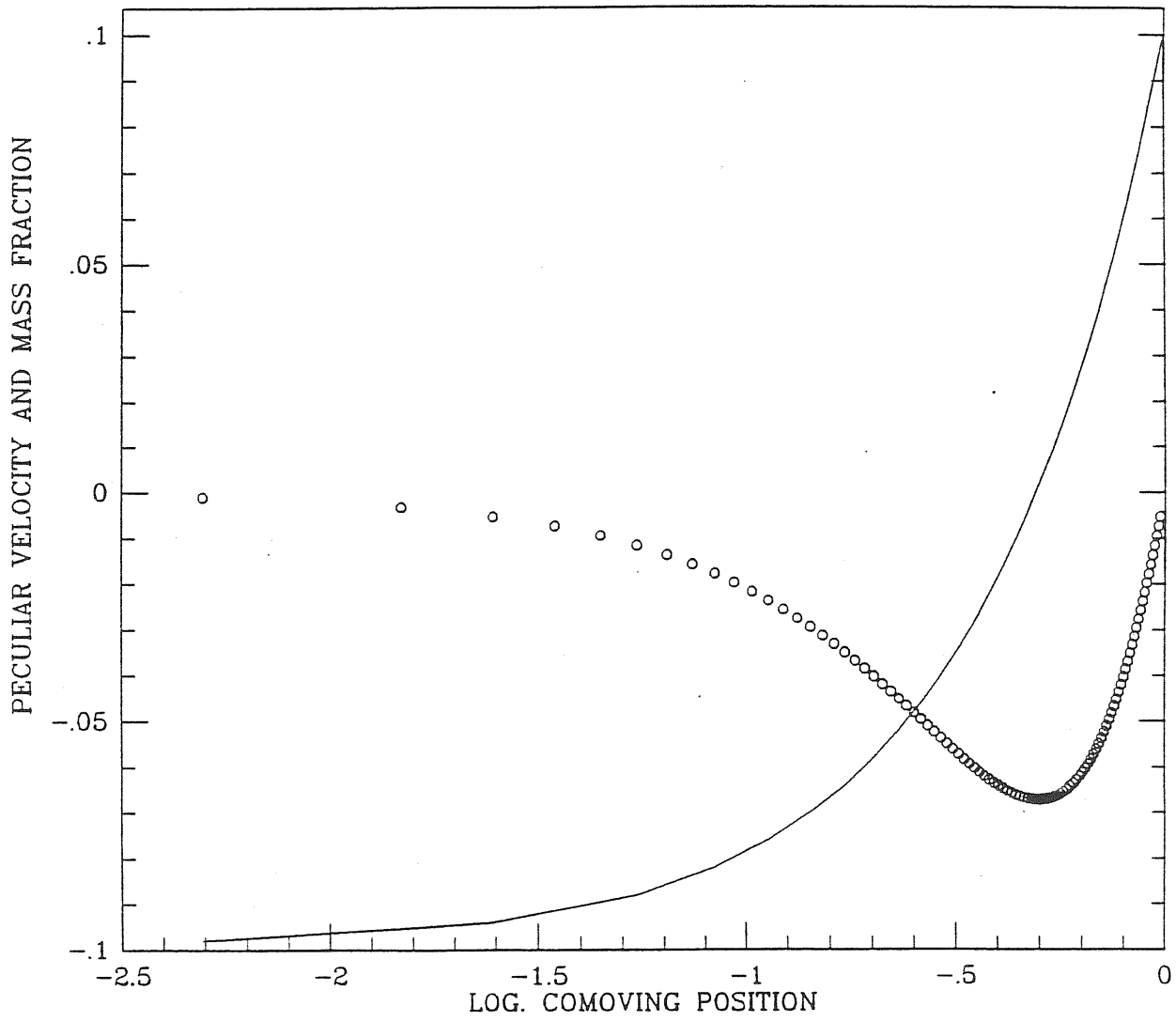


**Figure 5.** Canonical case: z=1000 (initial values); 100 planes.

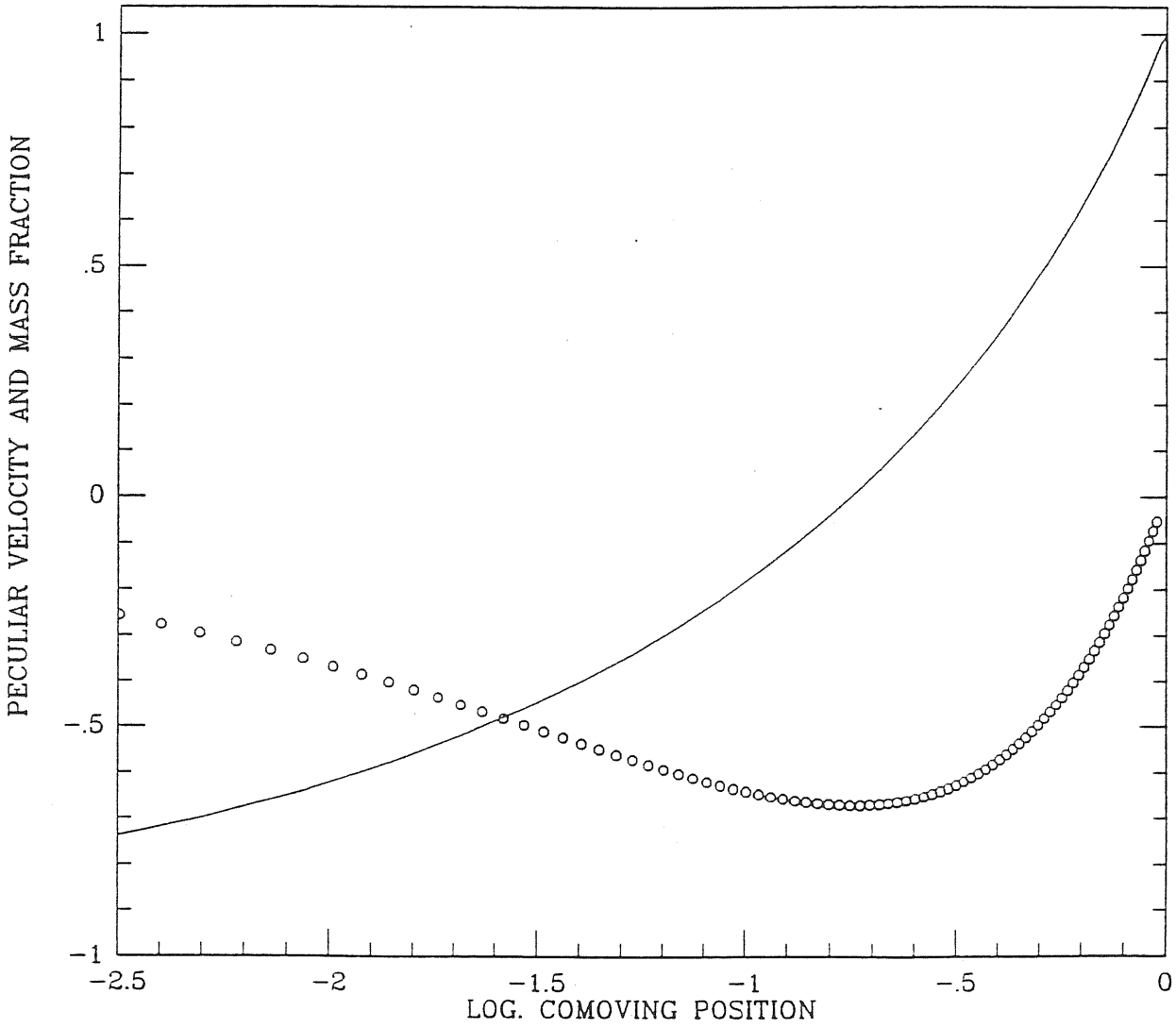


**Figure 6.** Canonical case: z=10; 100 planes.

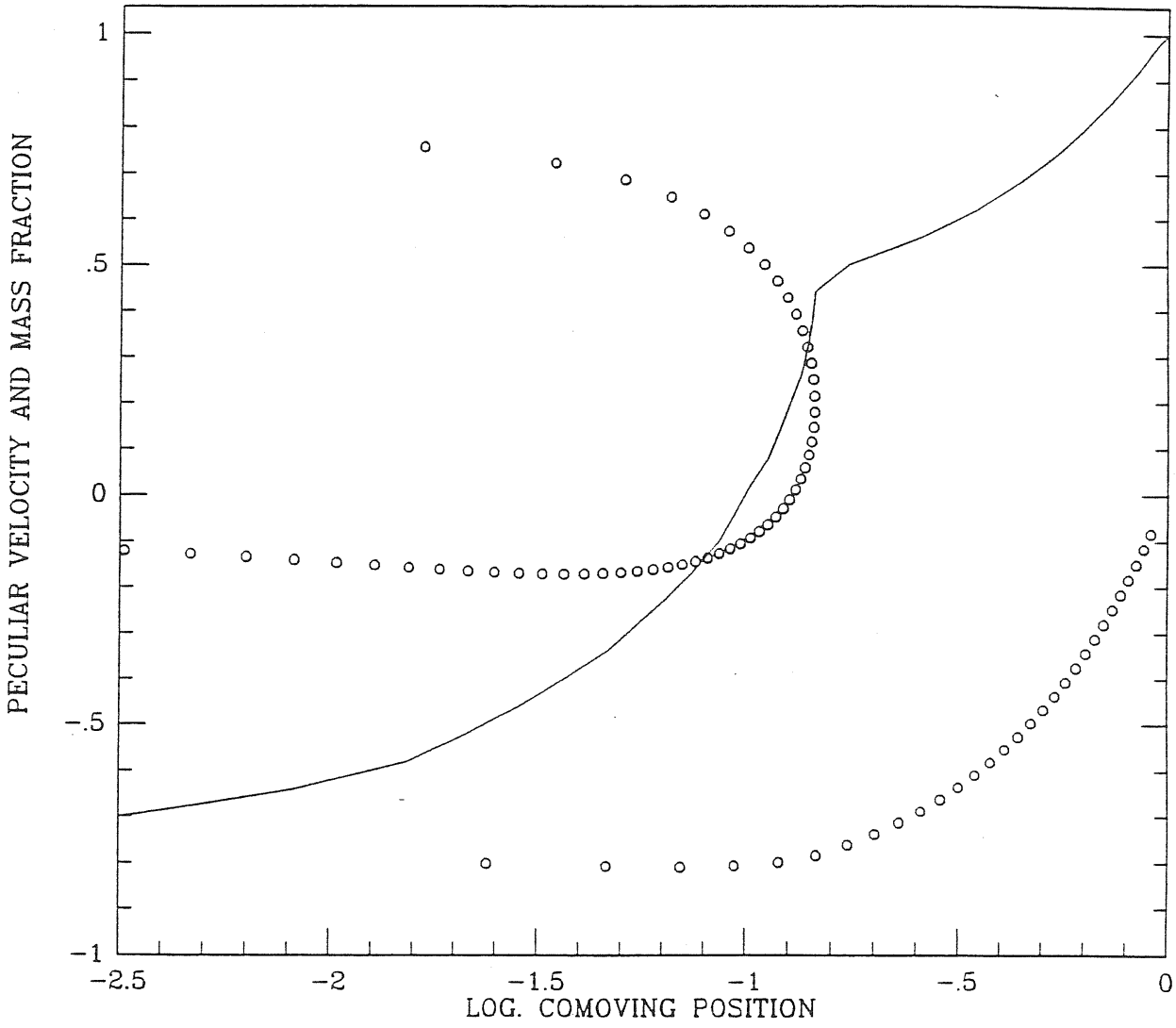


**Figure 7.** Canonical case: z=3; 100 planes.

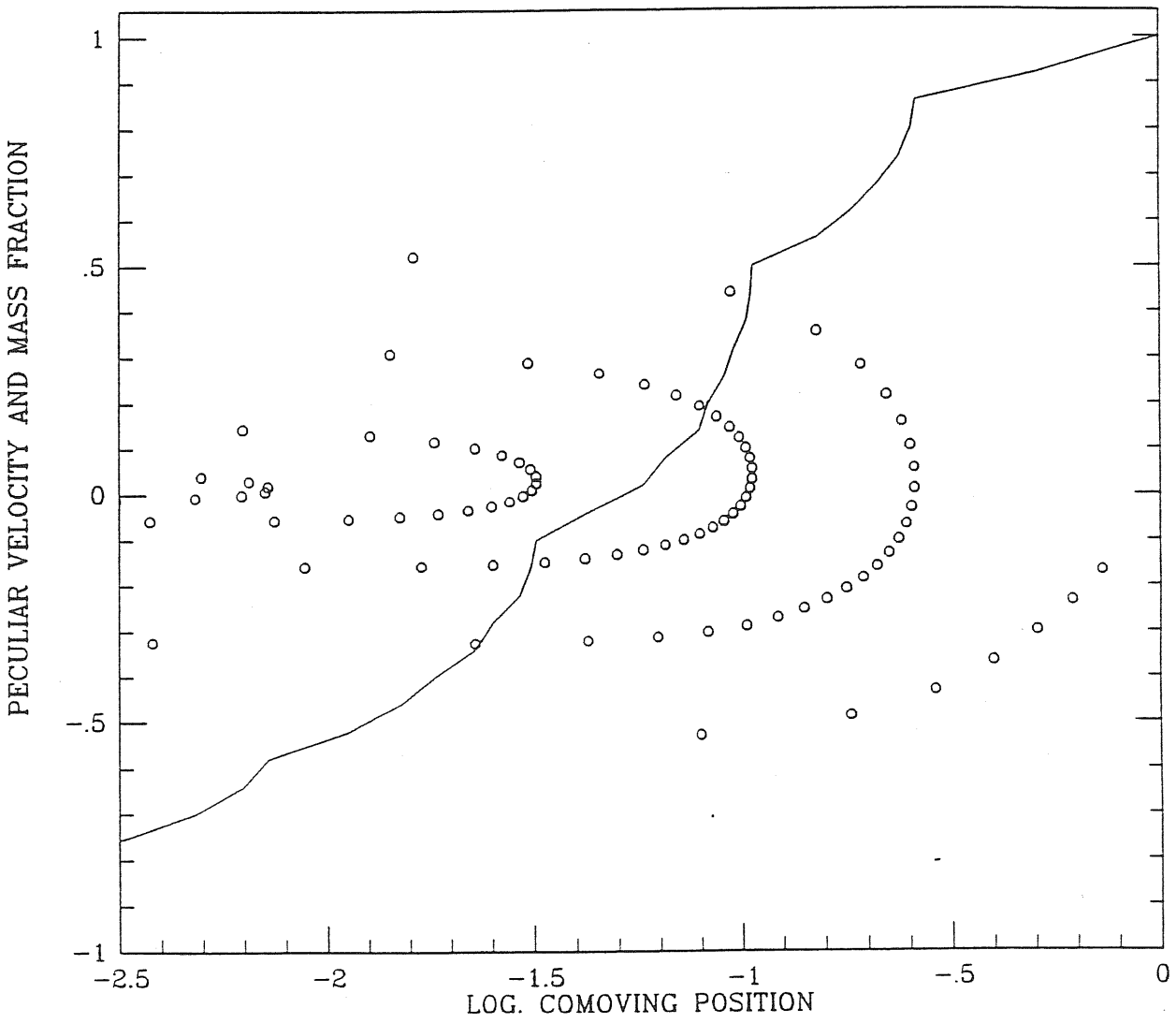


**Figure 8.** Canonical case: z=0; 100 planes.

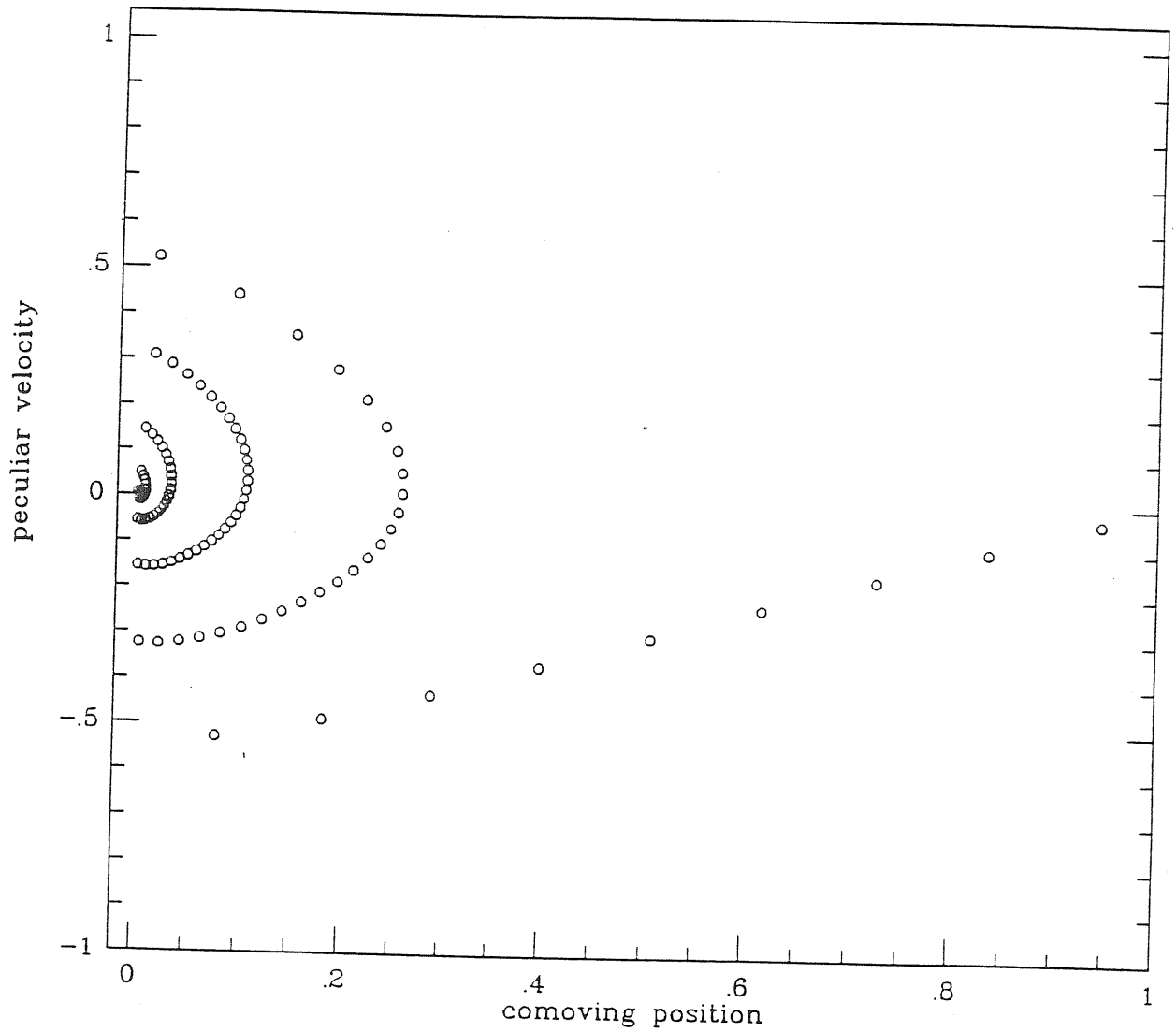


**Figure 9.** Canonical case: z=0; 100 planes.

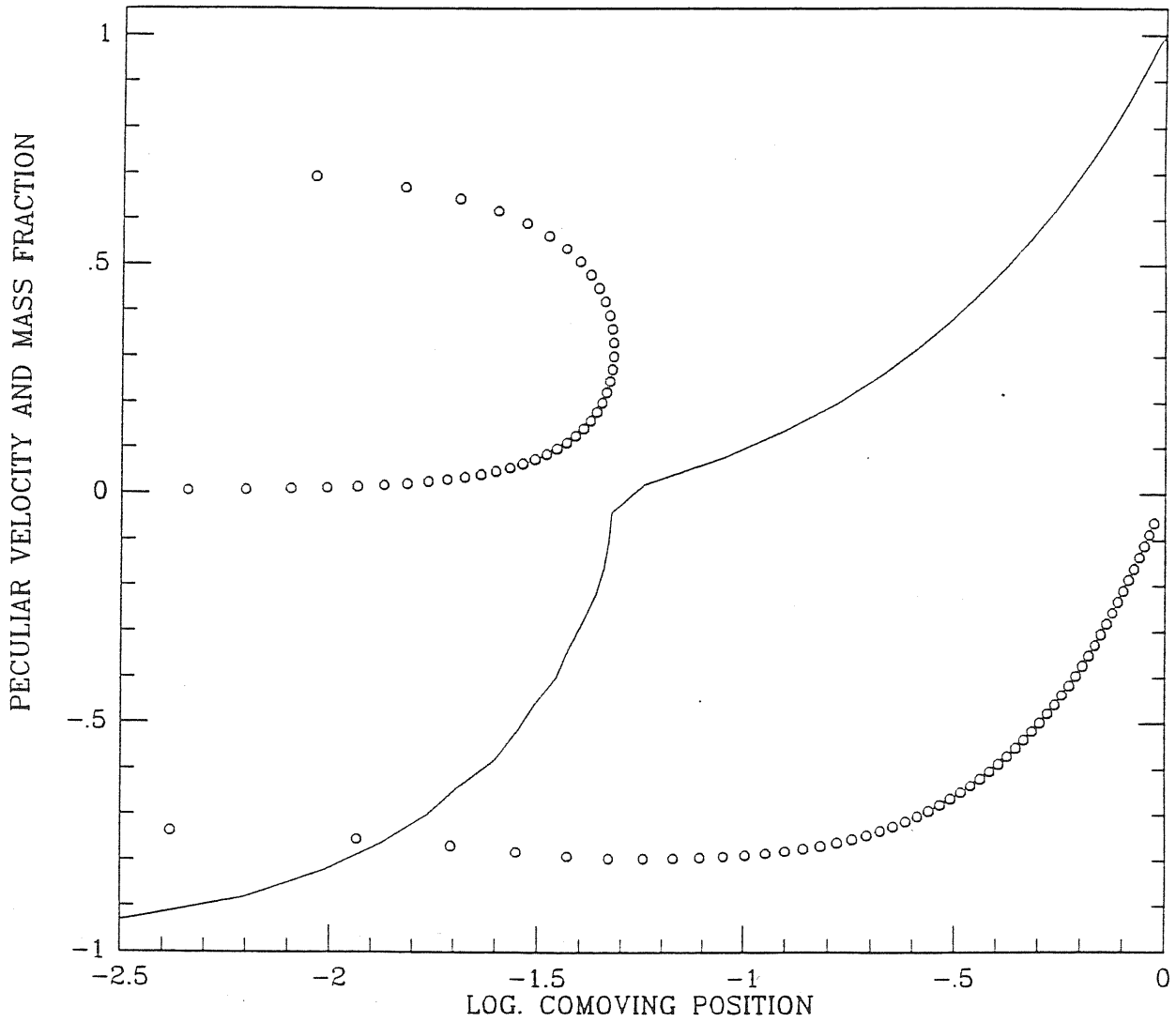


**Figure 10.** Canonical case: z=6; 100 planes.

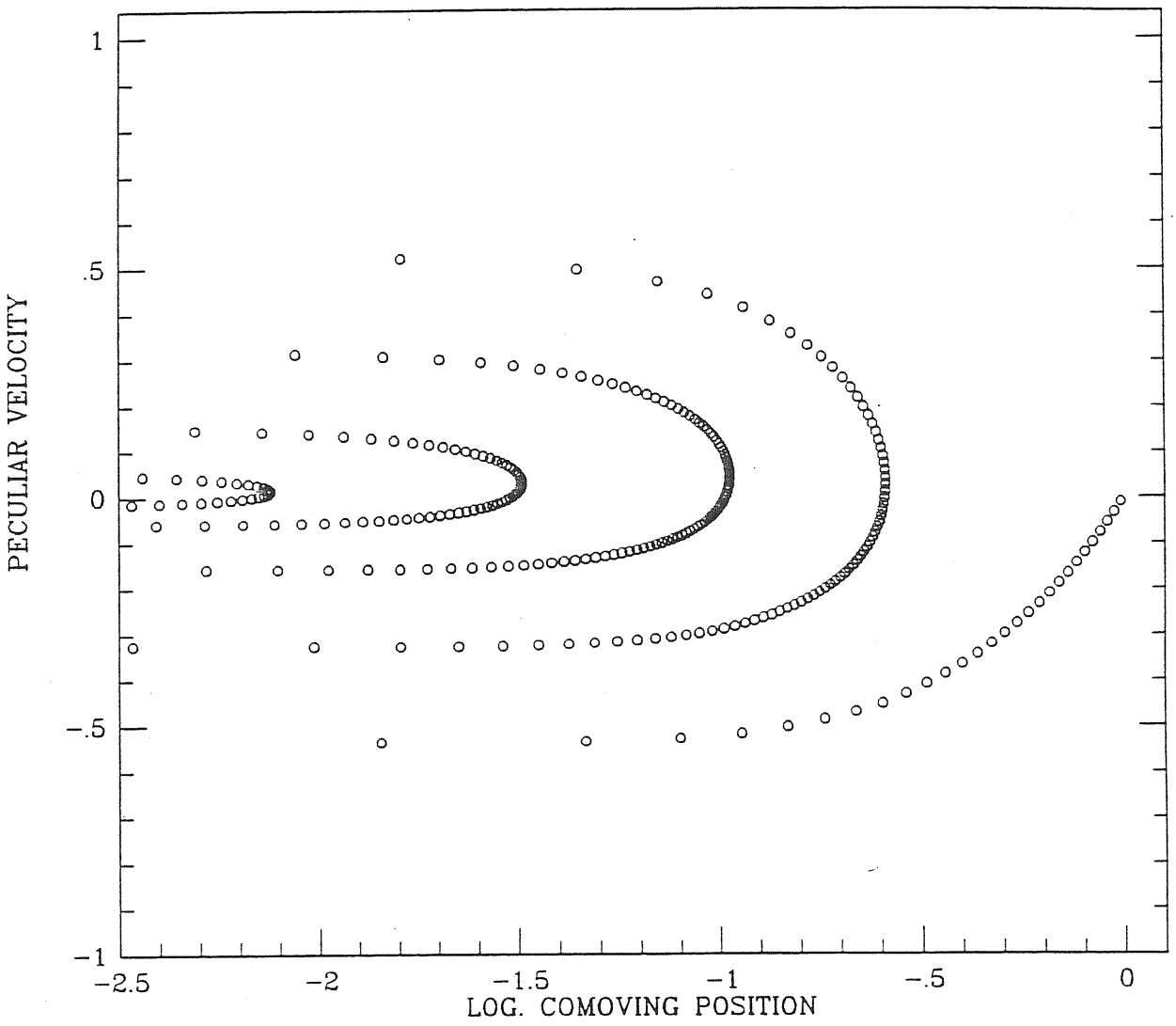


**Figure 11.** Canonical case: z=0; 300 planes.

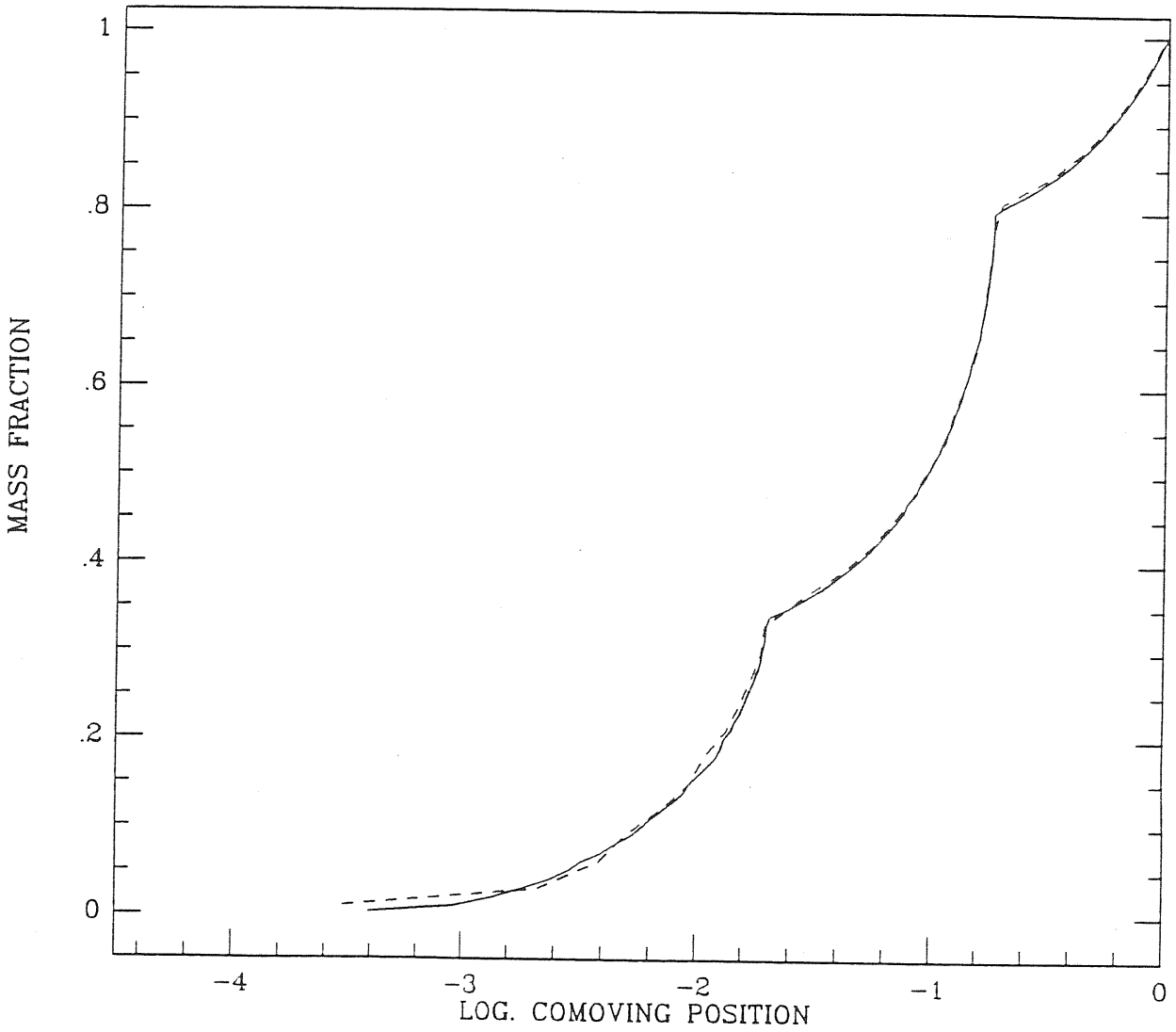


**Figure 12.** Canonical case: z=2; 300 planes solid line, 100 planes dashed line.

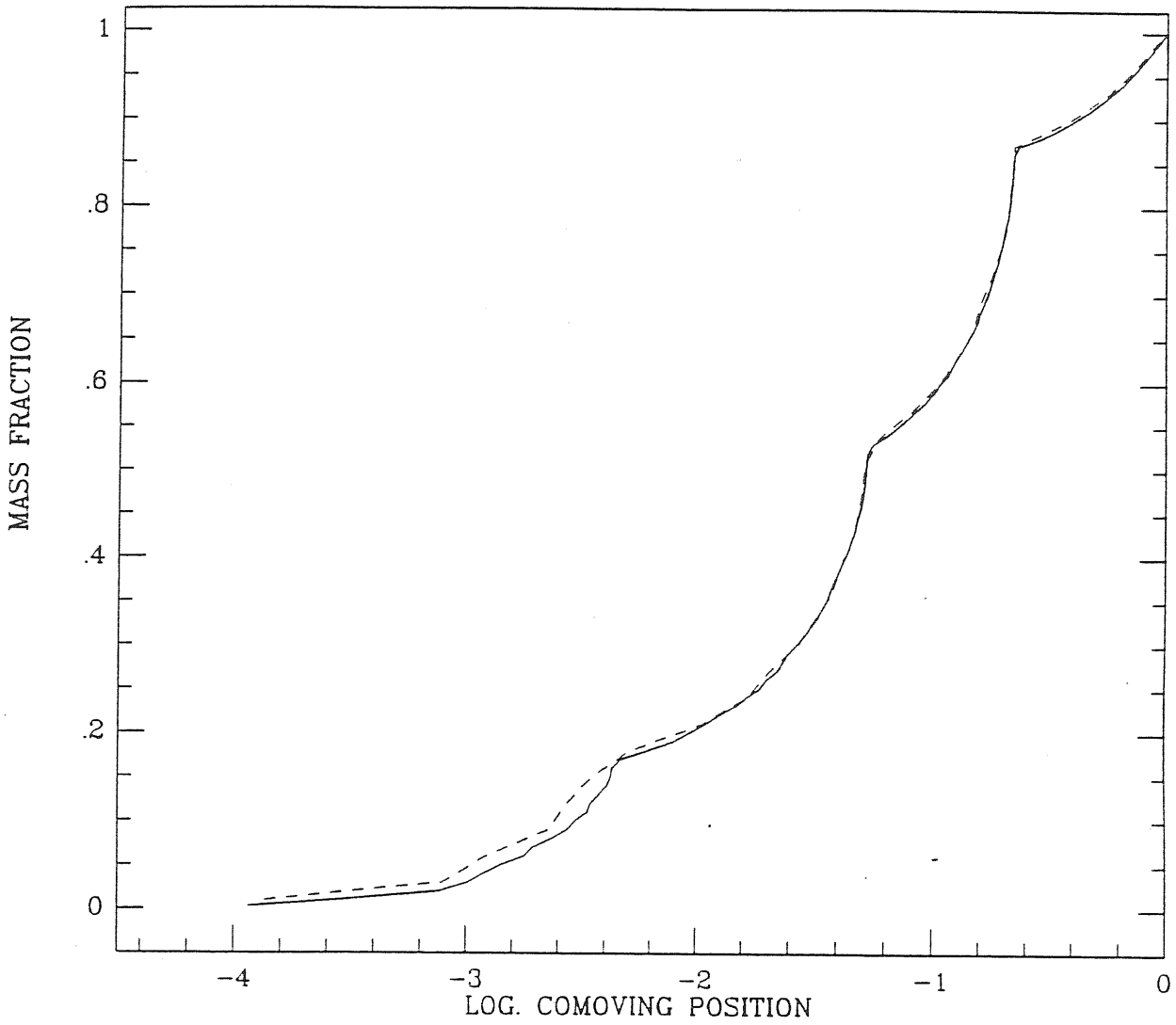


**Figure 13.** Canonical case: z=1; 300 planes solid line, 100 planes dashed line.

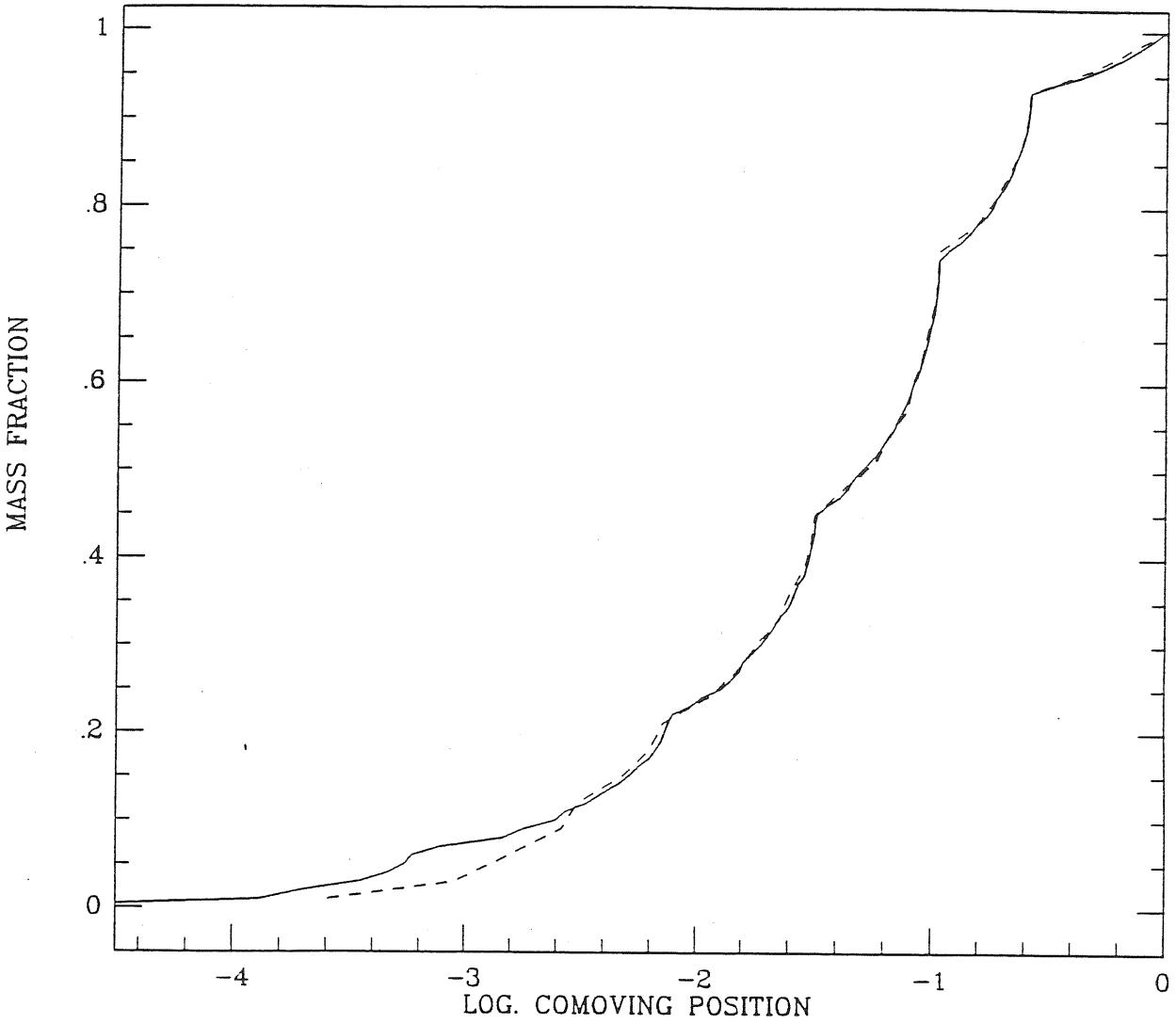


**Figure 14.** Canonical case: z=0; 300 planes solid line, 100 planes dashed line.

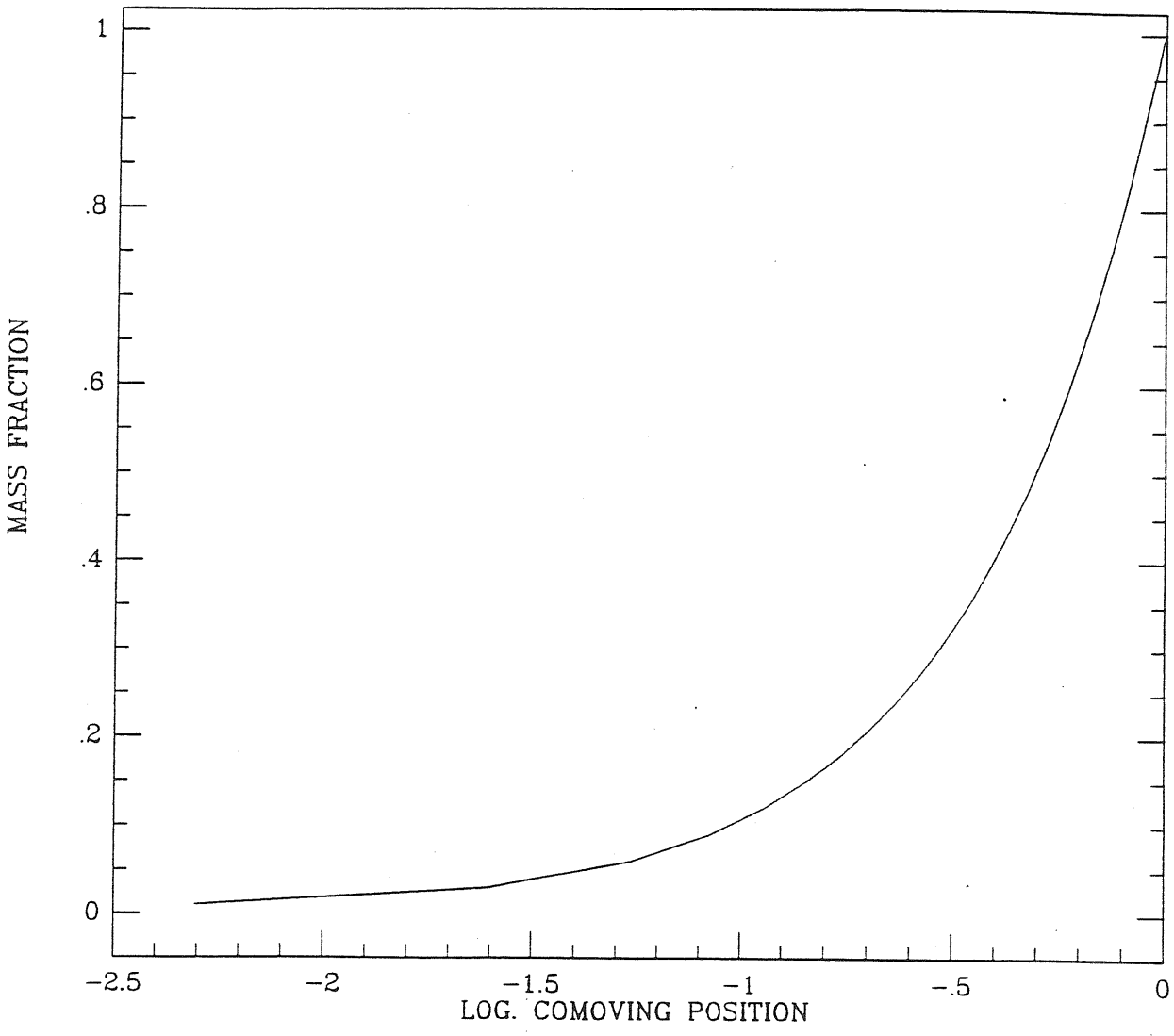


**Figure 15.** Cold case: z=1000.

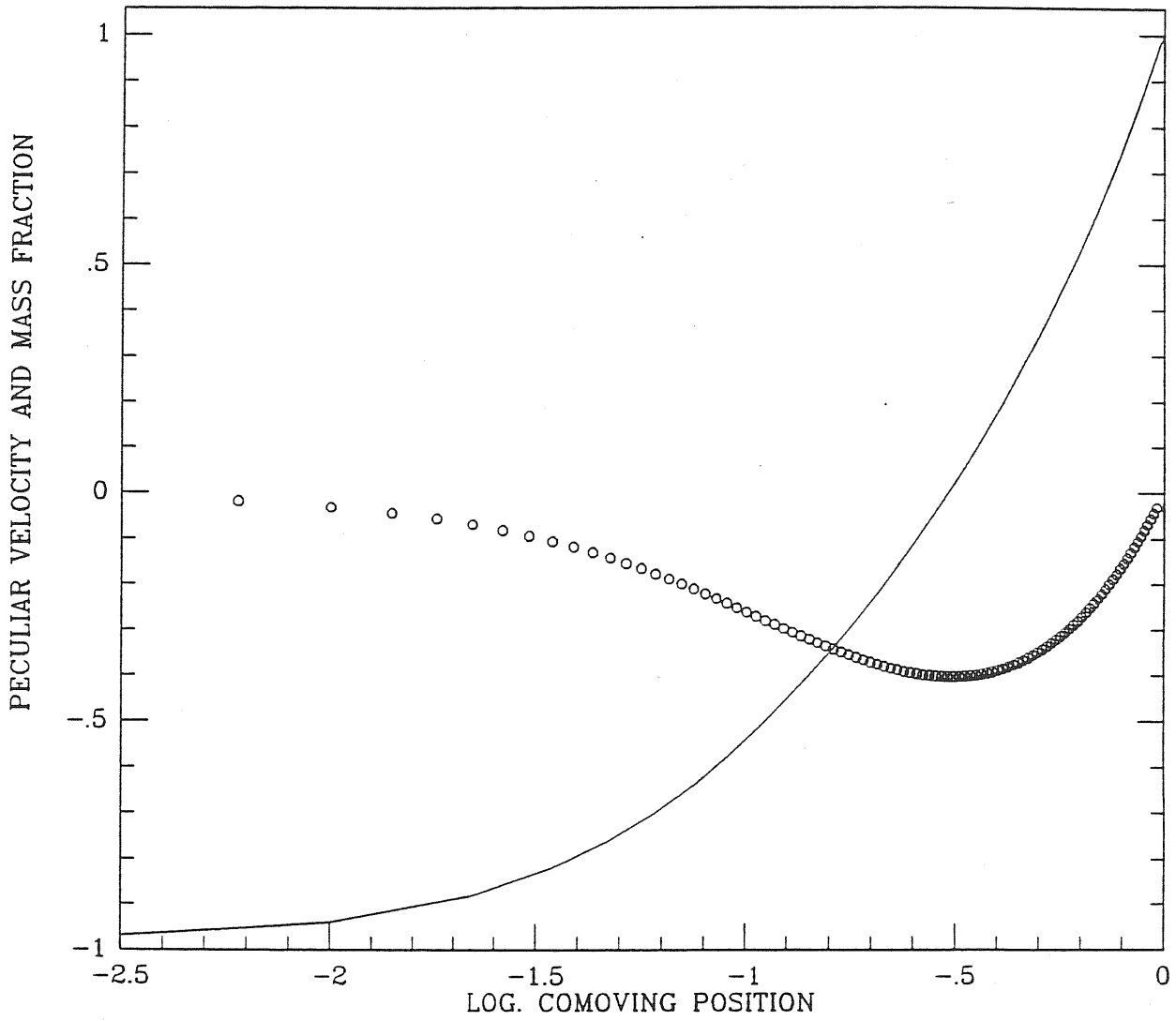


**Figure 16.** Cold case: z=10.

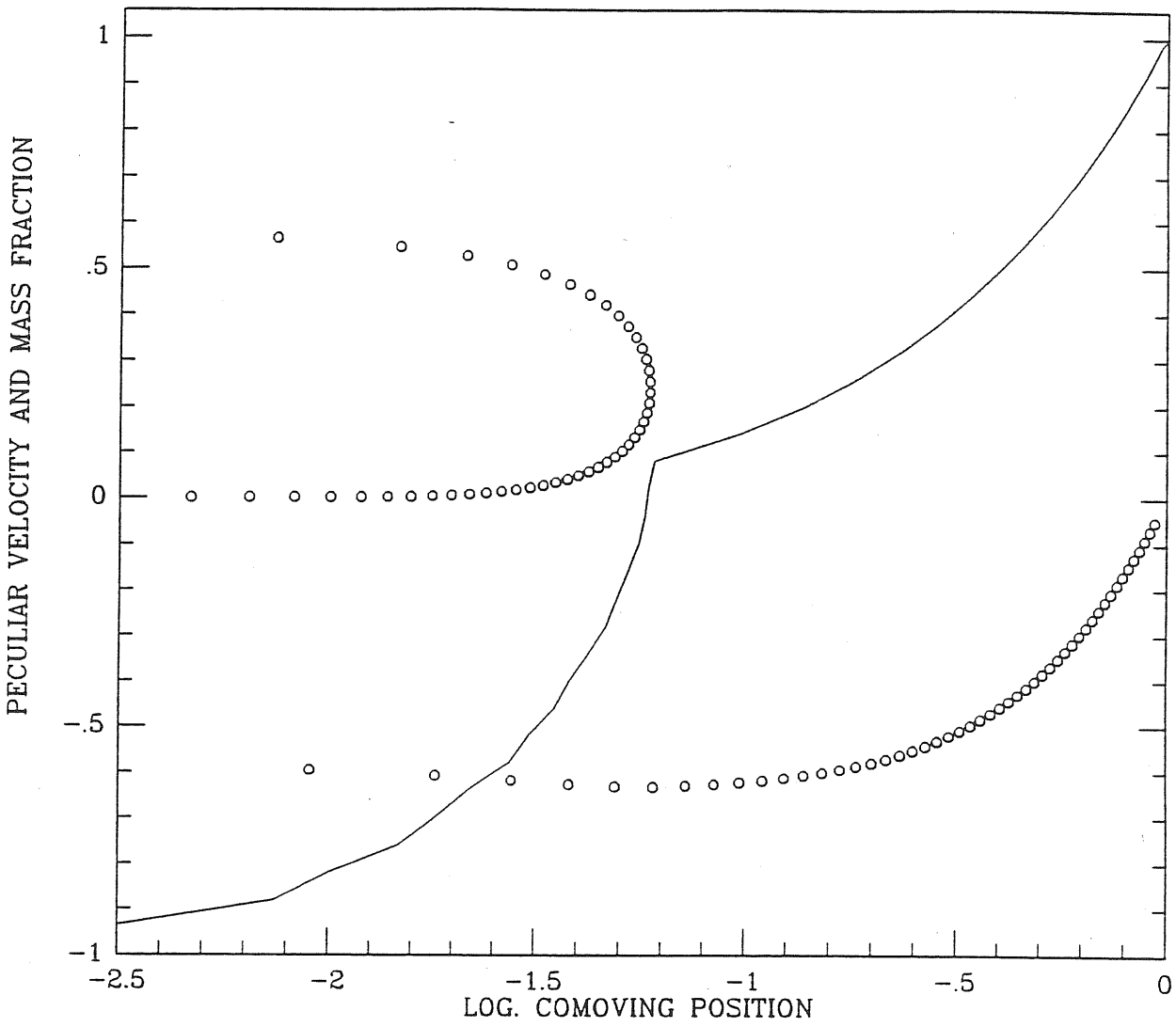


**Figure 17.** Cold case: z=3.

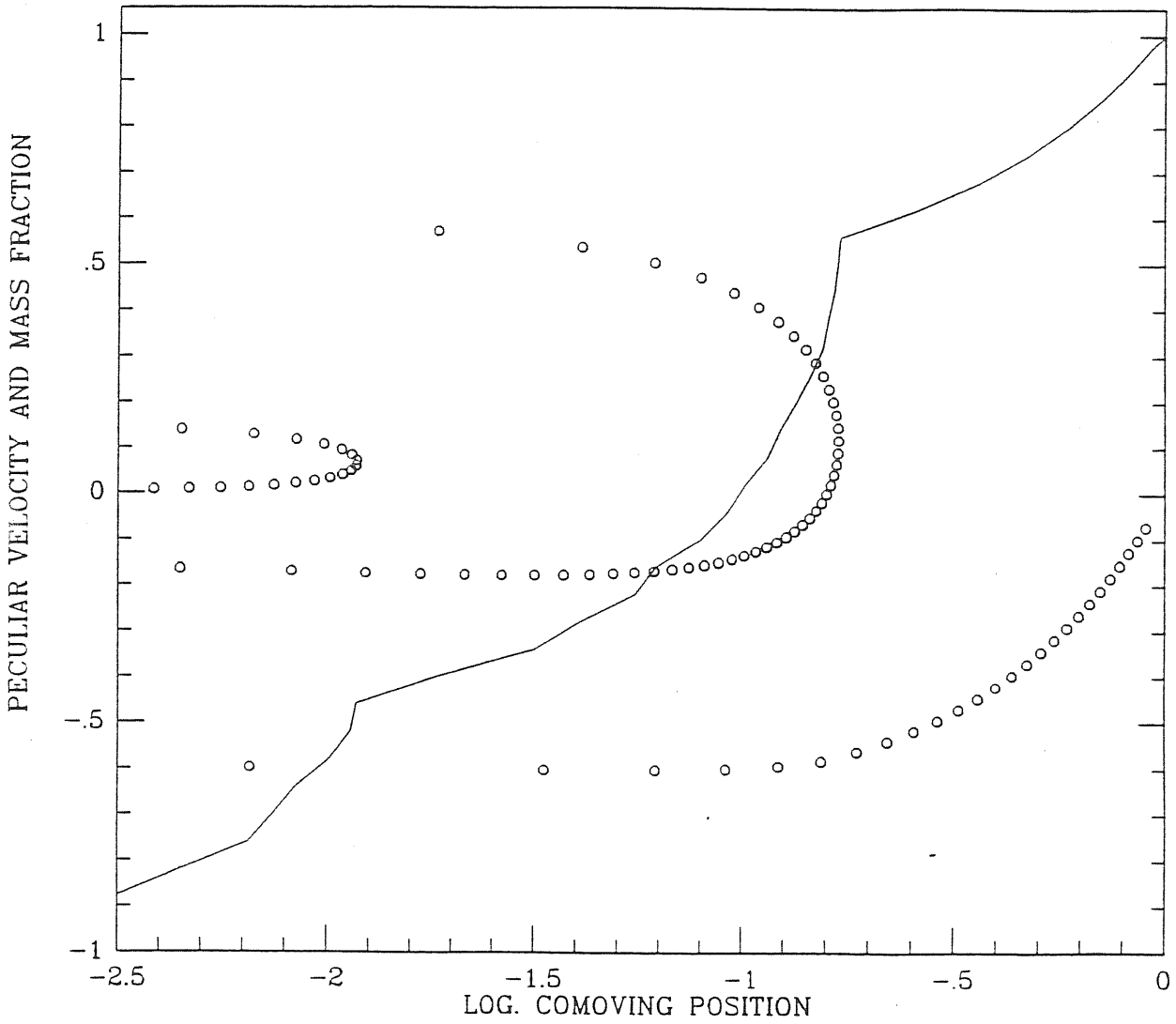


**Figure 18.** Cold case: z=1.

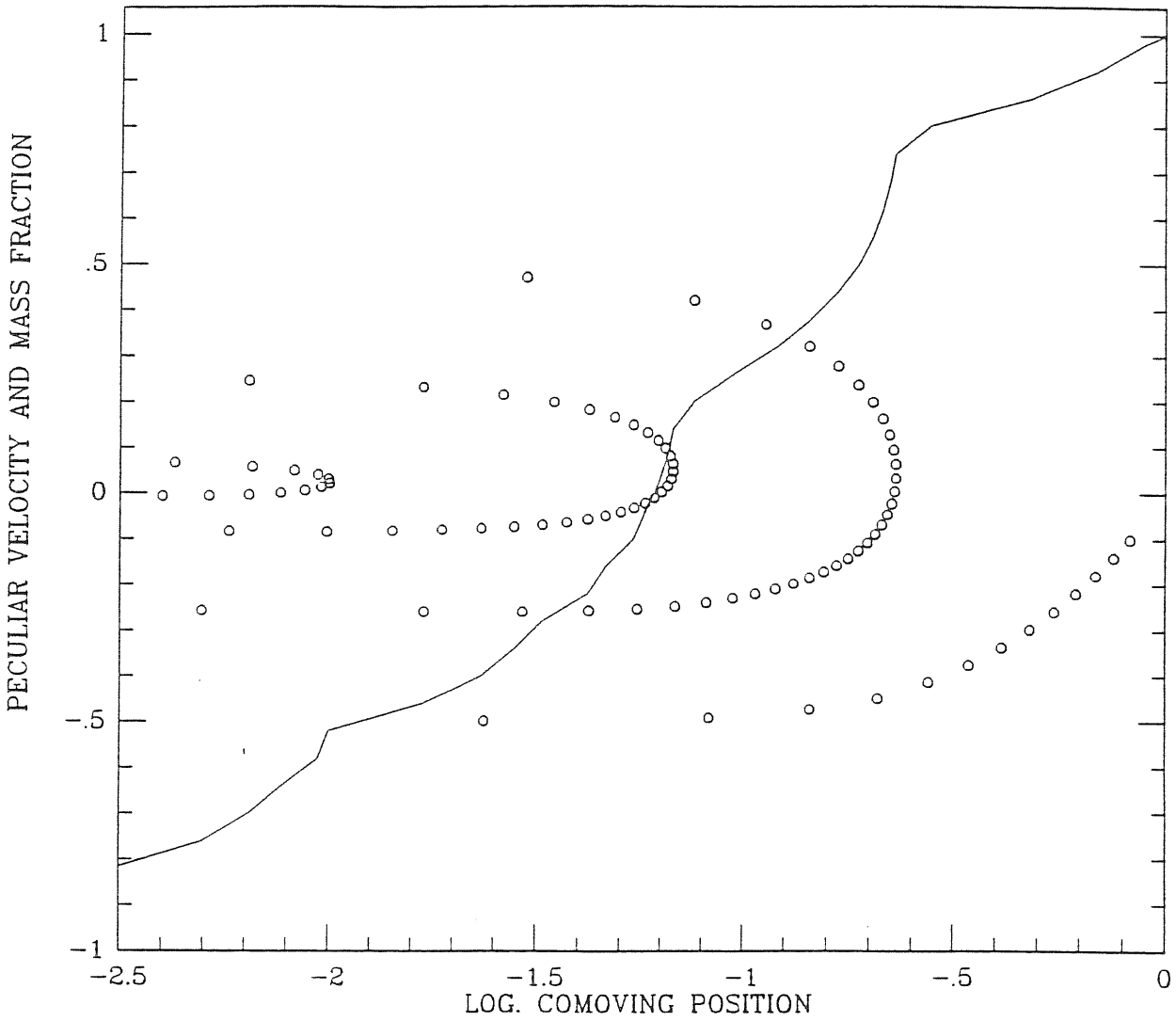


**Figure 19.** Cold case: z=0.

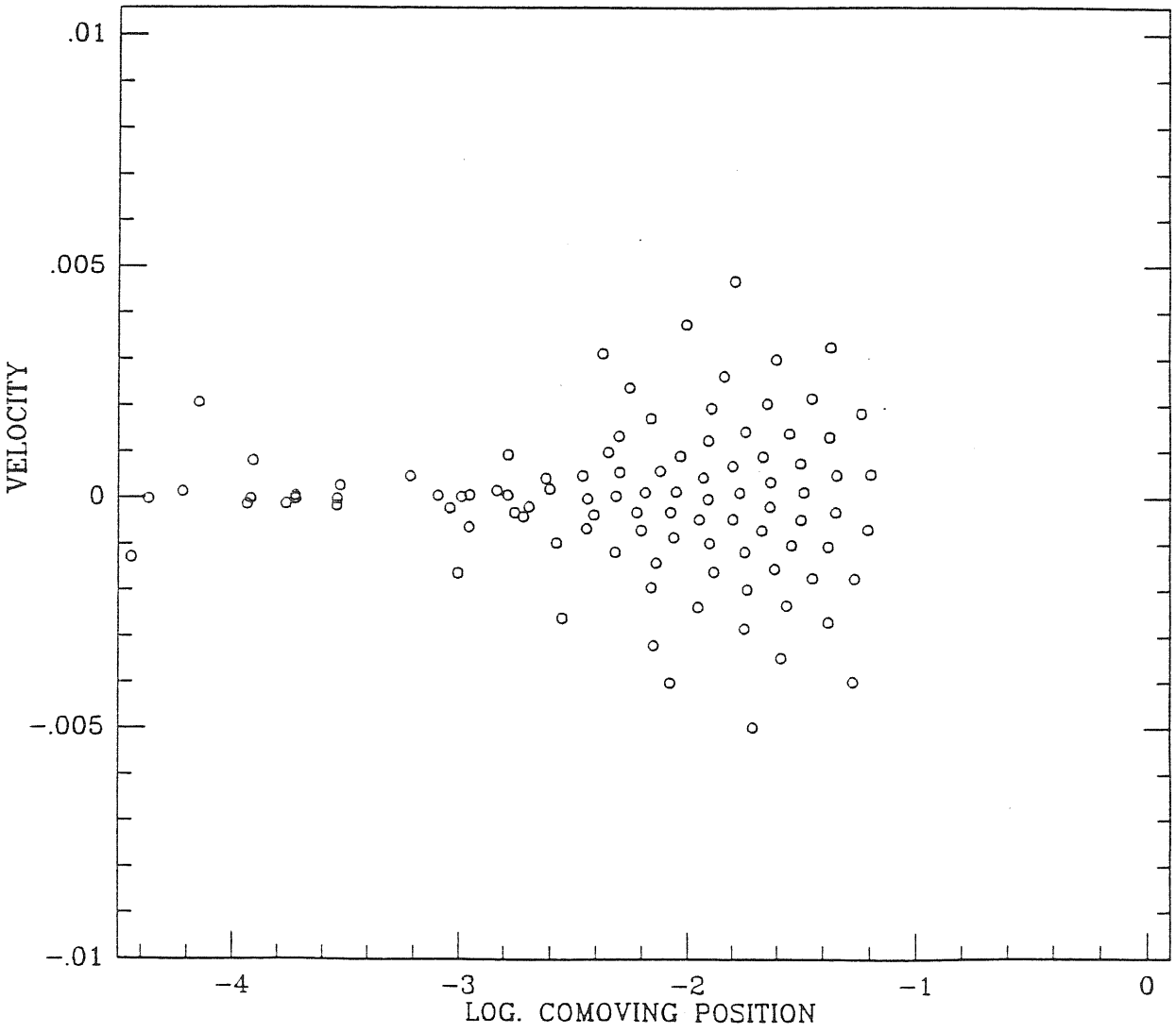


**Figure 20.** Cold case: a=70.

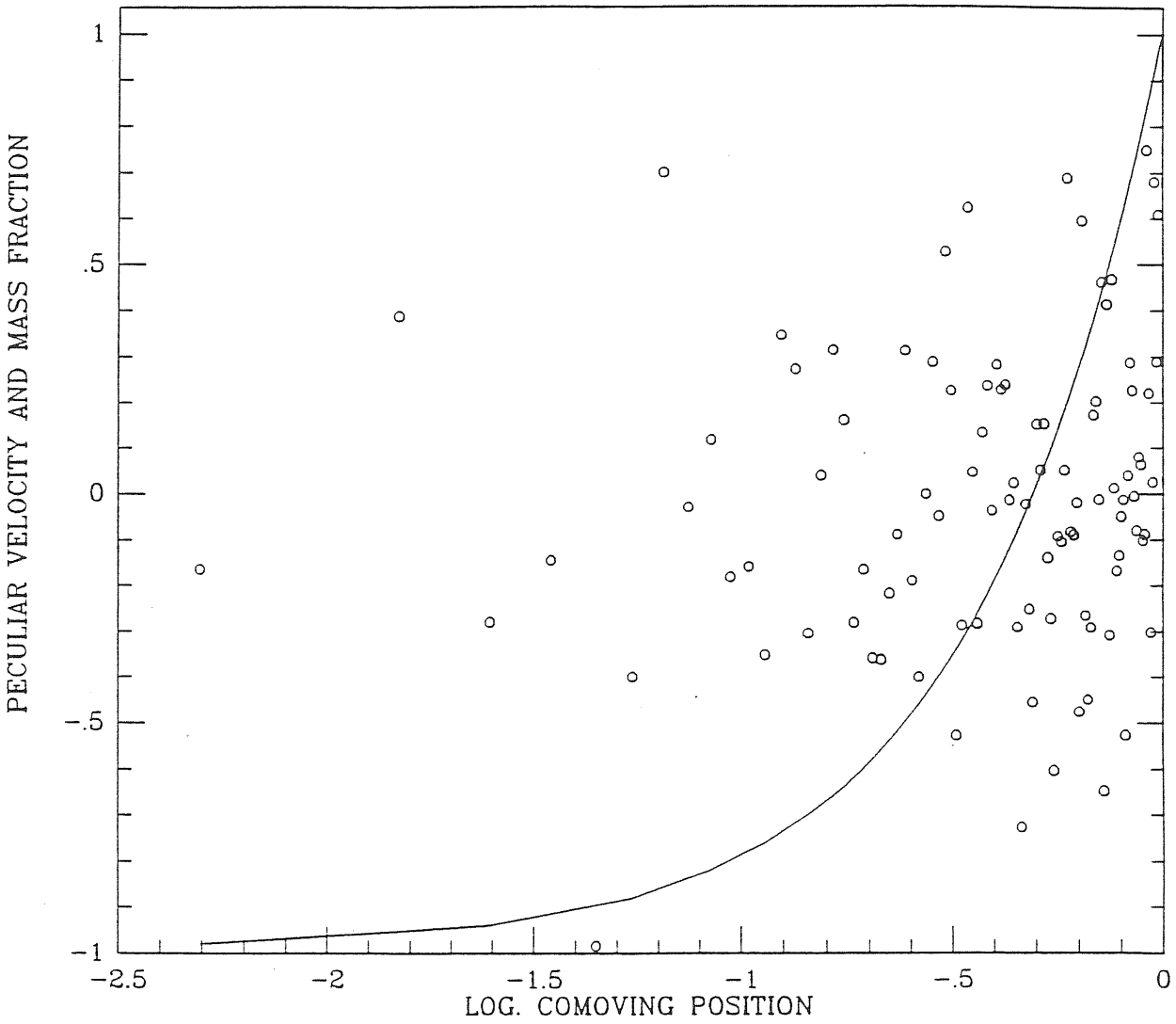


**Figure 21.** Case a: z=1000.

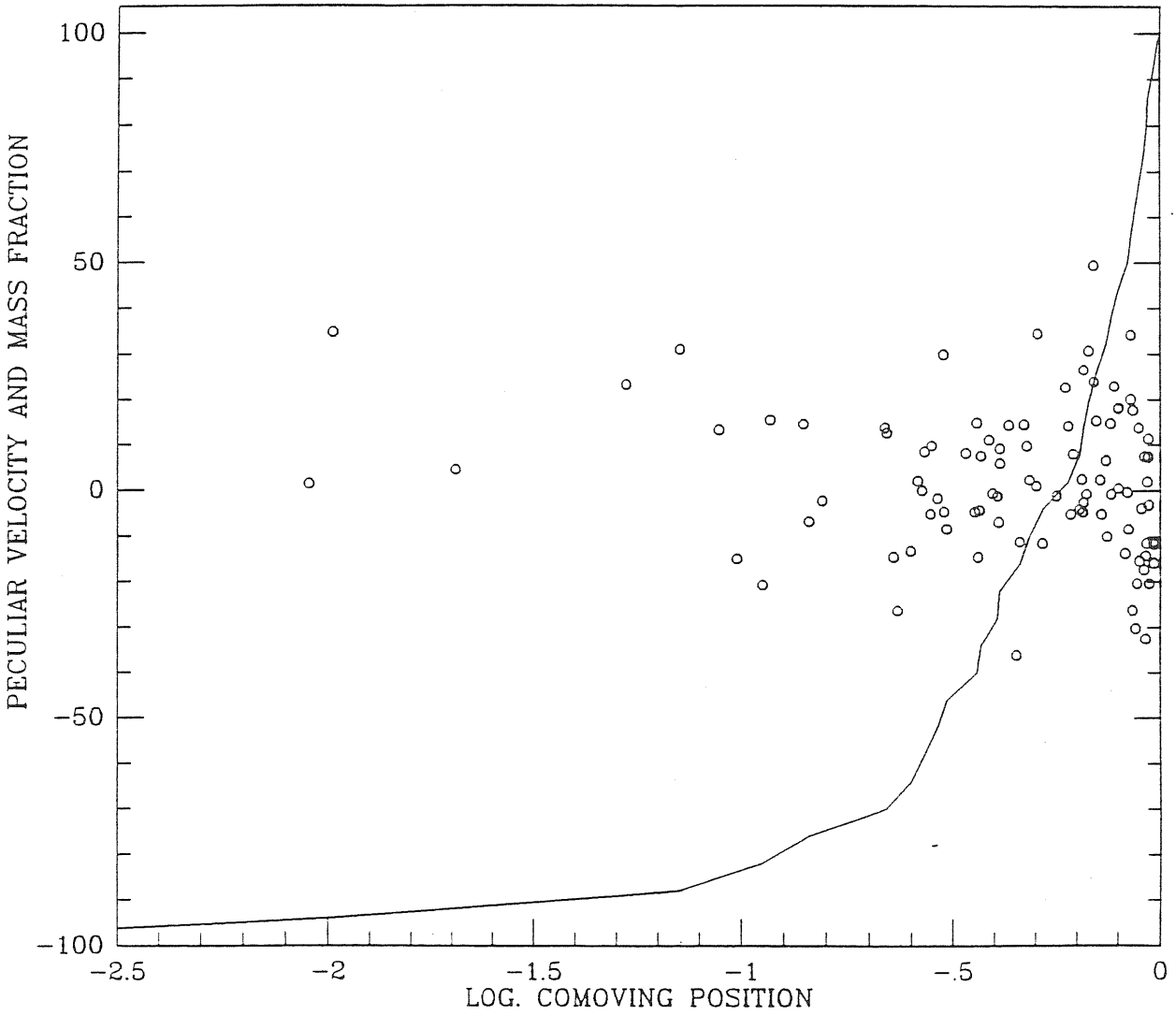


**Figure 22.** Case a: z=500; $\mathcal{F} = 1$.

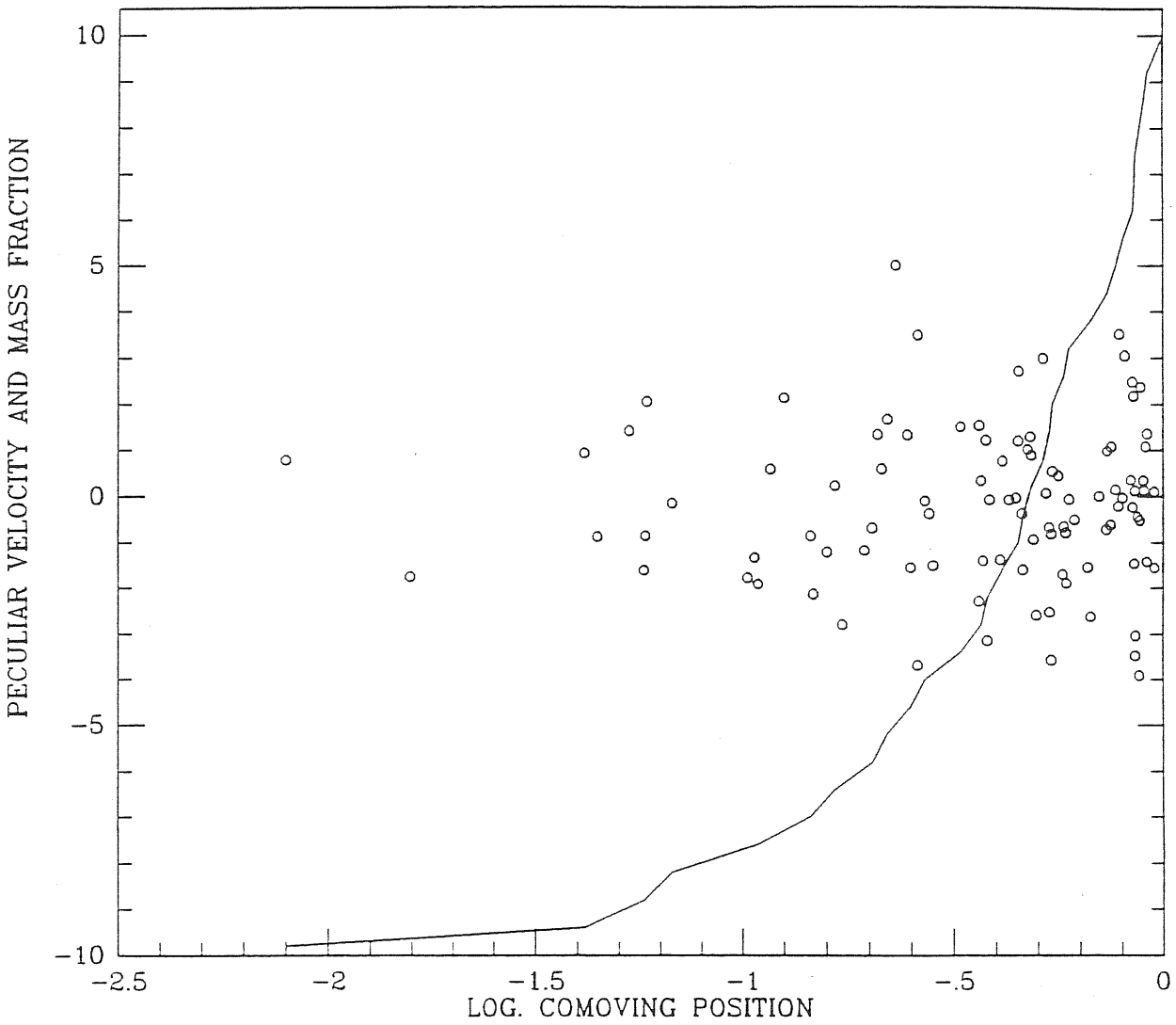


**Figure 23.** Case a: z=500; $\mathcal{F} = 10^{-1}$.

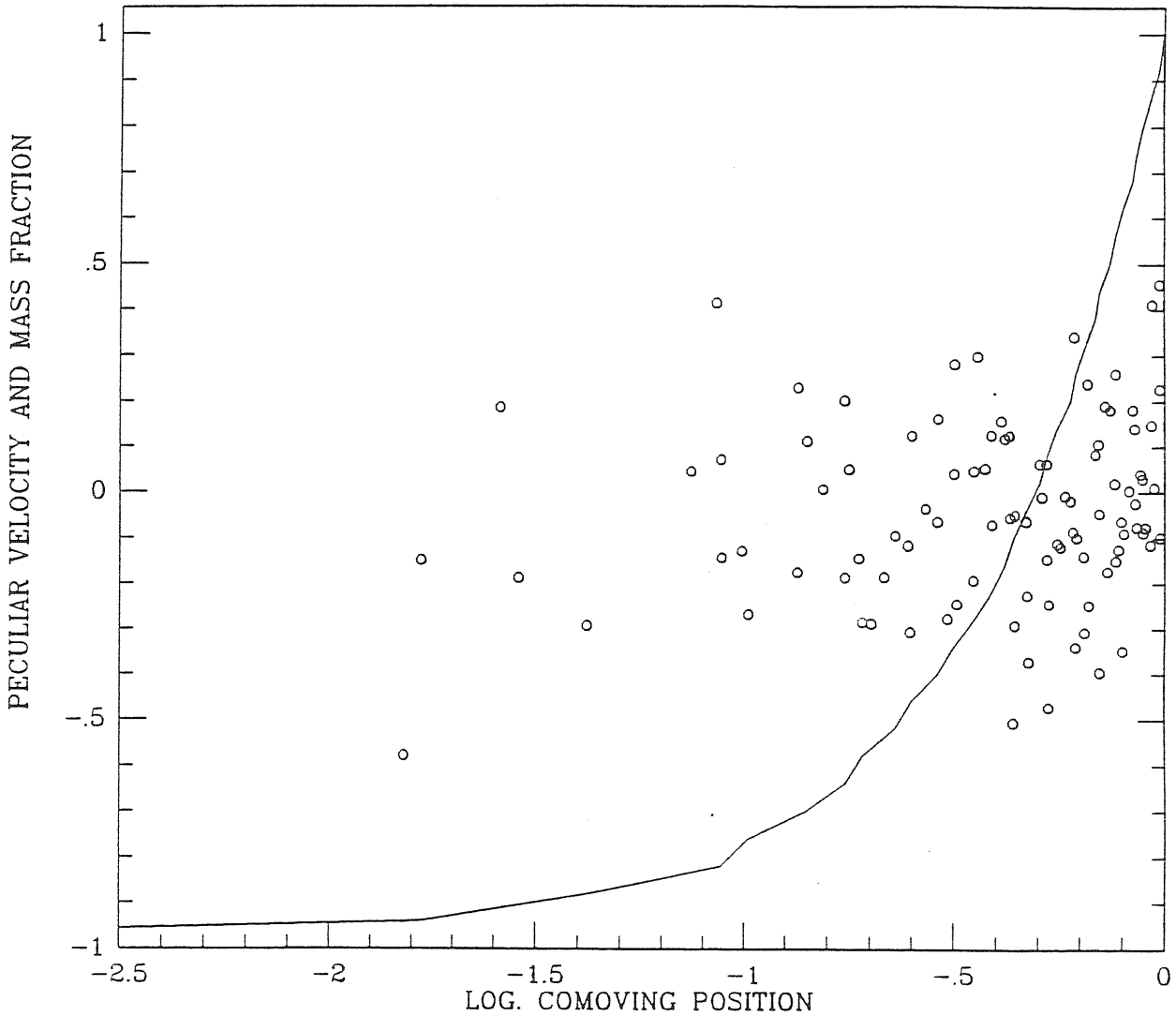


**Figure 24.** Case a: z=500; $\mathcal{F} = 10^{-2}$.

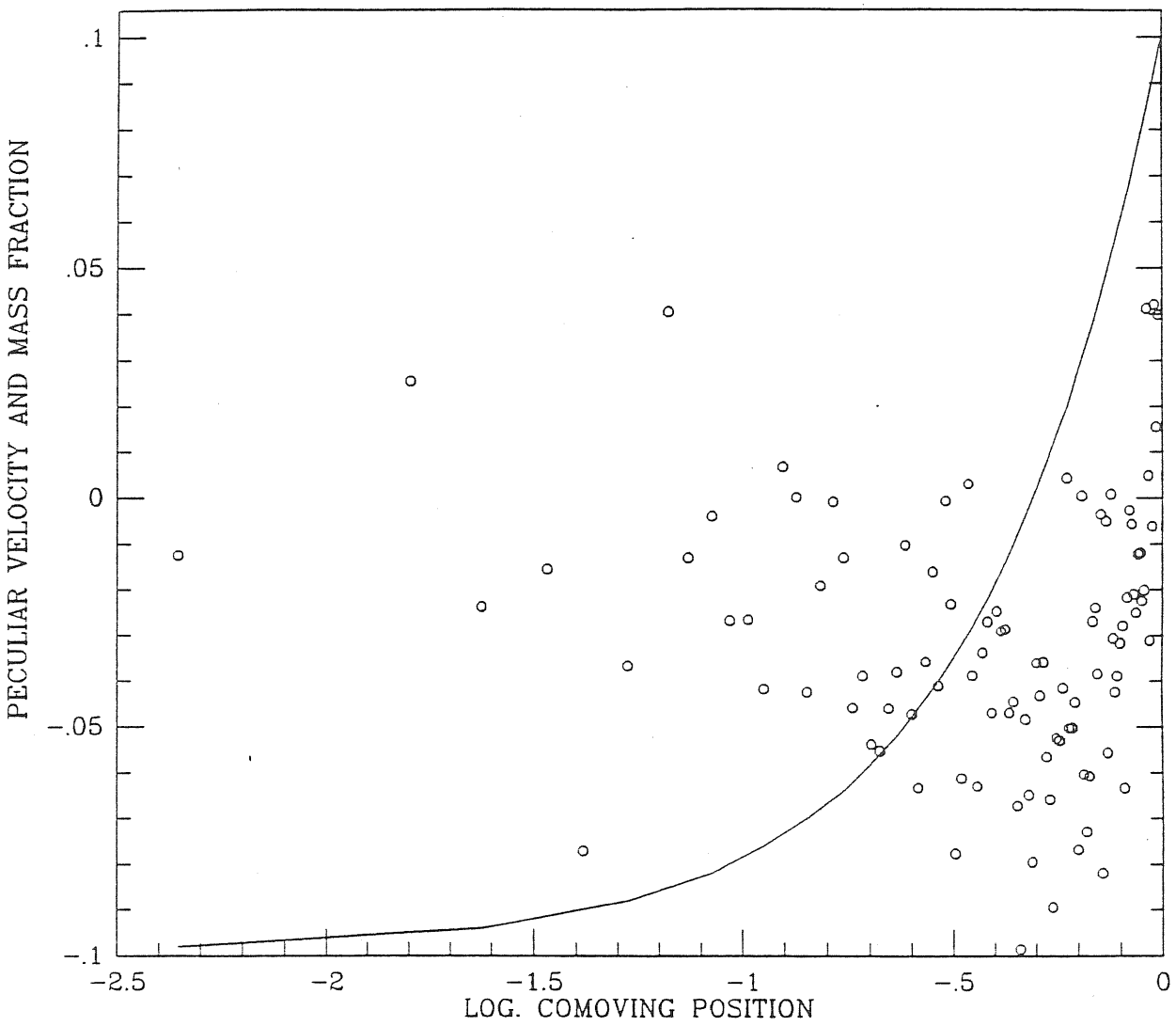


**Figure 25.** Case a: z=500; $\mathcal{F} = 10^{-3}$.

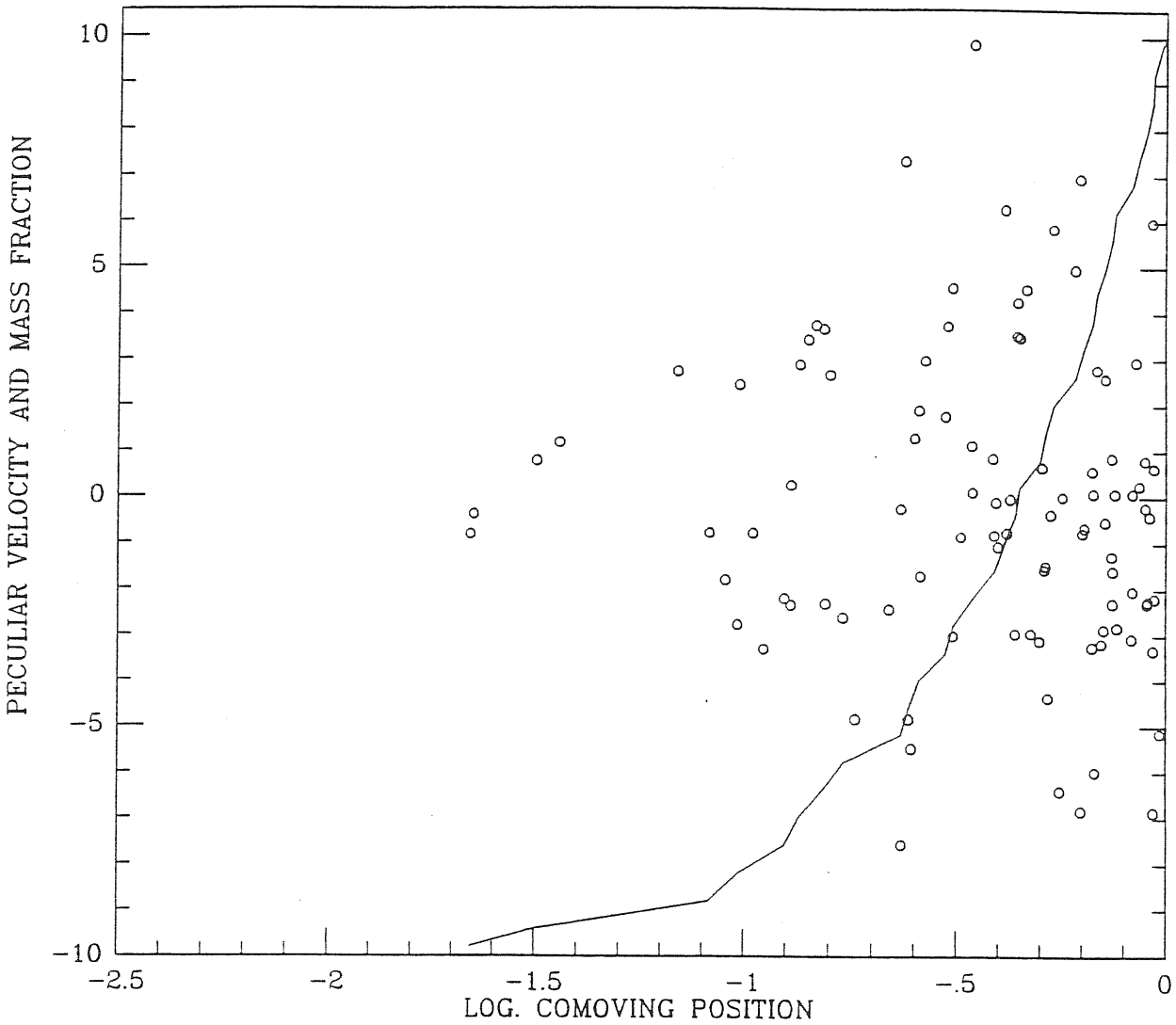


**Figure 26.** Case a: z=100; $\mathcal{F} = 1$.

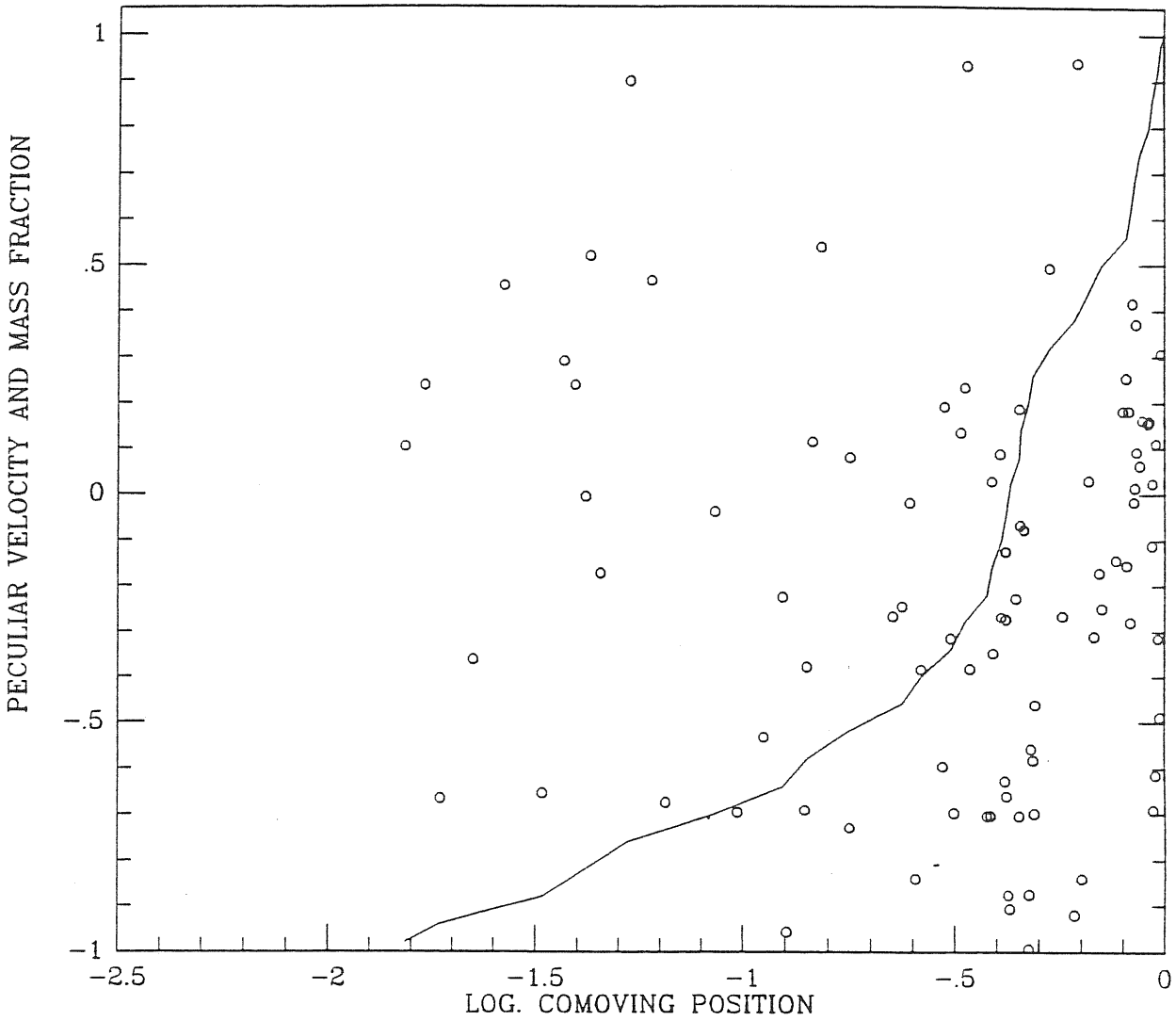


**Figure 27.** Case a: z=100; $\mathcal{F} = 10^{-1}$.

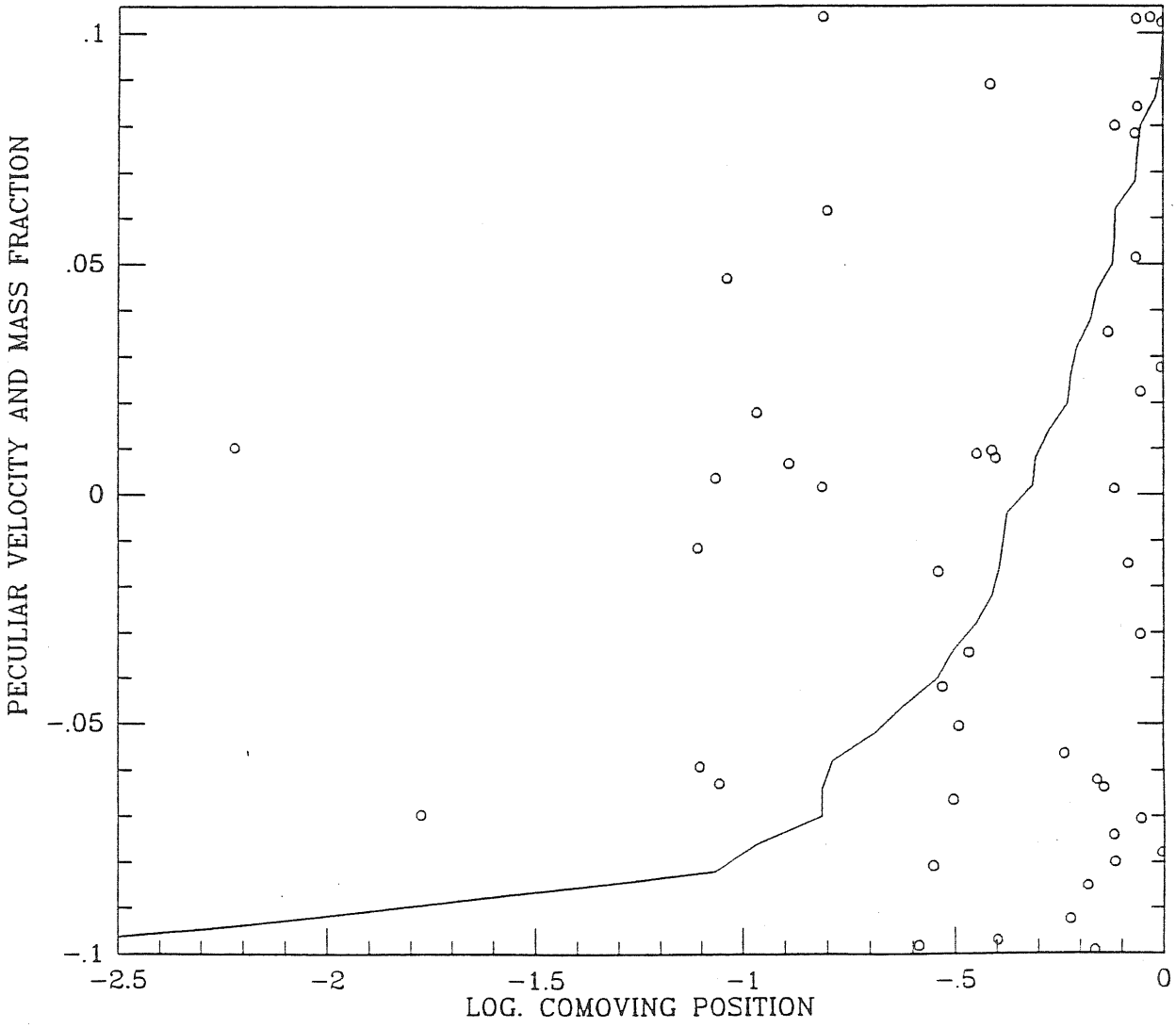


**Figure 28.** Case a: z=100; $\mathcal{F} = 10^{-2}$.

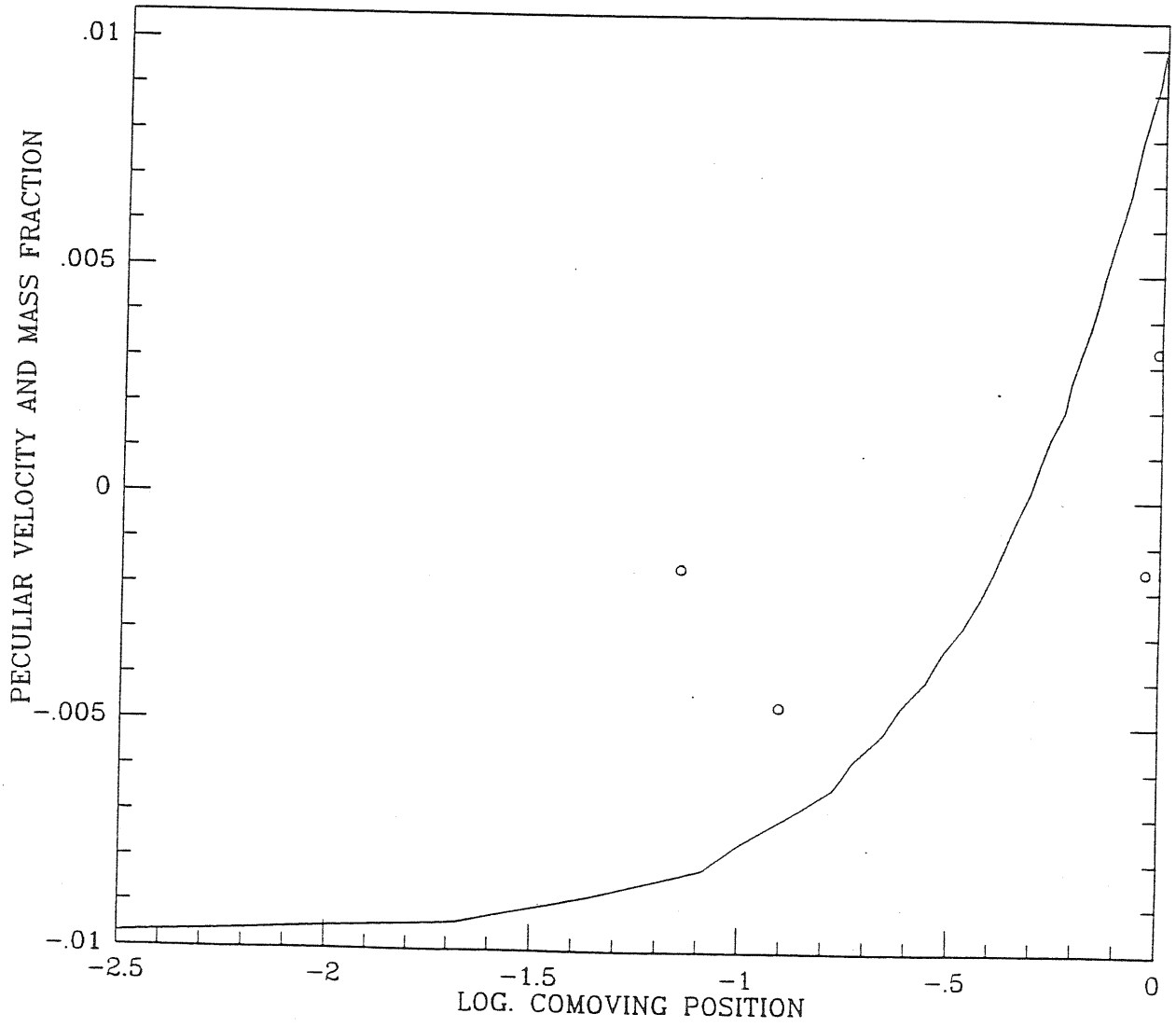


**Figure 29.** Case a: z=100; $\mathcal{F} = 10^{-3}$.

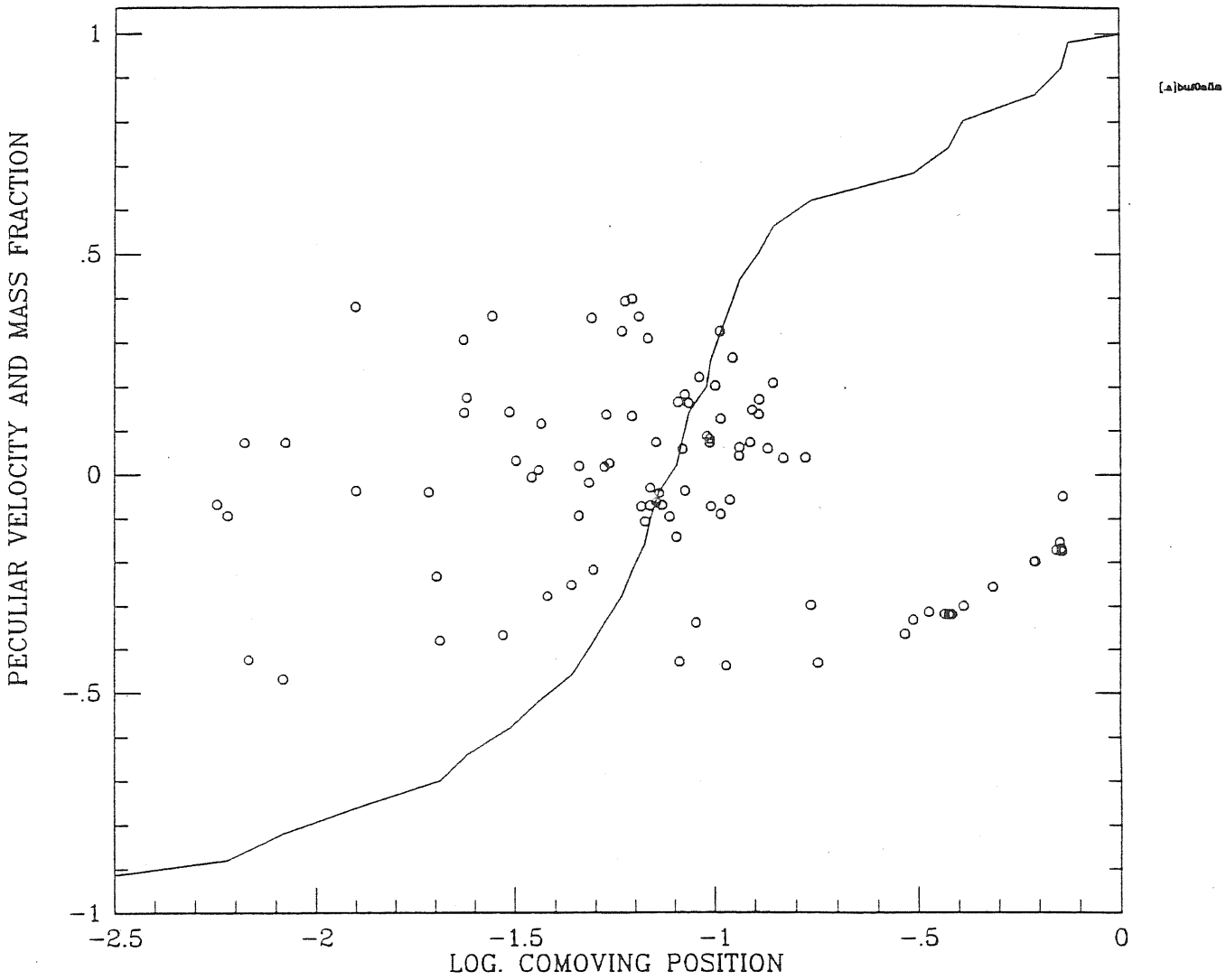


**Figure 30.** Case a: z=0; $\mathcal{F} = 1$.

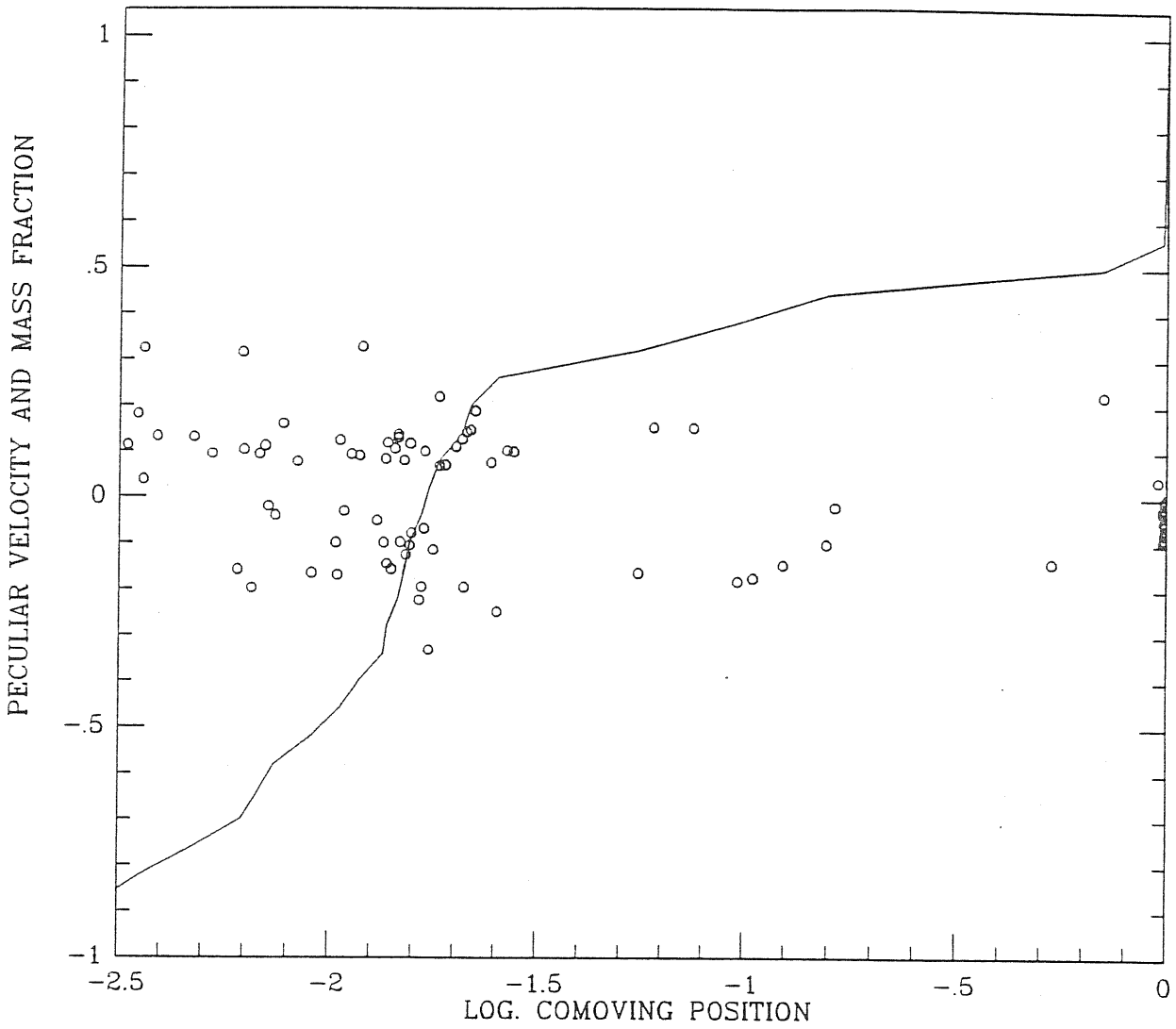


**Figure 31.** Case a: z=0; $\mathcal{F} = 10^{-1}$.

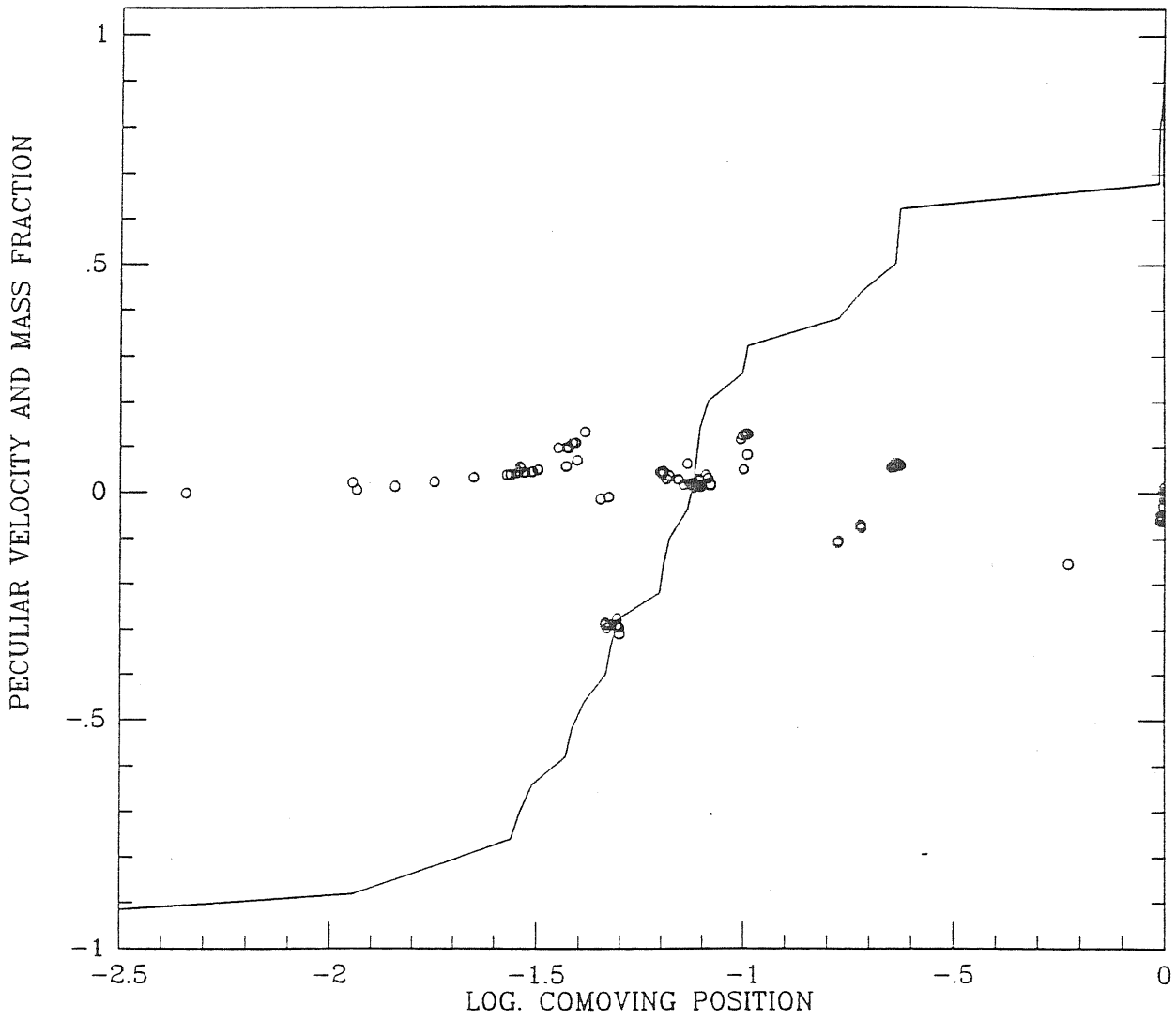


**Figure 32.** Case a: z=0; $\mathcal{F} = 10^{-2}$.

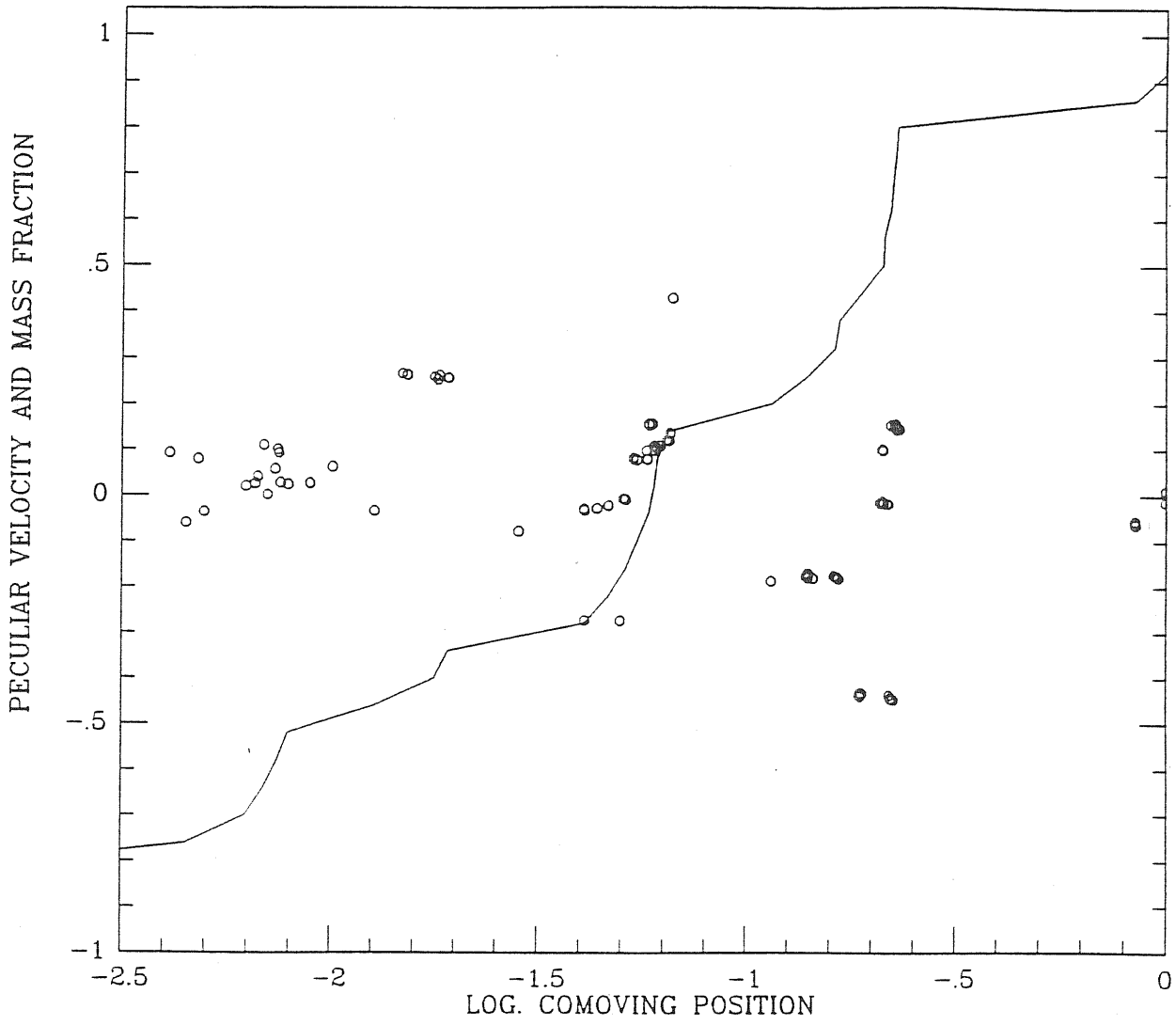


**Figure 33.** Case a: z=0; $\mathcal{F} = 10^{-3}$.

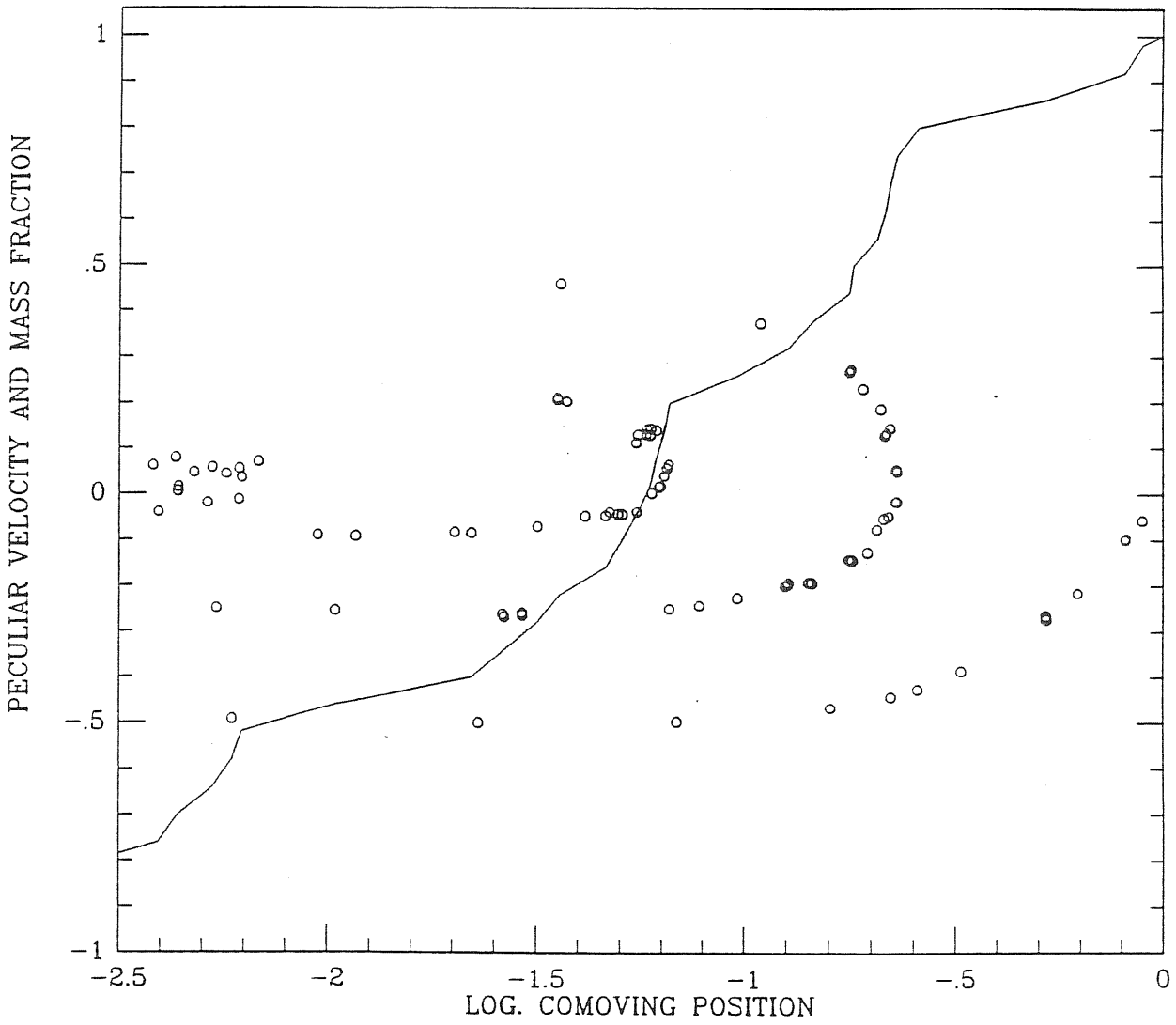


**Figure 34.** Case a: z=0; $\mathcal{F} = 10^{-4}$.

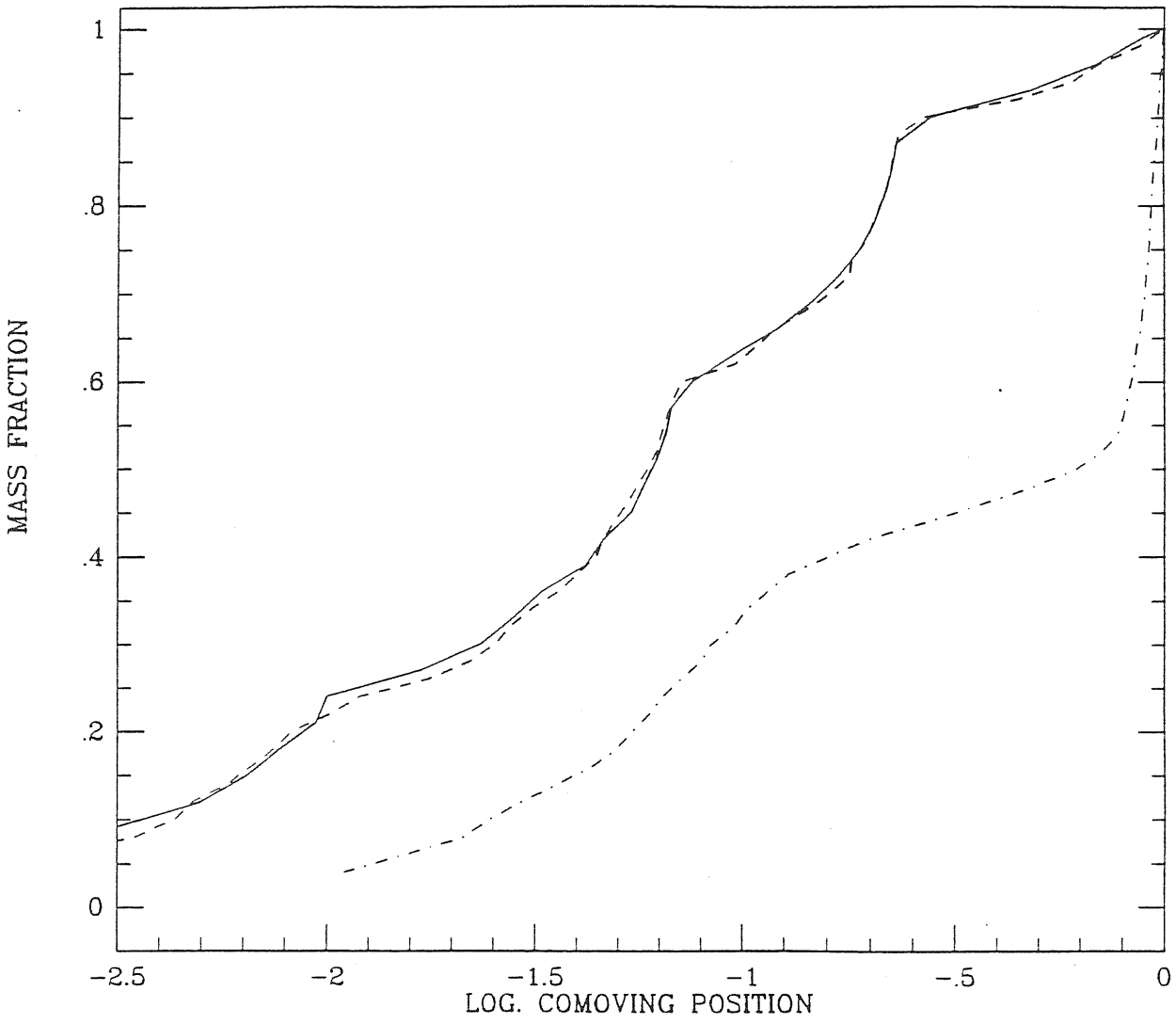


**Figure 35.** Z=0: Cold case case, solid line; sum of cases a, b, c, d, $\mathcal{F} = 10^{-4}$ dashed line; sum of cases a, b, c, d, $\mathcal{F} = 1$ point-dashed line.

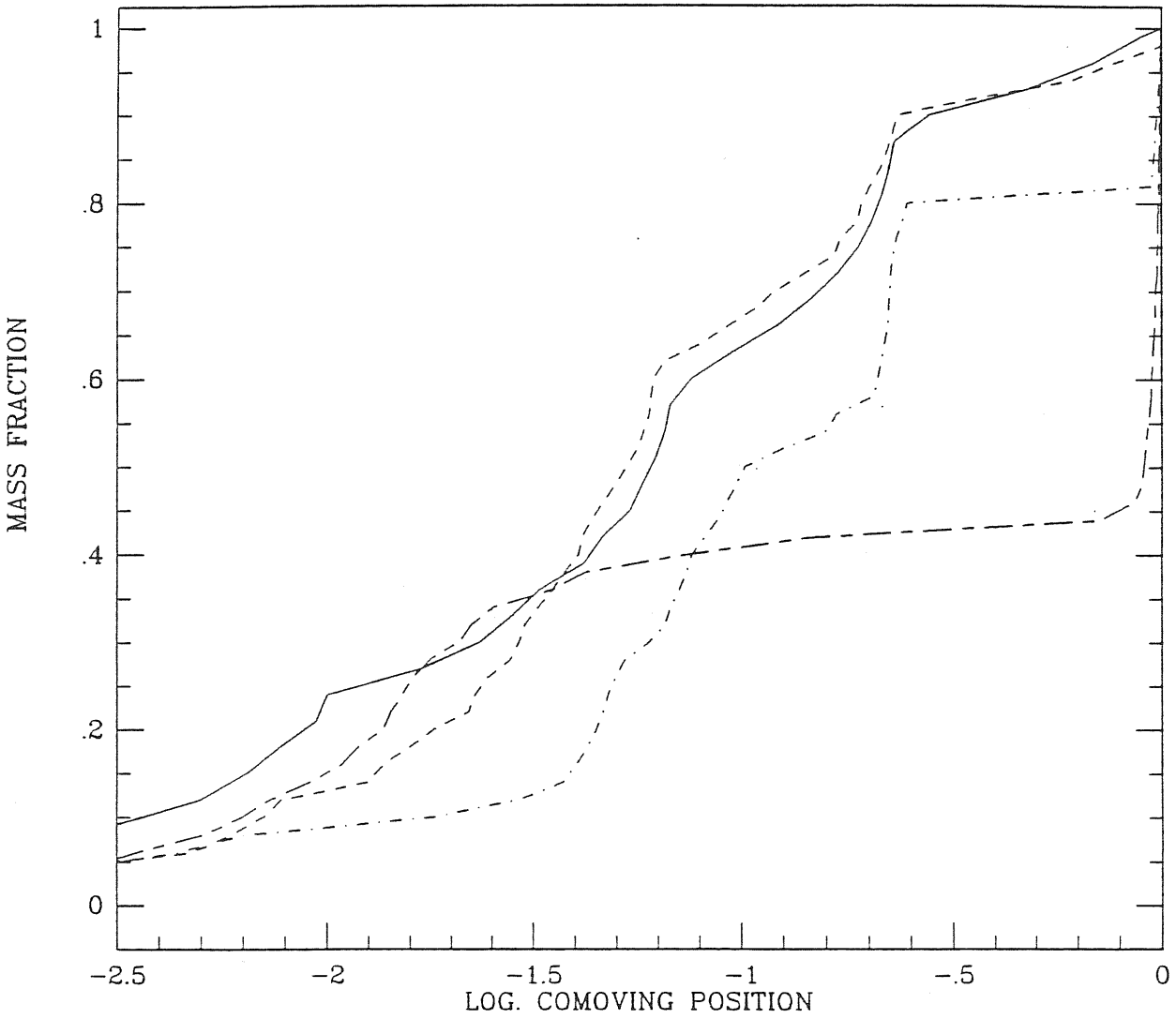


**Figure 36.** Z=0: Cold case case, solid line; sum of cases a, b, c, d, $\mathcal{F} = 10^{-3}$ dashed line; sum of cases a, b, c, d, $\mathcal{F} = 10^{-2}$ point-dashed line; sum of cases a, b, c, d, $\mathcal{F} = 10^{-1}$ short-long dashed line.

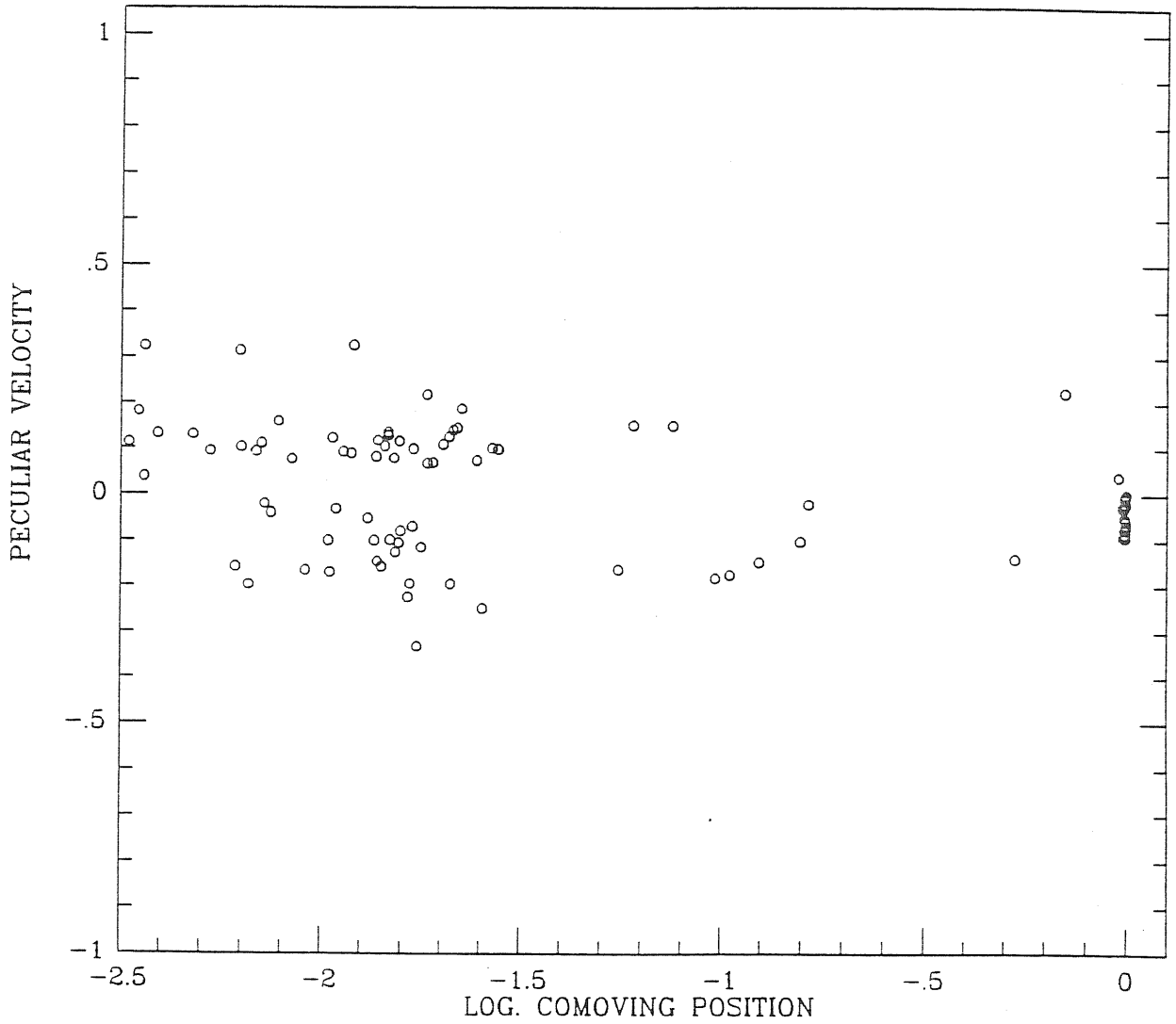


**Figure 37.** Case a: z=0 $\mathcal{F} = 10^{-1}$.

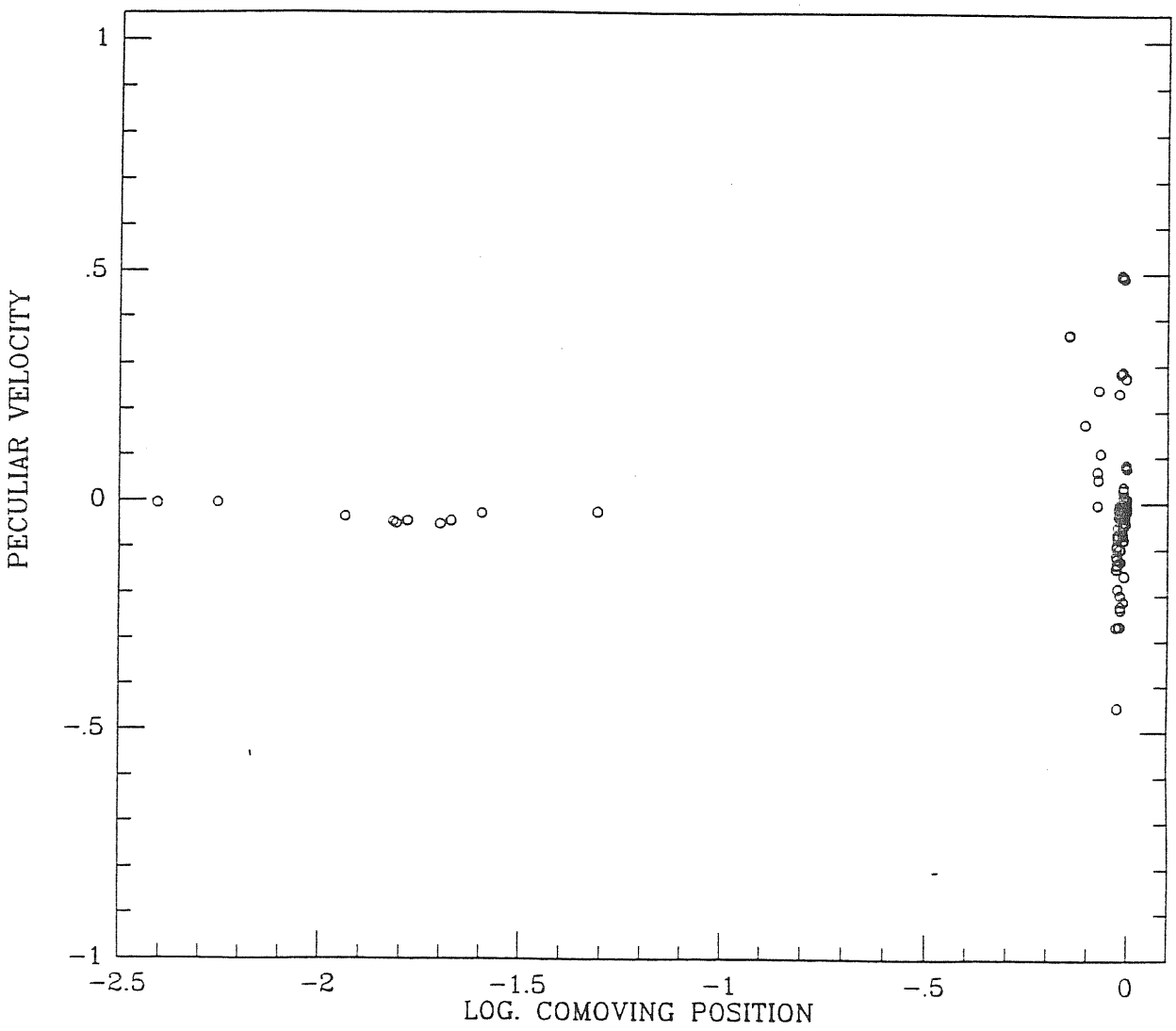


**Figure 38.** Case b: z=0 $\mathcal{F} = 10^{-1}$.

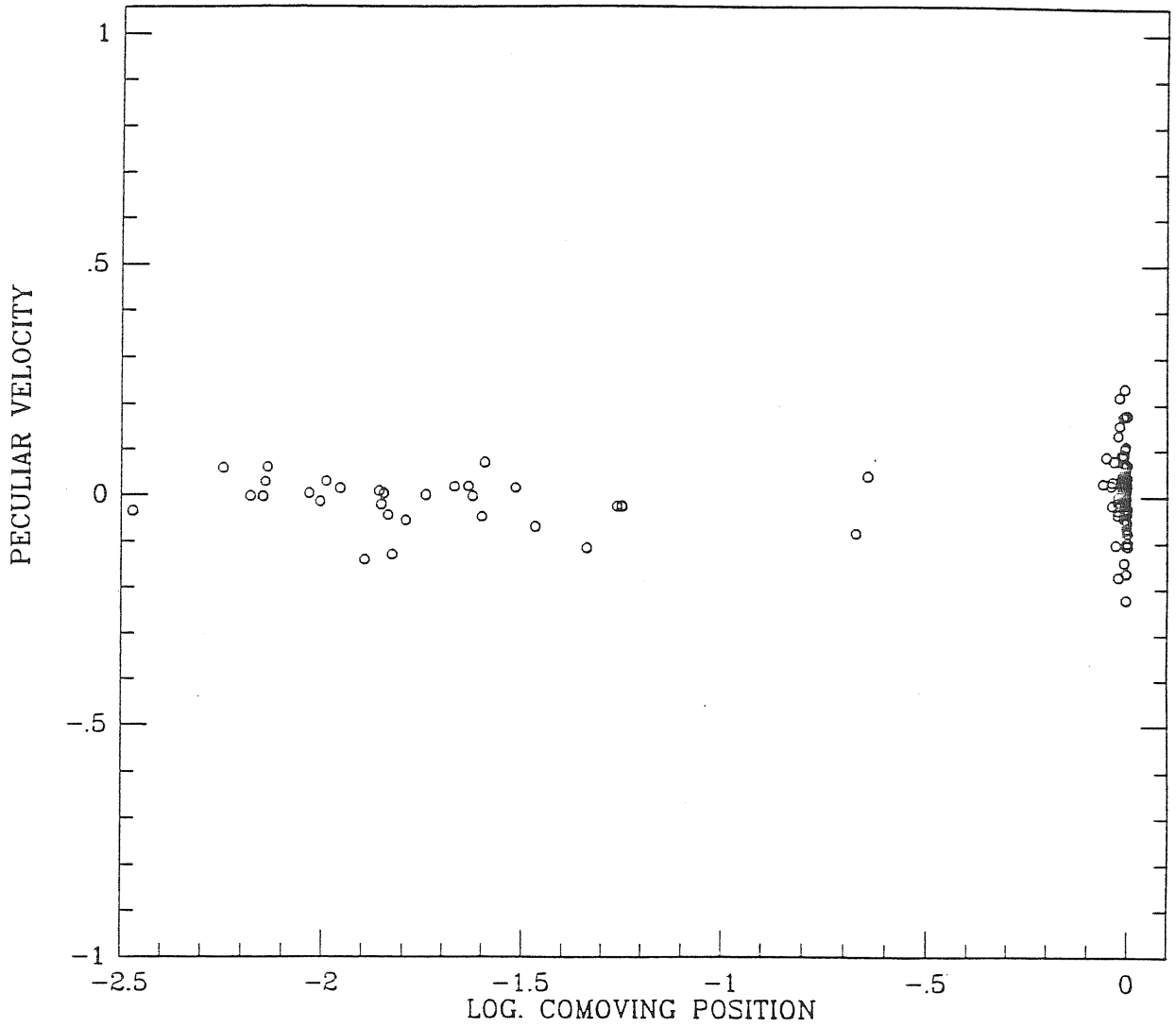


**Figure 39.** Case c: z=0 $\mathcal{F} = 10^{-1}$.

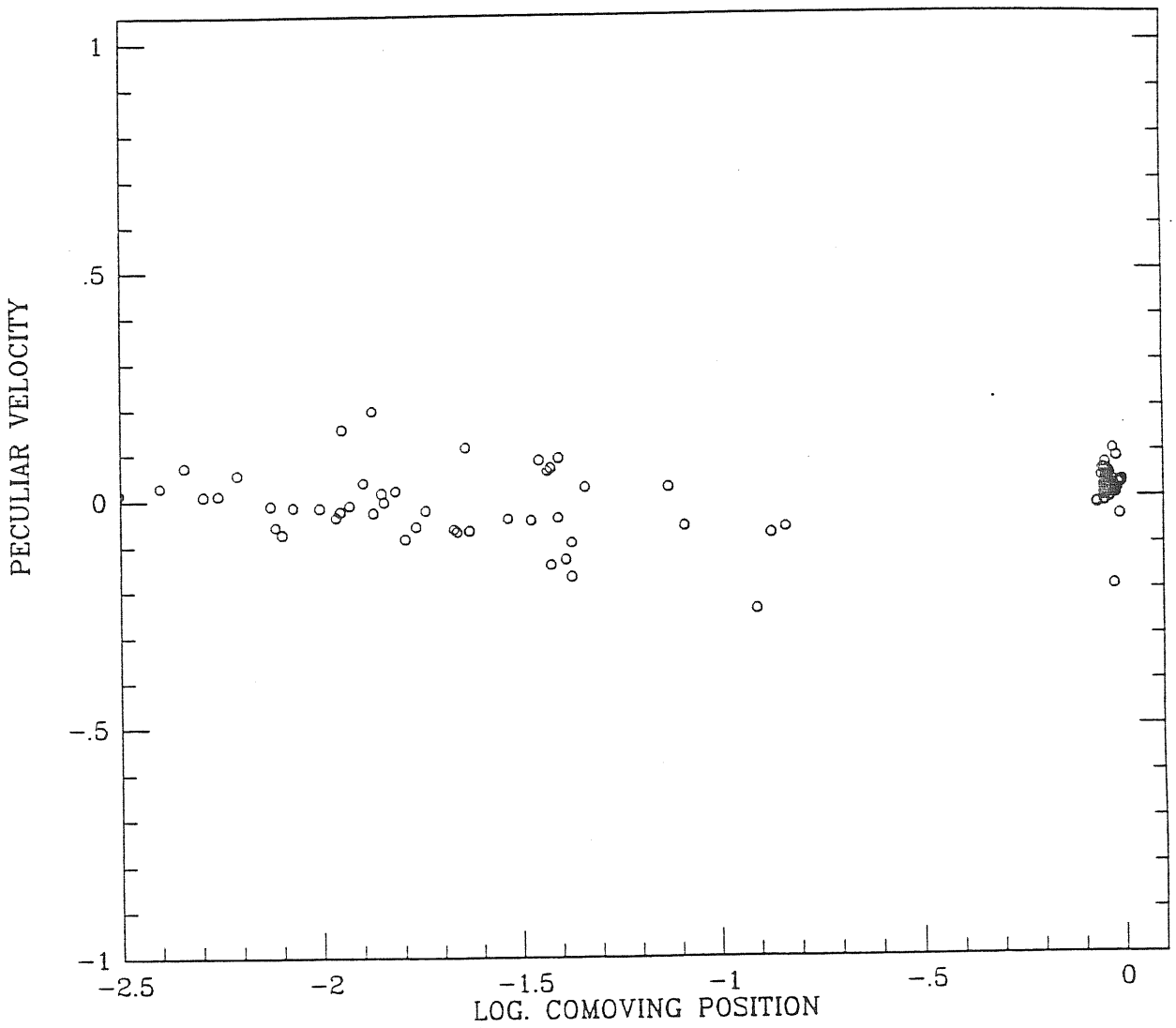


**Figure 40.** Case d: z=0 $\mathcal{F} = 10^{-1}$.

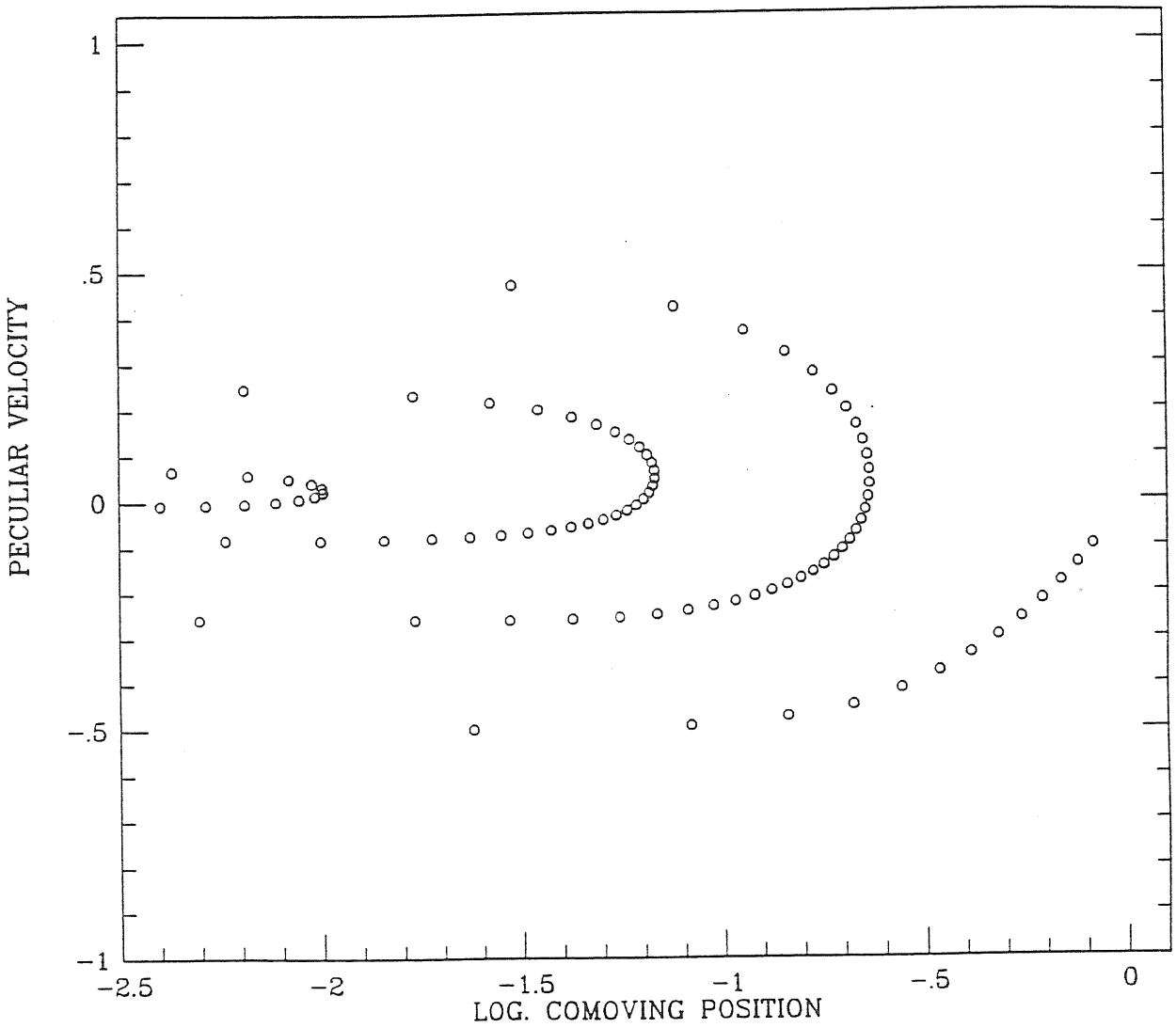


**Figure 41.** Cold case: z=0.

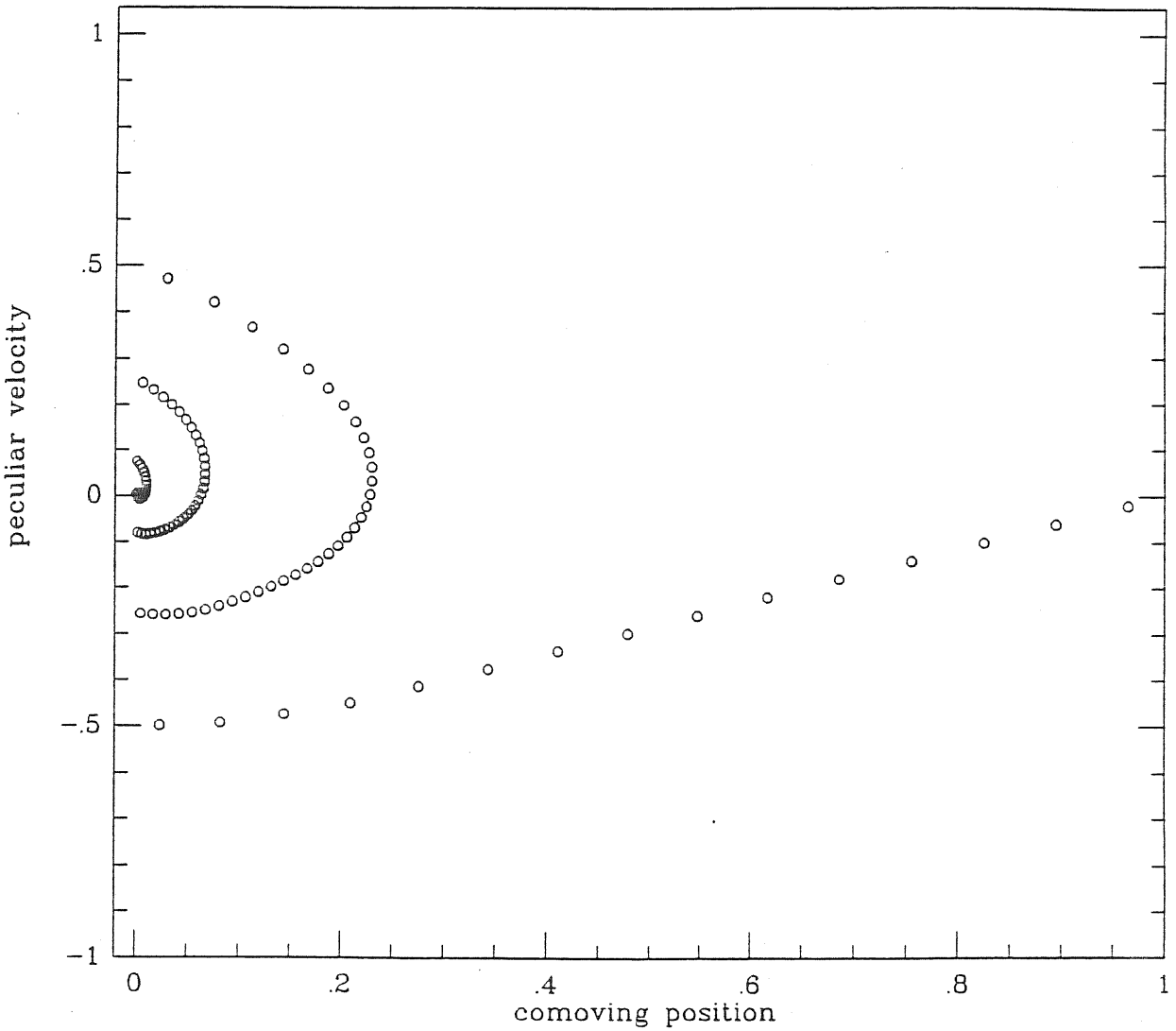


**Figure 42.** Cold case: z=0.

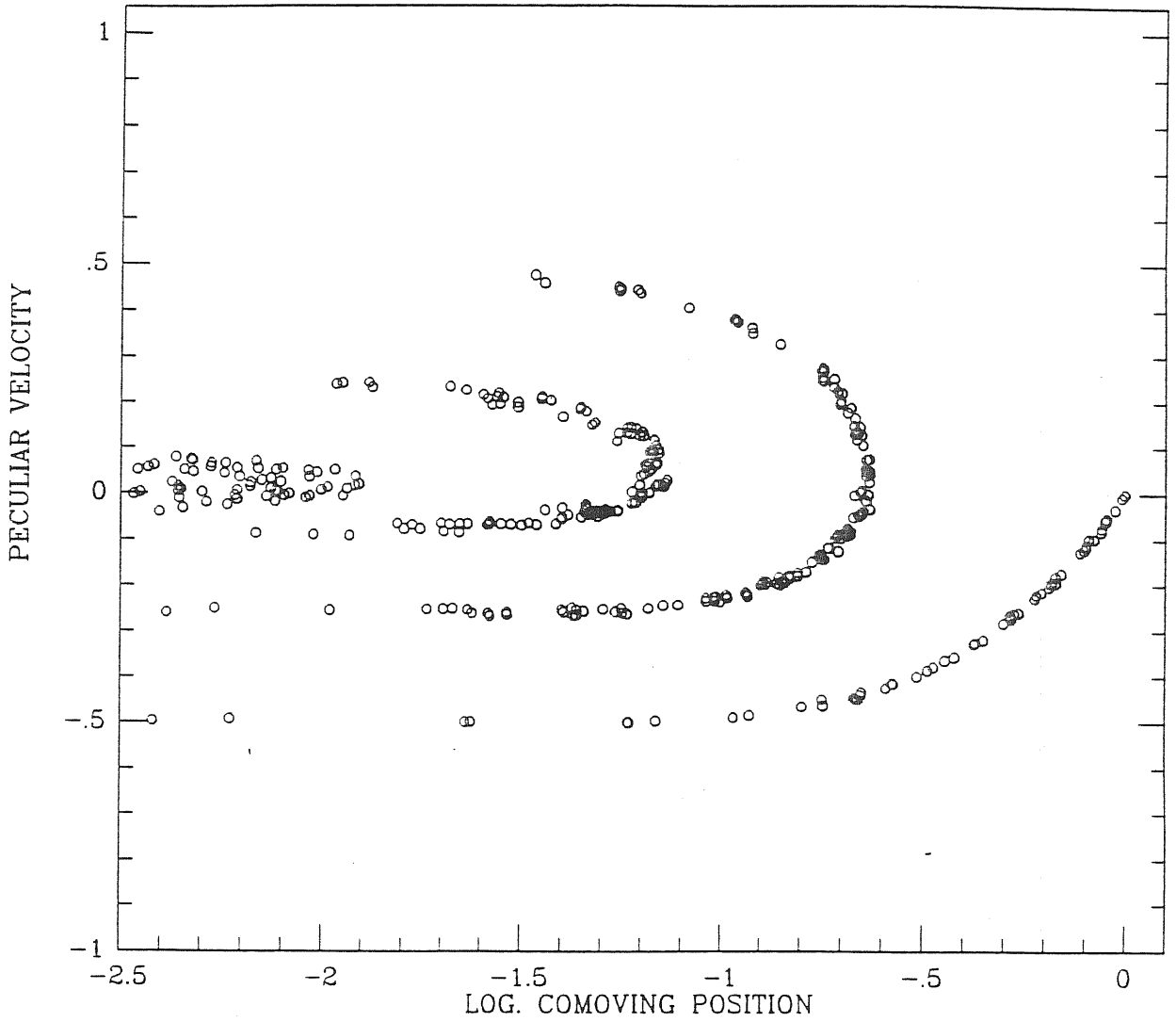


**Figure 43.** Sum of cases a, b, c, d: z=0; $\mathcal{F} = 10^{-4}$.

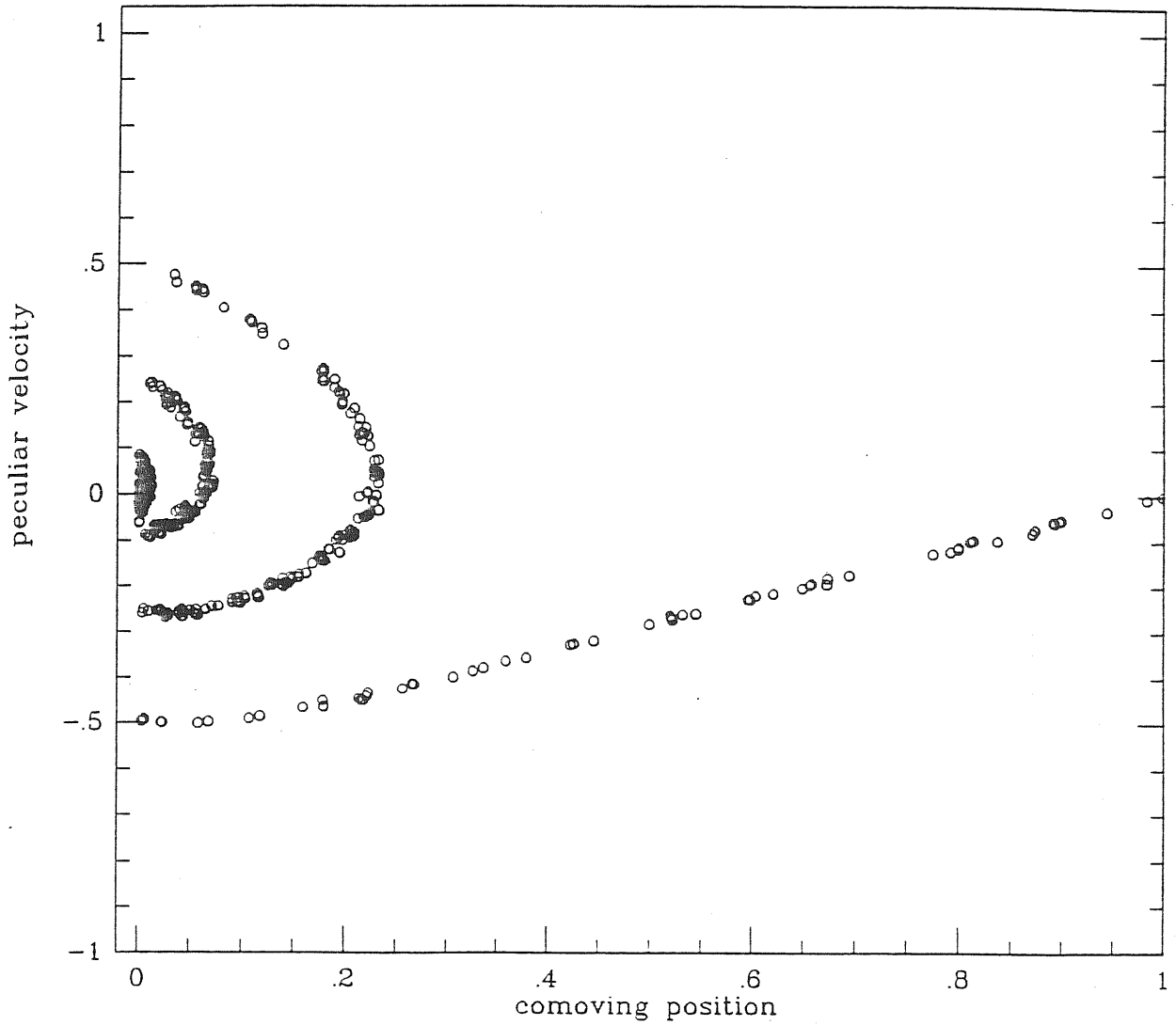


**Figure 44.** Sum of cases a, b, c, d: z=0; $\bar{\mathcal{F}} = 10^{-4}$.

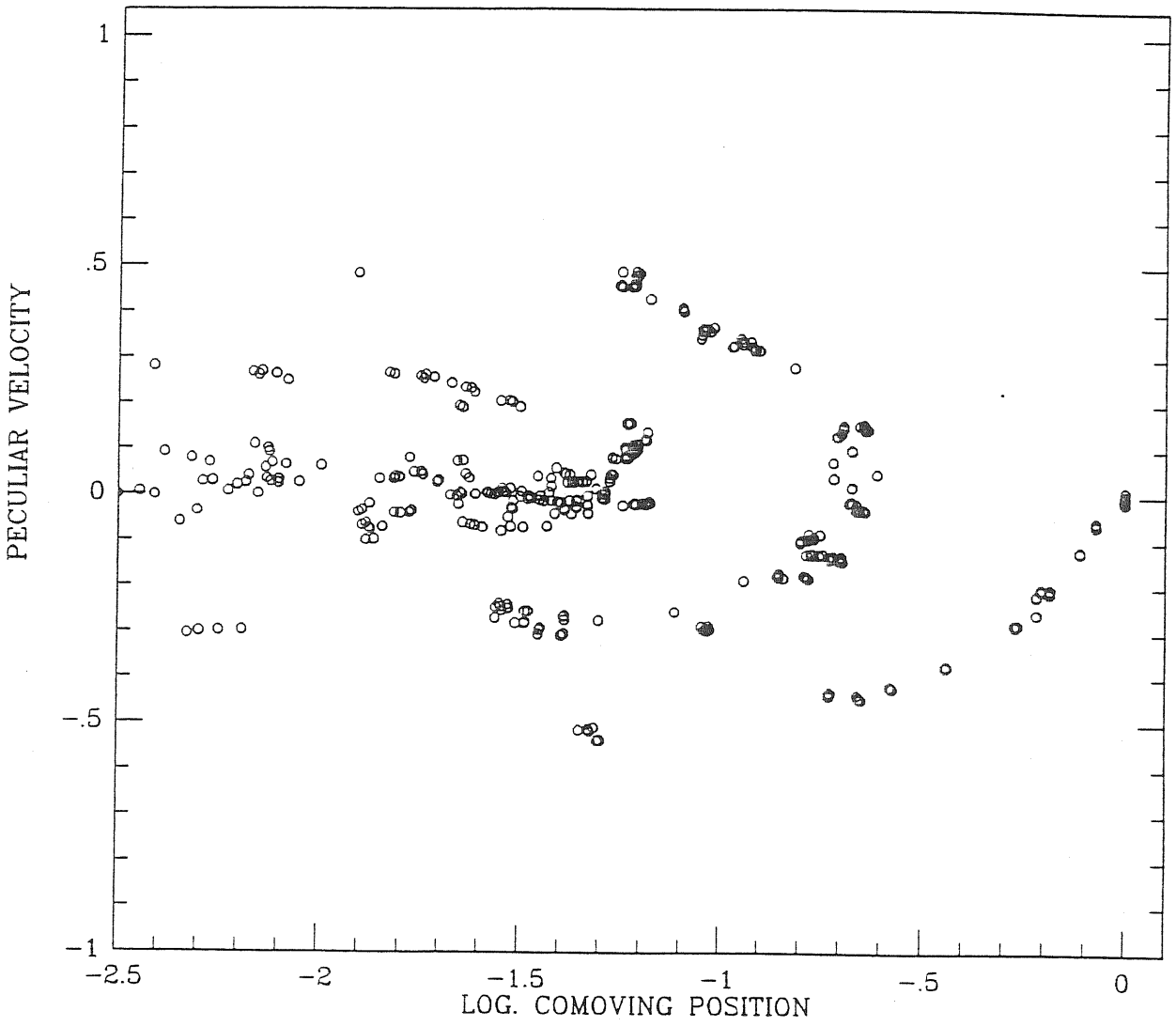


**Figure 45.** Sum of cases a, b, c, d: z=0; $\mathcal{F} = 10^{-3}$.

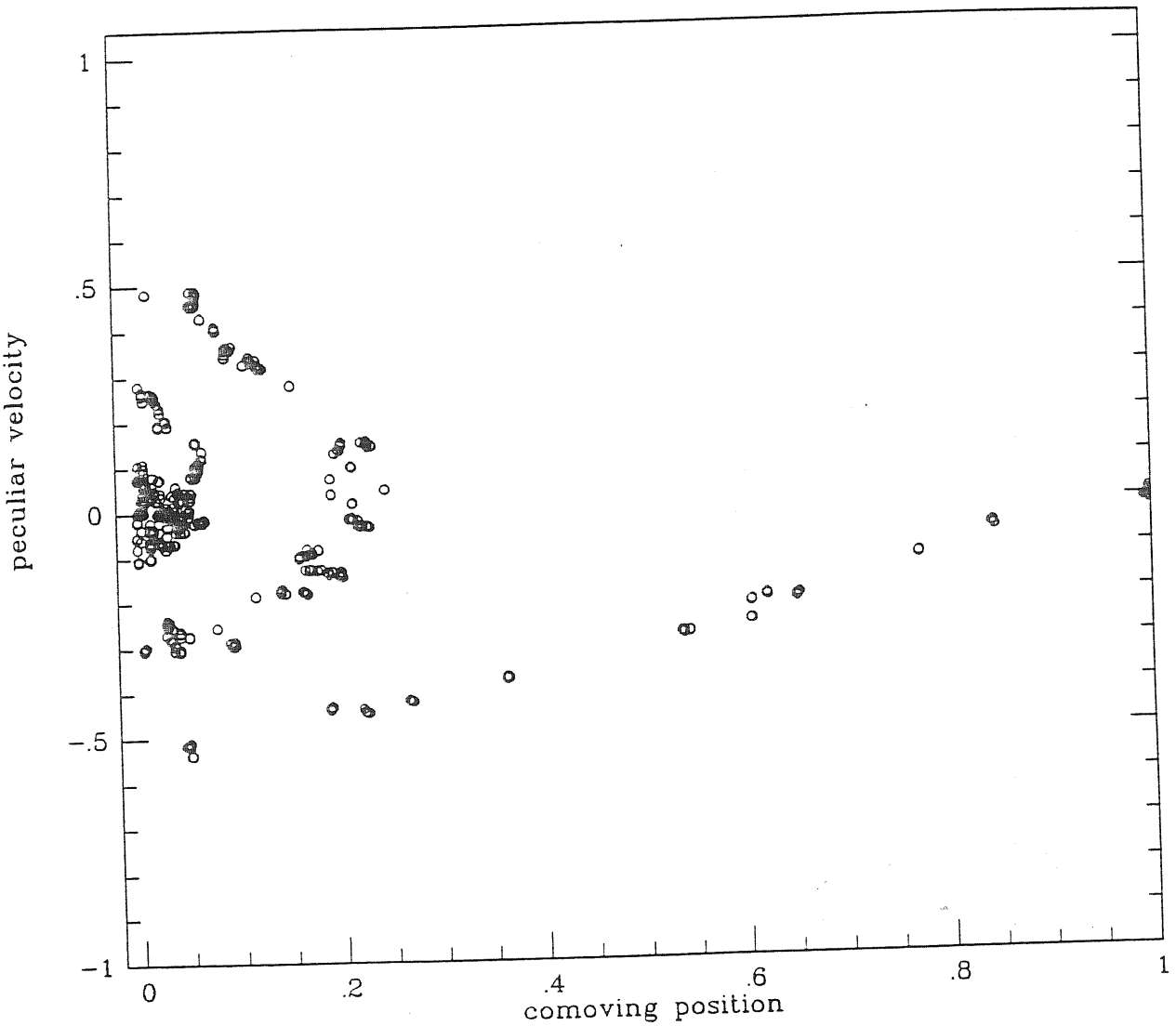


**Figure 46.** Sum of cases a, b, c, d: z=0; $\mathcal{F} = 10^{-3}$.

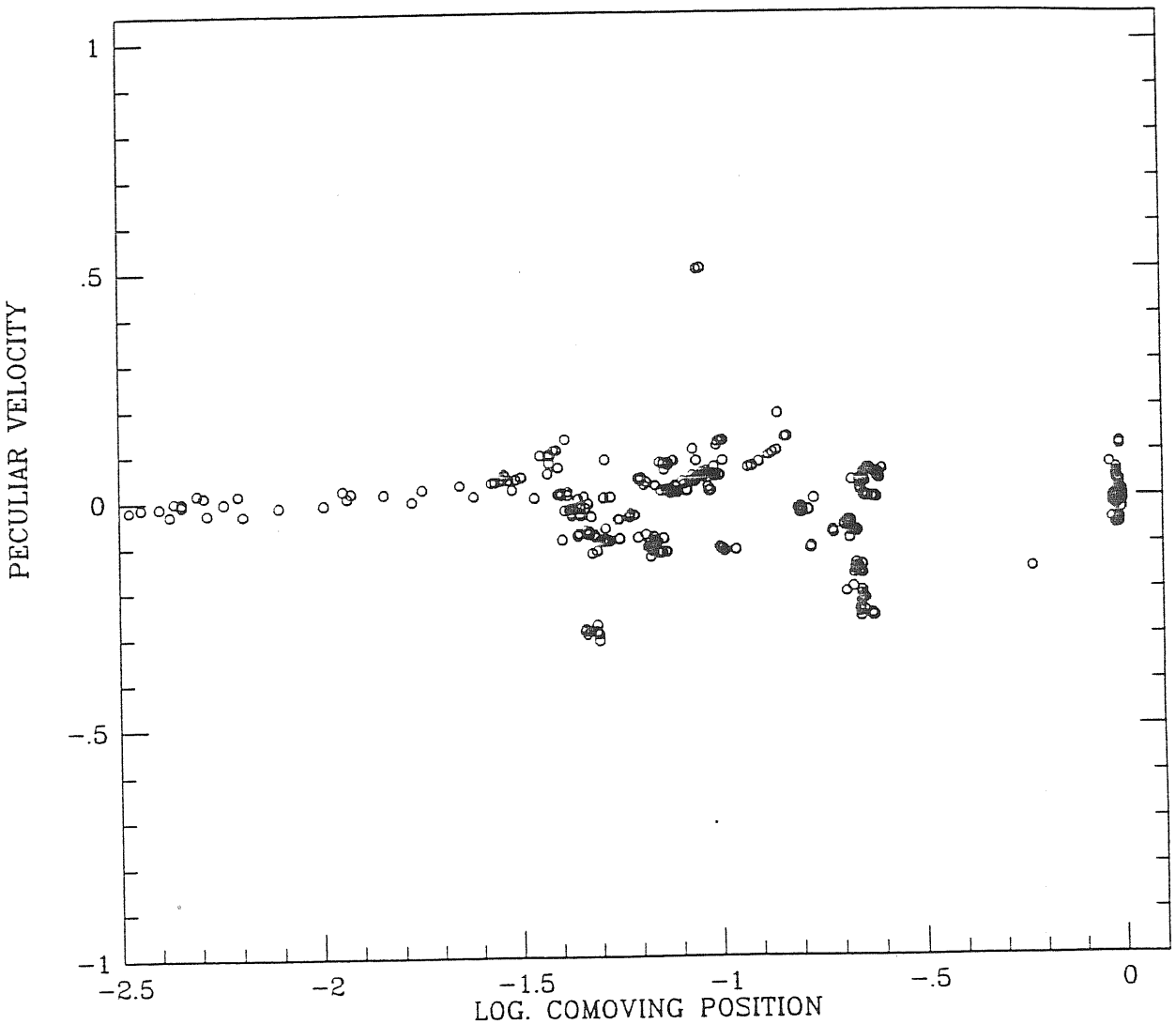


**Figure 47.** Sum of cases a, b, c, d: z=0; $\mathcal{F} = 10^{-2}$.

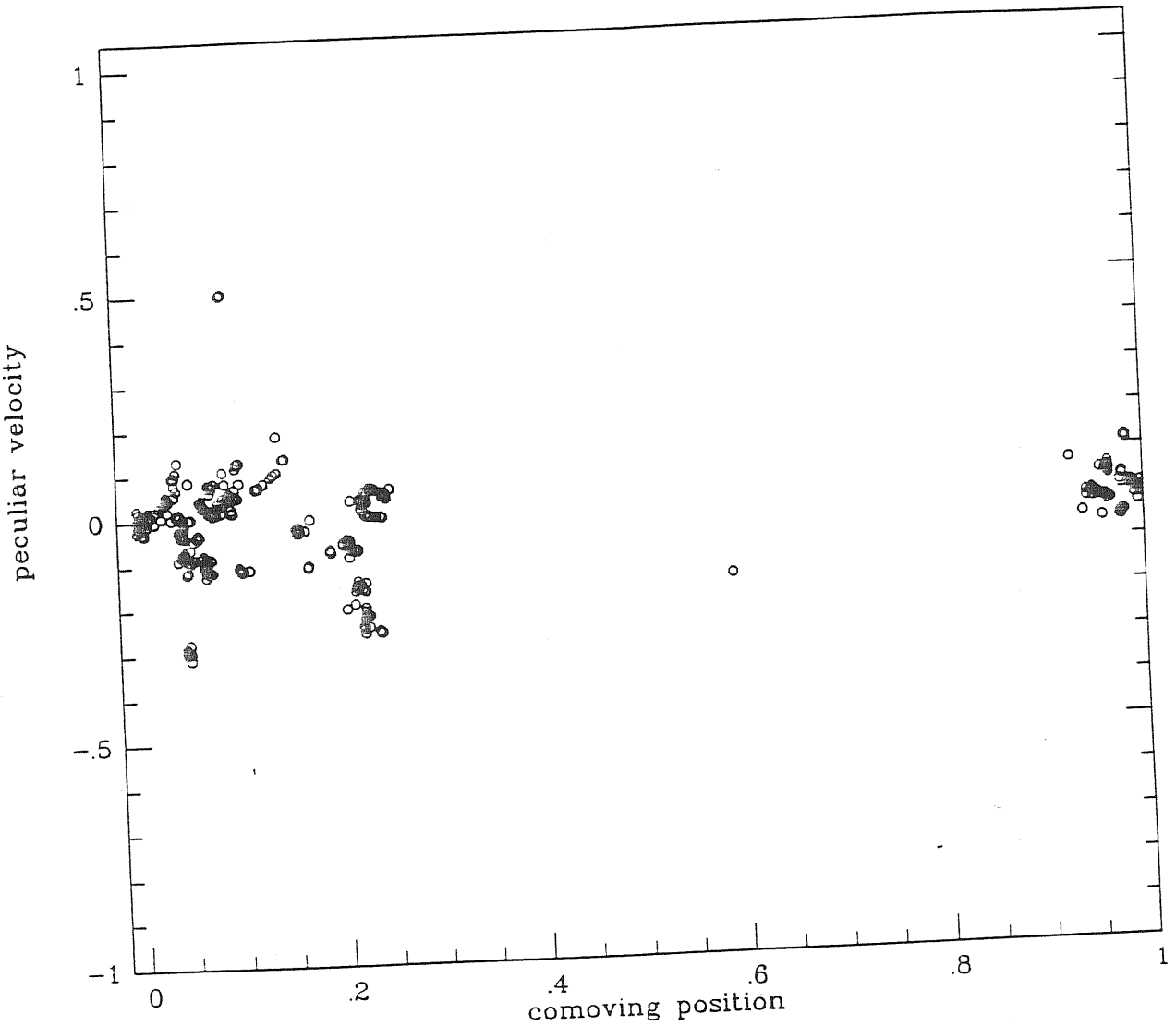


**Figure 48.** Sum of cases a, b, c, d: z=0; $\mathcal{F} = 10^{-2}$.

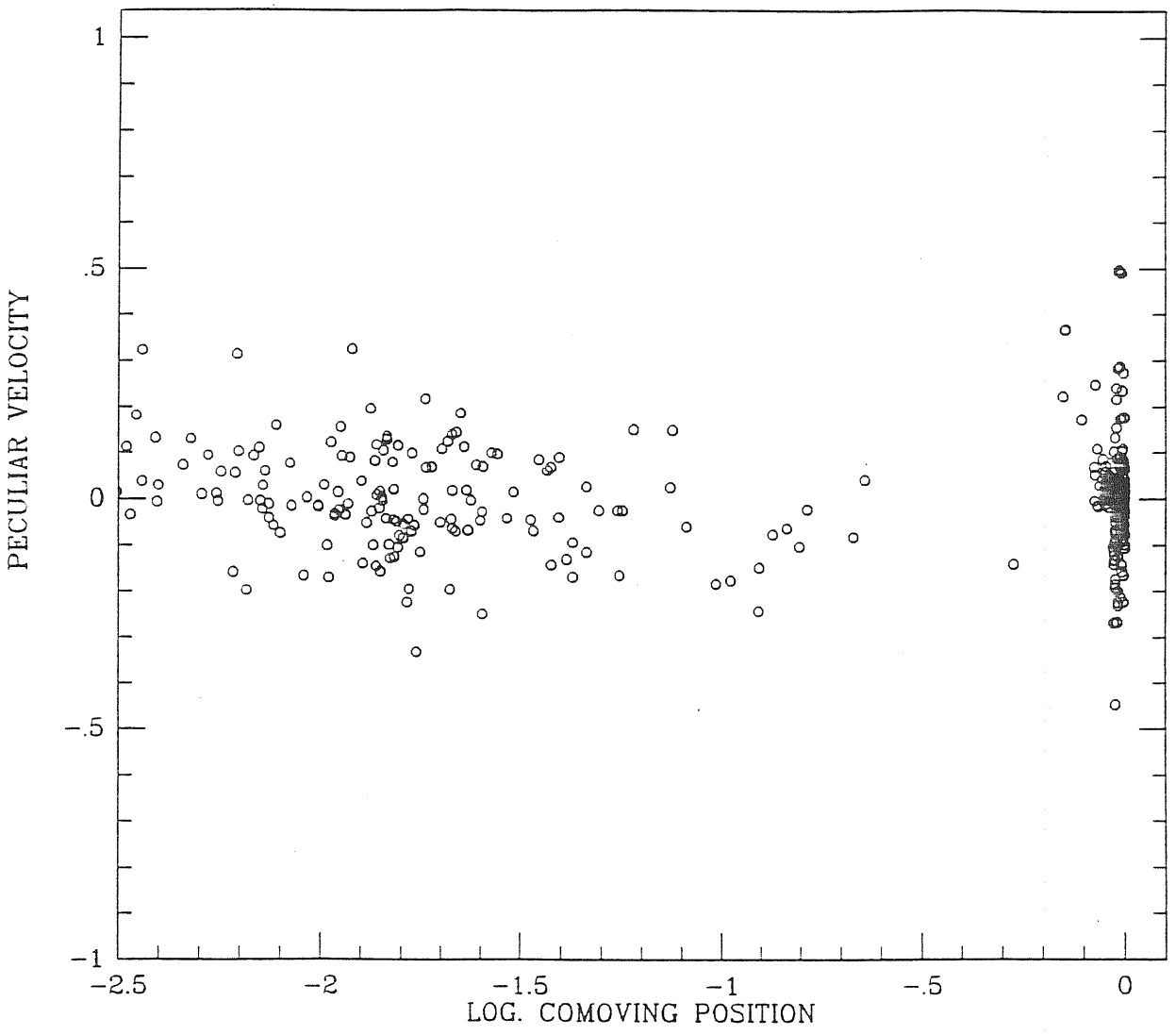


**Figure 49.** Sum of cases a, b, c, d: z=0; $\mathcal{F} = 10^{-1}$.

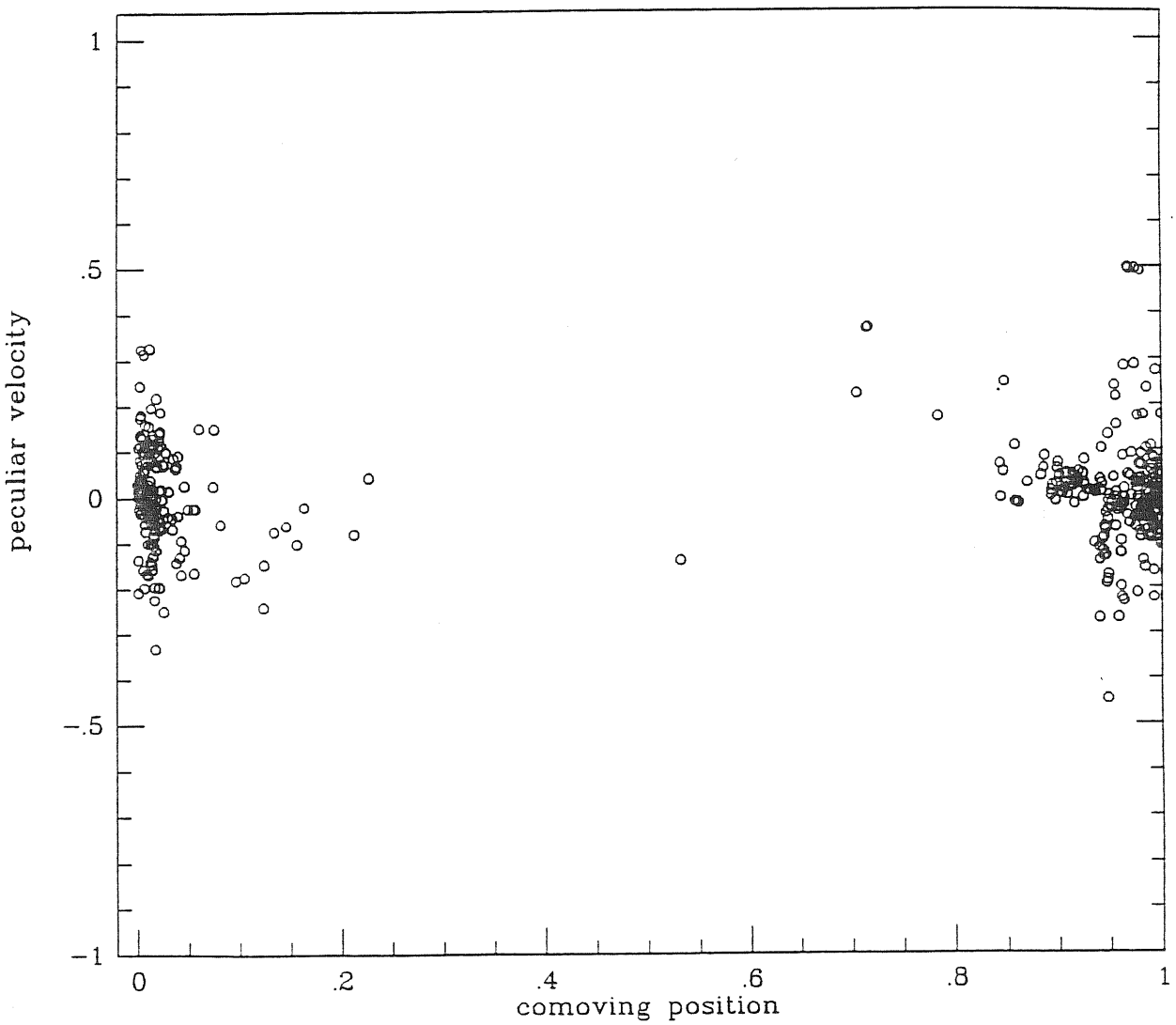


**Figure 50.** Sum of cases a, b, c, d: z=0; $\mathcal{F} = 10^{-1}$.

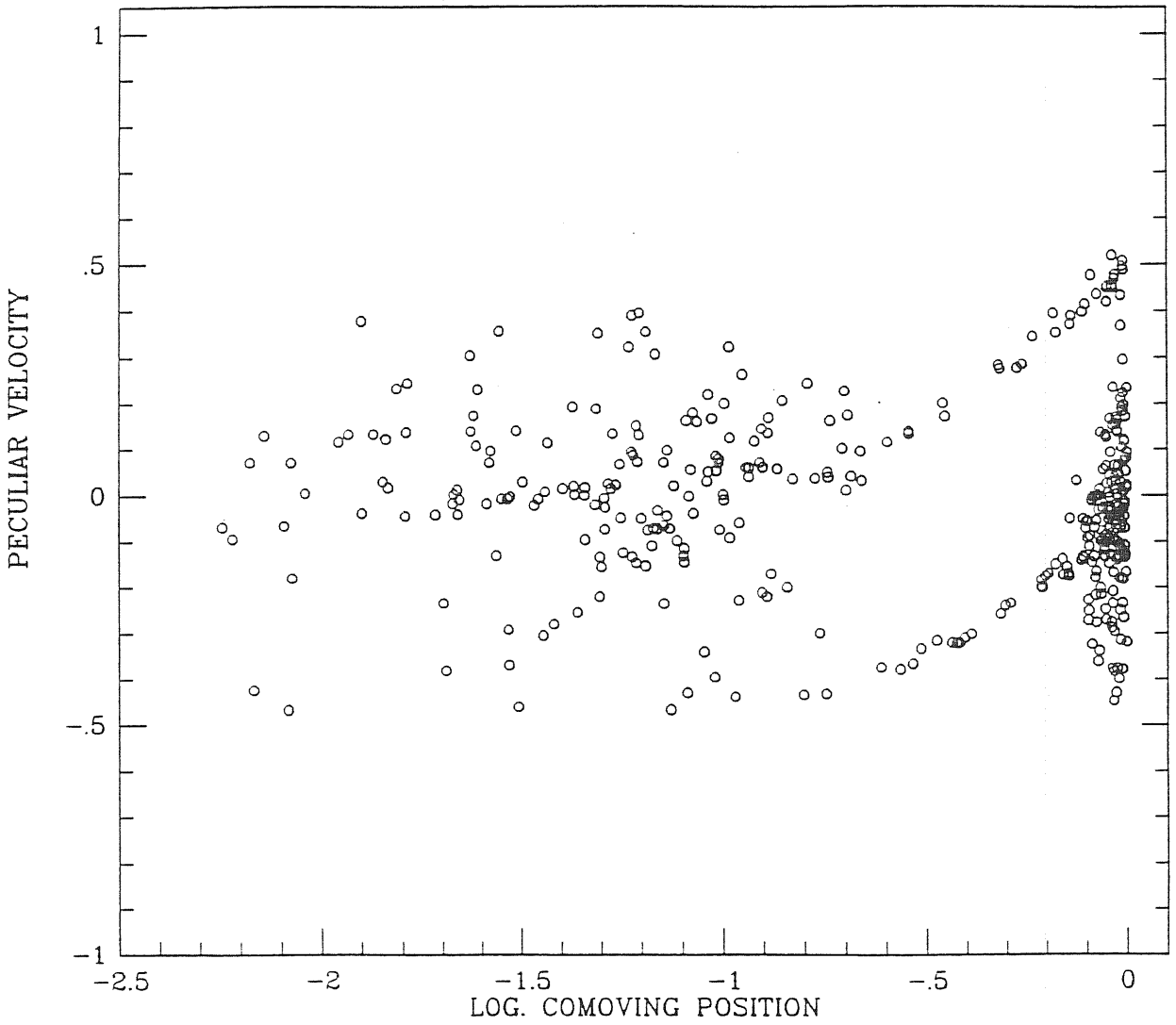


**Figure 51.** Sum of cases a, b, c, d: z=0; $\mathcal{F} = 1$.

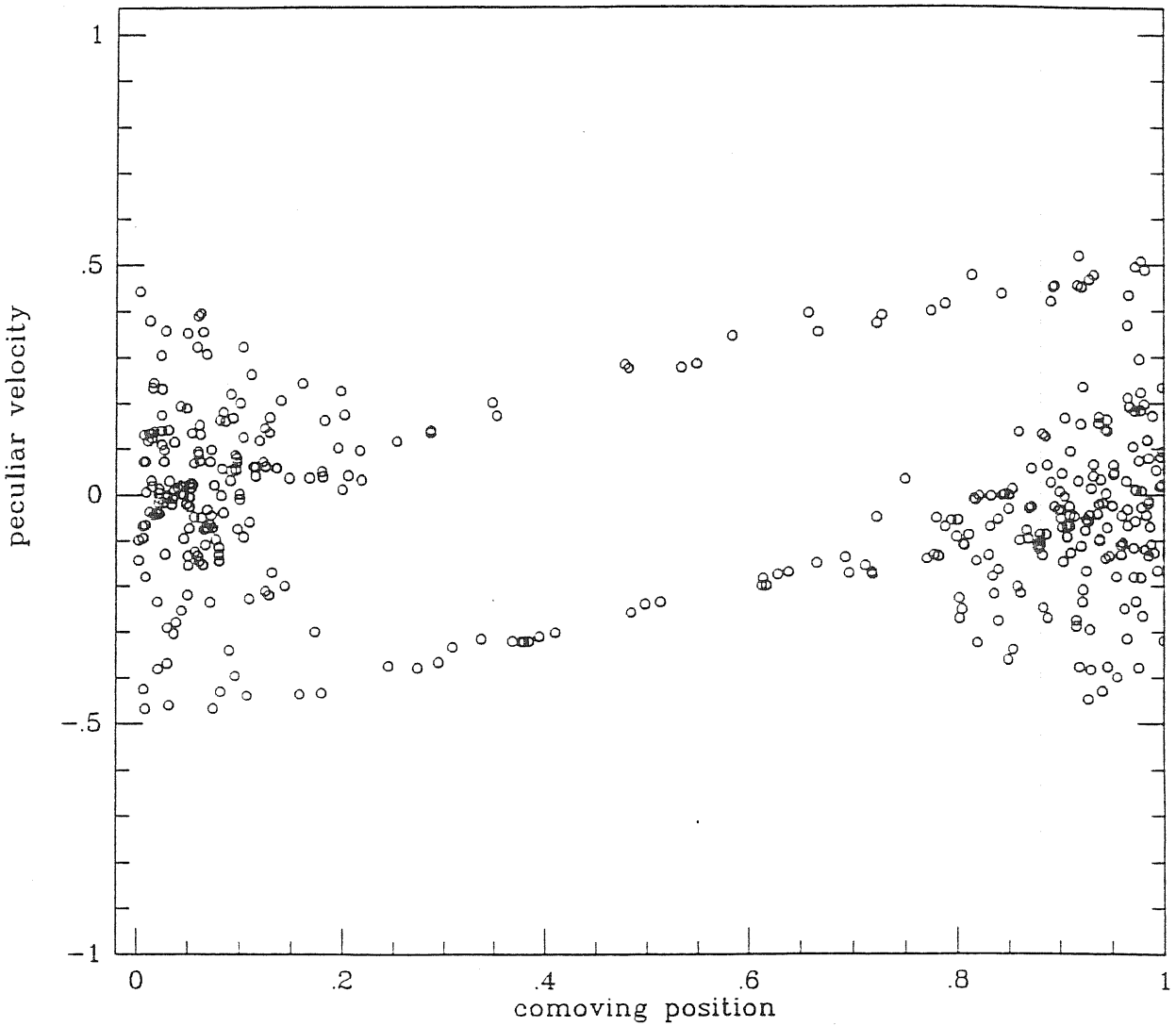


**Figure 52.** Sum of cases a, b, c, d: z=0; $\mathcal{F} = 1$.

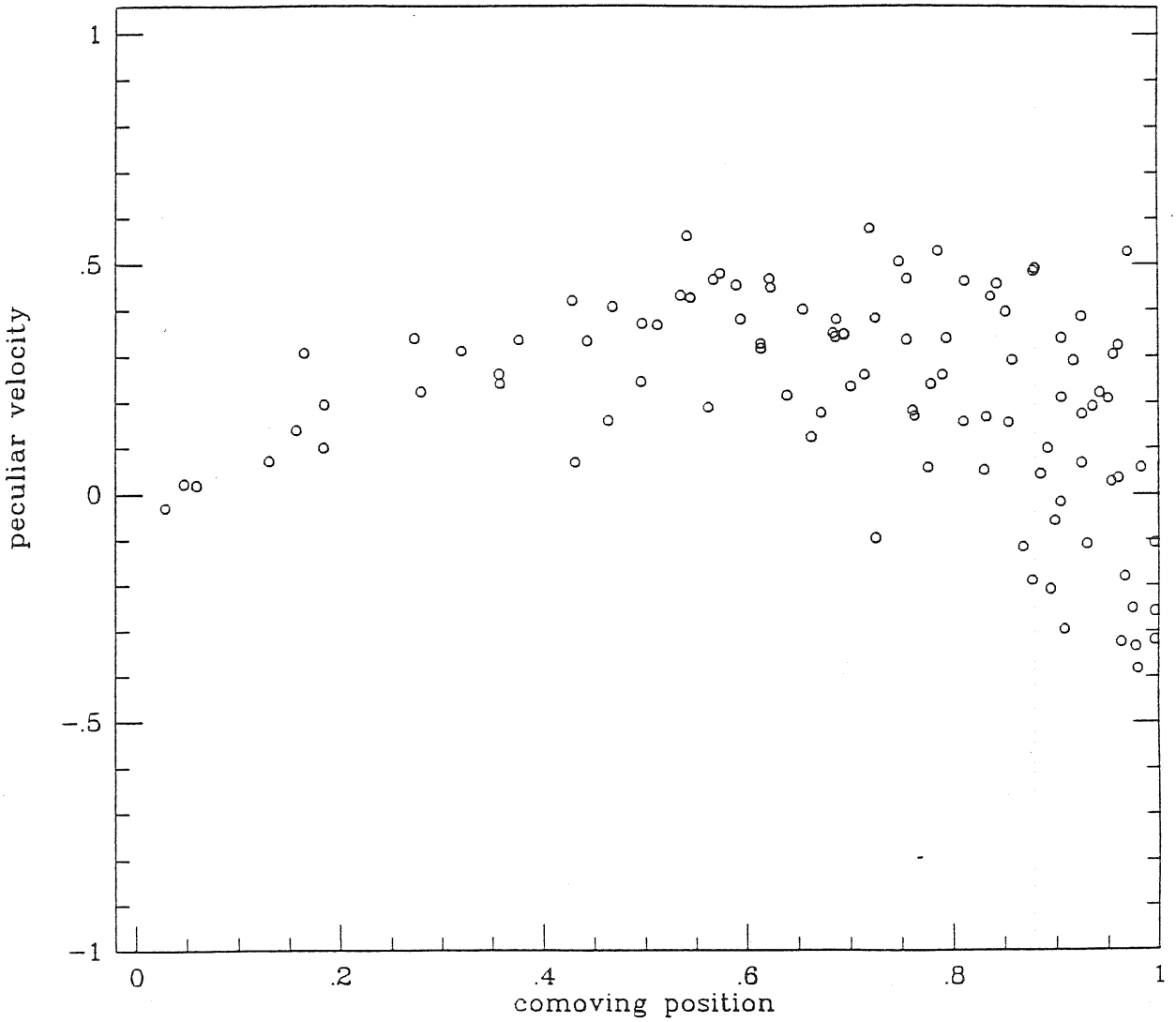


**Figure 53.** Case d: z=3.

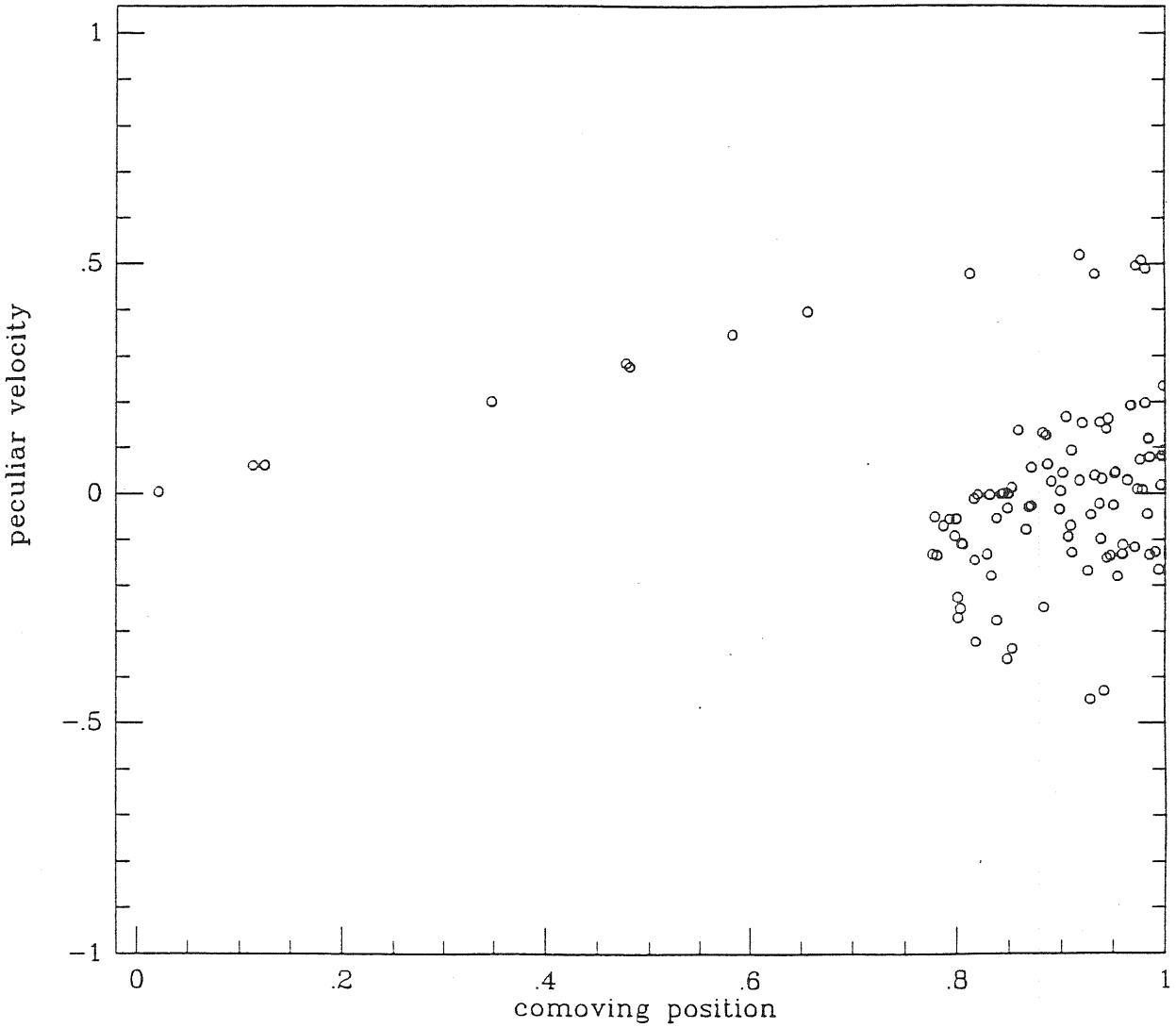


**Figure 54.** Case d: z=0.

# BIBLIOGRAPHY


Bahcall, J.N., 1984, *Astrophys. J.*, **276**, 156.

Bardeen, J., 1980, *Phys. Rev.* **22 D**, 1882.

Blumenthal, G.R., Pagels, H., and Primack, J.R., *Nature* **299**, 37.

Bond, J.R., and Szalay, A.S., 1983, *Astrophys. J.*, **274**, .

Doroshkevich, A.G., Ryaben'kii, V.S., and Shandarin, S.F., 1975, *Astrophysics*, 9, 144.

Carr, B.J., and Silk, J., 1983, *Astrophys. J.*, **268**, 16.

Centrella., J.M., 1980, *Astrophys. J.*, **241**, 875.

Centrella, J.M., and Melott, A., 1985, "Numerical Astrophysics", 334, Ed. Centrella, J.M., Le Blanc, J.M., Bowers, R.L.

Cuperman, S., Harten, A., and Lecar, M., 1971, *Ast. Sp. Sci.***13**, 411.

Davis, M., Efstathiou, G., Frenk, C.S., and White, S.D.M., 1985, *Astrophys. J.*, **292**, 391.

Fillmore, J.A., and Goldreich, P., 1984, *Astrophys. J.*, **281**, 1.

Groth, E.J., and Peebles, P.J.E., 1975, *Astron. Astrophys.*, **41**, 143.

Guth, A., 1982, *Phys. Rev.*, **D23**, 347.

Hoffmann, G.L., Olson, D.W., and Salpeter, E.E., 1980, *Astrophys. J.*, **242**, 861.

Hohl, 1967, *Astrophys. J.*, **147**, 1164.

Lecar, M., ad Cohen, L., 1971, *Ast. Sp. Sci.* **13**, 397.

Lifshitz, E.M., 1946, *Zh. esp. Theor. Phys.* **16**, 587.

Linde, 1983, *Phys. Lett.* **108 B**, 389.

Lynden-Bell, D., 1967, *Mon. Not. Roy. Astron. Soc.*, **136**, 101.

Melott, A.L., 1982, Phys. Rev. Lett., **48**, 894.

_____1983, *Astrophys. J.*, **264**, 59.

_____1985, *Astrophys. J.*, **289**, 2.

Milgrom, M., 1983, *Astrophys. J.*, **270**, 365.

Oort, 1932, *Bull. Astr. Inst. Netherlands* **6**, 249.

_____1960, *Bull. Astr. Inst. Netherlands* **15**, 45.

Pagels, E.,1984, *11th Texas Symp.*, Ann. N.Y. Acad. Sci. **422**, 15.

Peebles, P.J.E., 1980a, **"The Large Scale Structure of the Universe"**, Princeton University Press, Princeton N.J.

_____1980b, **"Physical Cosmology"**, 216, Ed. Balian, R., Audouze, J., and Schramm, D.N., Les Houches XXXII.

_____1982, *Astrophys. J. Lett.*, **263**, L1.

Press, W.H., and Vishniac, E.T., 1980, *Astrophys. J.*, **239**, 1.

Press, W.H., Flannery, B.P., Teukolsky, S., and Vetterling, W.T., 1985, **"Numerical Recipes"**, in press.

Rubin, V.C., *IAU Symp.* **100**, 3, Ed. Athanassoula, E., Reidel.

Salpeter, E.E., 1984, *11th Texas Symp.*, Ann. N.Y. Acad. Sci. **422**, 95.

Severne.,G., and Luwel, M., 1980, *Ast. Sp. Sci.* **72**, 293.

Shu, F.H., 1978, *Astrophys. J.*, **225**, 83.

Shandarin, S.F., 1981a, *Astrophysics*, **16**, 439.

_____1981b, "**The Origin and Evolution of Galaxies**", Ed. Jones and Jones, NATO Proceedings, Erice, Italy.

Shapiro, P.R., Struck-Marcell, C., and Melott, A.L., 1983, *Astrophys. J.*, **275**, 413.

Shapiro, P.R., and Struck-Marcell, C., 1985, *Astrophys. J. Suppl.*, **57**, 205.

Shukurov, A.M., 1982, *Astrophysics*, **17**, 263.

Silk, J., 1968, *Astrophys. J.*, **151**, 459.

Shaeffer, R., and Silk, J. 1985, *Astrophys. J.*, **292**, 319.

Szalay, A.S., and Zel'dovich, Y.B., 1982, "**Neutrino '82**", Ed. Frenkel, Jenik.

Tremaine, S., 1985 preprint.

Uson, J.M., and Wilkinson, D.T., 1984, *Astrophys. J. Lett.*, **274**, L1.

Wilson, J.R., Bond, J.R., Centrella, J.M., and Szalay, A.S., 1985, "**Numerical Astrophysics**", 325, Ed. Centrella, J.M., Le Blanc, J.M., Bowers, R.L.

White, S.D.M., Frenk, C., and Davis, M., 1983, *Astrophys. J. Lett.*, **274**, L1.

Zel'dovich, Y.B., 1970, *Astron. Astrophys.*, **5**, 84.

Zel'dovich, Y.B., and Novikov, I.D., 1983, "**The Structure and Evolution of the Universe**", Chicago University Press.

Zwicky, F., 1930, *Helv. Phys. Acta* **6**, 110.